Ministero dell'Istruzione,
dell'Università
e della Ricerca

Università degli Studi di Palermo
Dottorato in Ingegneria dell'Innovazione
Tecnologica

ELECTROSPUN NANOFIBROUS MATS IN FIBRE REINFORCED EPOXY LAMINATES

PhD thesis of **Maria Di Filippo**

SSD Chim/07

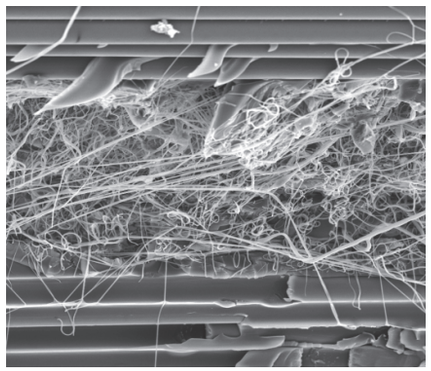

Supervisor
Prof.ssa. Clelia Dispenza

Head of the PhD board
Prof. Salvatore Gaglio

Ciclo XXIX

M. Di Filippo Electrospun nanofibrous mats in fibre reinforced epoxy laminates

UNIVERSITÀ DEGLI STUDI DI PALERMO
Dottorato in Ingegneria dell'Innovazione Tecnologica
Dipartimento dell'Innovazione Industriale e Digitale – Ingegneria Chimica, Gestionale, Informatica, Meccanica
SSD: CHIM/07

ELECTROSPUN NANOFIBROUS MATS IN FIBRE REINFORCED EPOXY LAMINATES

IL DOTTORE
MARIA DI FILIPPO

IL COORDINATORE
Prof SALVATORE GAGLIO

IL TUTOR
Prof.ssa CLELIA DISPENZA

CICLO XXIX
2017

ACKNOLEDGEMENTS

Firstly, I would like to express my sincere and heartfelt thanks to my supervisor, Prof.ssa Clelia Dispenza, for her continuous support and guidance through my Ph.D studies. I learnt a lot from her.

I gratefully acknowledge Dr.ssa Sabina Alessi, that helped me with very useful suggestions in the whole research project. I also thank her for support in SEM analysis.

Sincere appreciation is extended to Prof. Giuseppe Pitarresi for his advises and training in mechanical tests.

My thankfulness goes to Prof. Giuseppe Spadaro, for his recommendations.

I also want to thank Dr.ssa Maria Antonietta Sabatino for her continuous encouragements and all members of the "BioNanomaterials and Composites" Lab., in particular Lorena and Alessia for their support and friendship.

I acknowledge Prof. Andrea Zucchelli, Ing. Roberto Palazzetti, Prof.ssa Maria Letizia Focarete e Prof.ssa Chiara Gualandi, Alma Mater Studiorum – Università di Bologna, for producing and providing some electrospun mats.

Finally, my gratitude goes to Prof. Giuseppe Palmese, Department of Chemical and Biological Engineering, Drexel University, Philadelphia (USA), that allowed me to be part of his research group for 10 months, also giving me the opportunity to live a new life experience in USA.

TABLE OF CONTENTS

LIST OF FIGURES

1. Fibre-reinforced composite materials

2. Electrospinning

3. The influence of electrospun mats on the properties of epoxy resins

4. Electrospun Nylon 6,6 mats in high performance epoxy laminates

5. Comparative analysis of Nylon 6,6 and PVDF electrospun mats in low performance epoxy-carbon fibre laminates

6. Hydrothermal aging of epoxy resins

7. Hydrothermal aging of laminates with nanofibrous mats as interlayers

LIST OF TABLES

1. Fibre-reinforced composite materials

2. Electrospinning

3. The influence of electrospun mats on the properties of epoxy resins

4. Electrospun Nylon 6,6 mats in high performance epoxy laminates

6. Hydrothermal aging of epoxy resins

7. Hydrothermal aging of laminates with nanofibrous mats as interlayers

1. FIBRE-REINFORCED COMPOSITE MATERIALS

1.1 Introduction

A composite material can be defined as the combination of two or more materials, different in form and chemical composition. Each component retains its physical and chemical identity in the final material. [1]

Generally, the two main constituents are a continuous phase, the matrix, and a reinforcement.

Composites are classified according to the type of matrix or the geometry of the reinforcement. For the first case, they are distinguished in metal matrix composites (MMC), ceramic matrix composites (CMC) and polymer matrix composites (PMC); according to reinforcement they are classified in particulate reinforced and fiber reinforced composite materials. [2]

The most common form in which fiber reinforced composites are used in structural applications is the laminate. As the name indicates, it is constituted of a number of layers of long fiber fabrics and the matrix, stacked and consolidated together, the properties being influenced by fiber orientation in the layer and by the ply stacking sequence. [2]

It is well-known that the major strength points of fiber reinforced polymers, with respect to the traditional metallic materials, are the high strength to weight ratio and the high modulus to weight ratio. In addition, good fatigue strength, excellent chemical and corrosion resistance and design flexibility make them perfect replacement of traditional metallic materials for structural components in aeronautical, high performance automotive and other industries.

1.2 Matrix

The matrix is the Achille's heel in the laminate, limiting the fibers in exhibiting their full potential in terms of properties. It fulfills several functions; it holds the

fibers together transferring and distributing the loads among them, it provides out-of-plane mechanical properties to the laminate and contributes to the energy absorption features of the composite material. The matrix controls also the thermal properties, i.e. the heat capacity and the heat distortion temperature, and the flame resistance properties. [1]

Polymeric matrices for fiber-reinforced composites can be divided in thermoplastic and thermosetting polymers. Regarding the thermosetting polymers, the two most used types are epoxy resins and unsaturated resins, such as polyester or vinyl ester. Both these two systems meet the requirements of matrices for composite material, that are [3]:

- Long shelf-life.
- Relatively low viscosity for good fibers impregnation.
- High reactivity upon curing (low curing times and relatively low curing temperatures).
- Ease of control of the curing reaction kinetics, without volatile products formation.
- Good mechanical properties and thermal resistance of the cured resin.

In this work, the author focused the attention on epoxy matrices, that are characterized by a fairly rigid three-dimensional network.

The basic formulation of an epoxy matrix formulation consists of one or many epoxy monomers and one or many curing agents. Typical epoxy monomers for matrices in composite laminates are presented in Tab. 1.1.

Regarding the curing agents, amino-hardeners are the most used in conjunction with epoxy resins. Scheme 1.1 shows the mechanism of cure of primary amines with epoxy monomers. The initial step involves the primary amine active hydrogen addition to the epoxy group. This is followed by the resulting secondary amine addition to the epoxy group (Scheme 1.1a). When the monomer and the amine are di-functional, i.e. a diepoxide and a diamine, respectively, the resulting product is an infusible polymer (Scheme 1.1b). [3]

Table 1.1 Typical epoxy monomers used for composite materials.

Difuctional:

Diglycidyl ether of bisphenol A (n=0), MY 750

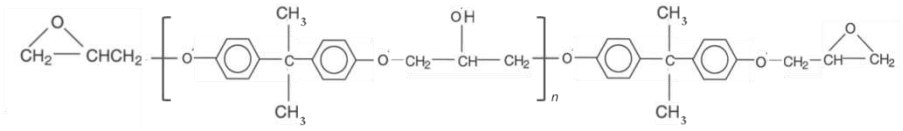

Trifunctional:

MY 0510

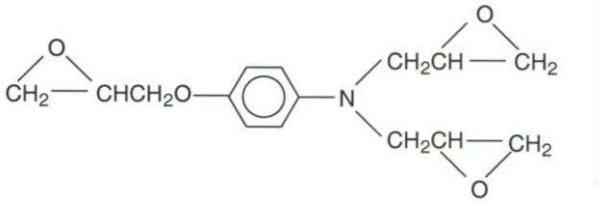

XD 7342.00L

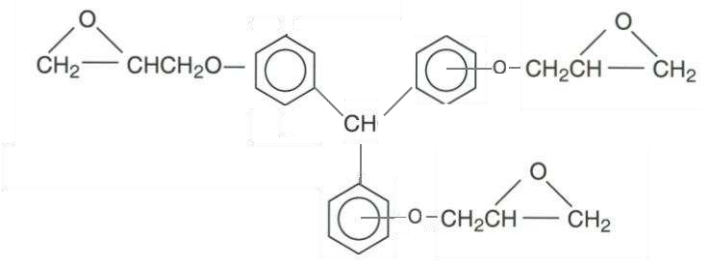

Tetrafunctional:

MY720

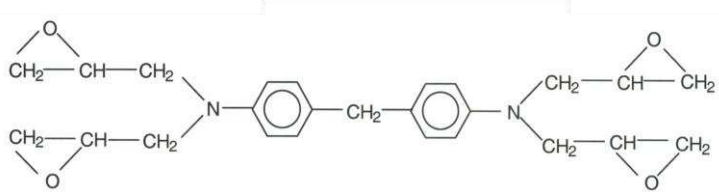

PGA-X

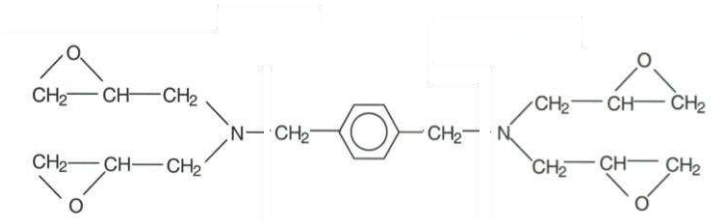

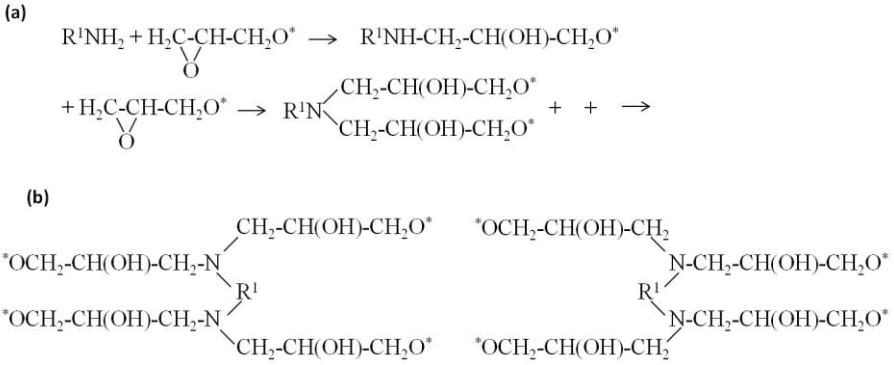

Scheme 1.1 Mechanism of cure of primary amines. $-CH_2O^*$ indicates that only the reactive epoxy group is shown.

Amino-curing agents include aliphatic and cycloaliphatic amines, aromatic amines, polyamides and dicyandiamide. [3, 4]

In addition to the two main ingredients, i.e. epoxy monomer and curing agent, numerous other materials are frequently employed in the formulation, in order to modify the properties and characteristics of epoxies, both uncured and in their cured form, depending on the final application of the matrix and, thus, of the composite material. Among them we have: diluents, fillers, toughening agents and plasticilisers/flexibilisers.

Diluents are usually used as a means of reducing viscosity of the resin, in order to aid the processability as well as to facilitate the incorporation of other solid components, such as fillers. They are divided in two broad classes: reactive and non-reactive diluents. As the name indicates, reactive diluents are materials capable of chemical reaction with the epoxy resin components.

Apart from the resin and the hardener, fillers are the most common ingredients added to the epoxy formulations. The function of the filler can be: to improve toughness, to reduce water absorption, to decrease the exotherm of the cure reaction, to reduce the formulation costs. Some of the commonly used fillers are alumina, silica, mica and kaolin. [3]

Toughening agents are additives added to the formulation to the aim to improve the fracture toughness of the matrix. Today, rubbers and thermoplastic polymers are

widely used as toughening agents in epoxy matrices. More details on these components will be provided in paragraph 1.5.1.

The inherently hard and brittle characteristic of epoxies can be also alleviated by means of the use of plasticisers/flexibilisers. Plasticisers act in a non-reactive manner, while the term "flexibilisers" indicates materials that react with the epoxy system during cure. Several groups of plasticisers/flexibilizers are used in epoxy resins to modify their mechanical properties. These include:

- Monofunctional epoxy compounds (e.g., epoxidized oils) which influence molecular weight of the cured resin.
- Low molecular weight polyamide resins. These are curing agents that, when added at certain proportions to other hardeners in the system, may help to modify properties.
- Mercaptan terminated materials (for example polysulfides).

1.3 Fiber reinforcement

The role of the reinforcement in a composite material is to provide strength and stiffness the final material. More in detail, the main functions of the fiber reinforcement in a composite are [1]:

- To carry the load (in a structural composite, 70 to 90% of the load is carried by fibers).
- To provide stiffness, strength, and other structural properties in the composites.
- To provide electrical conductivity, depending on the type of fiber used.

A first classification of the fiber reinforcement can be made based on the material of the fibers: nowadays, the most common reinforcements are glass, carbon, aramid and boron fibers.

In this work, the author focused the attention on carbon fibers. Carbon fibre is produced by processes of oxidation, carbonization and graphitisation of carbon-rich organic precursors, which are already in fibre form. The most common precursor is polyacrylonitrile (PAN), but fibres can also be produced from pitch or cellulose.

Once formed, surface treatments and chemical sizing are carried out in order to improve matrix bonding and to protect the fiber during handling.

Carbon fibres are usually grouped according to the modulus band in which their properties fall. These bands are commonly referred to as: high strength(HS), intermediate modulus (IM), high modulus (HM) and ultra high modulus (UHM).

For a big number of applications, the fibres are arranged in the form of sheet, known as fabrics, to make their handling possible. In particular, in the composite materials field, a fabric is defined as a manufactured assembly of long fibres to produce a flat sheet of one or more layers of them. These layers are held together either by mechanical interlocking of the fibres themselves or with a secondary material (stitching lines). Fabric types are classified by the orientation of the fibres used, and by the various construction methods used to hold the fibres together. Focus the attention on the fibre orientation the main categories are: unidirectional, 0/90°, multiaxial, and other/random.

In a unidirectional (UD) fabric the majority of fibres runs only in one direction. A small amount of fibre or other material may run in other directions, the aim being to hold the primary fibres in position.

For applications where more than one orientation of fiber is required, a fabric combining orientations at 0° and 90° is useful. In this case the most used method to keep the fibres together is the weaving, and the two more commonly found weave styles are *plain* and *twill*. In a plain fabric, each warp yarn passes alternately under and over each weft yarn, the fabric being symmetrical, with reasonable porosity. In twill style, one or more warp yarns alternately weave over and under two or more weft yarns in a regular repeated manner. With reduced crimp, the fabric as a smoother surface and slightly higher mechanical properties. [5]

In recent years, multiaxial fabrics have begun to find favor in the field of composite materials. These fabrics consist of one or more layers of long fibres held in place by a secondary non-structural stitching tread. The stitching process allows a variety of fibre orientations to be combined into one fabric.

1.4 Damage and failure mechanisms in composite laminates

The term "failure" for a structure indicates a condition in which the system does not work satisfactorily. The criteria to decide the satisfactory functioning is in general quantitative and refers to some specific properties of the structure. The term "damage" refers, instead, to a local failure of the material. Thus, a damage in a material does not necessarily mean the final failure.

The complex structure of composite laminates, due to the presence of more components and their anisotropic layered structure, leads to the development of different modes of damage, and thus to different failure modalities.

Rigorously, the damage mechanisms of fiber reinforced composites are classified in intralaminar damage, i.e. damage inside the ply, and interlaminar damage, i.e. damage established at the interface between two consecutive plies, specifically delamination. [6, 7]

Examples of intralaminar damages are matrix cracking and fibers fracture/breakage. Matrix cracking damage occurs when the stress overcomes the strength of the matrix. The matrix is the weakest component, usually highly brittle, thus the first one to fail.

Delamination is one of the most critical damages in composite materials, and consists in the process of separation between adjacent layers of the laminate. This phenomenon arises because the fiber reinforcement, placed in the plane of the laminate, does not provide reinforcement through the thickness of the laminate, and thus the assignment to carry loads in this direction is given to the matrix. [8] Delamination can occur due to several causes. Among these [7]:

- Loads generating out-of-plane stresses.
- Manufacturing defects.
- Aging, due to temperature, humidity, contact with chemicals, etc.

Figure 1.1 shows a schematic representation of delamination damage in a fiber reinforced laminate.

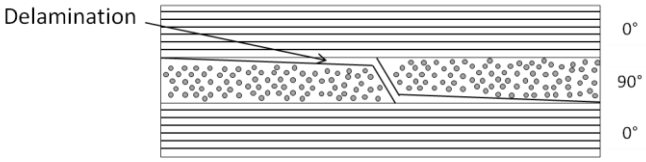

Figure 1.1 Schematic representation of the section of a delamination damaged composite laminate.

1.5 Toughening strategies: a review

The interlaminar fracture toughness, measured in terms of the critical strain energy release rate, is defined as the amount of strain energy released in propagating delamination by a unit length. This parameter is frequently used for comparing the resistance of various resin systems against the growth of delamination failure.

Delamination may occur in Mode I (opening mode or tensile mode of crack propagation), Mode II (sliding mode or in-plane shear mode of crack propagation), Mode III (tearing mode or antiplane shear mode of crack propagation), or a combination of these modes. Mode I and Mode II are the most common ones. In Mode I, crack propagation occurs as the crack surfaces pull apart due to a normal stress perpendicular to the crack plane. In Mode II, crack propagation occurs as the crack surfaces slide over each other due to a shear stress parallel to the crack plane. [2, 9, 10]

Over the years, several strategies have been devised to increase the interlaminar fracture toughness, and thus to improve the delamination resistance. Among them, the two most important are to increase directly the fracture toughness of the matrix resin, by blending with thermoplastic polymers or elastomers, or to introduce a thin layer of a tough material between adjacent fabric plies, as an interlayer. In the next paragraphs the state of the art of these two main approaches is briefly presented.

1.5.1 Use of toughened matrices

Thermoplastic-toughened epoxy matrices

The inclusion of thermoplastic into epoxy formulations have for long time been in the focus of academic and industrial research. Polysulphone (PSF), Polyethersulphone (PES) and Polyetherimide (PEI) are the most commonly used polymers for this purpose.

It is well known that most thermoplastic/epoxy blends show either lower critical solution temperature, and they are called (LCST)-type, or upper critical solution temperature, and they are named (UCST)-type. [11-15] In a LCST-type system, for example, a temperature jump from T_1 to T_2 thrusts the solution, i.e. the initially homogeneous system of composition φ, to enter into the two-phase region. Thus, the phase separation process begins, to obtain two phases of equilibrium composition φ' and φ'' (see Fig. 1.2). [11]

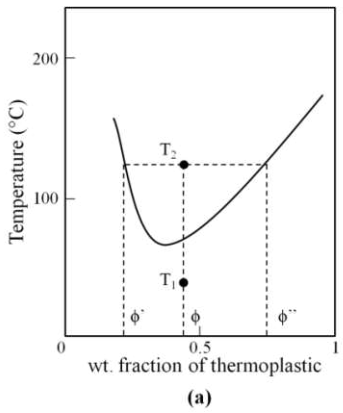

Figure 1.2 Schematic representation of LCST-type phase diagram.

Phase separation can take place via two different modes, called "spinodal decomposition" (SD) and "nucleation and growth" (NG). [11, 16, 17] The SD process involves different stages, as showed in Fig. 1.3. In the first stages a co-continuous-type structure is noted (panel (a) and (b) of Fig. 1.3), with two characteristic features: (i) a periodicity exists in all directions and (ii) both phases

are continuous. Then, co-continuity is lost to yield fragmented particles (panel (c)), thus spherical particles (panel (d)). Here, particle sizes are uniform and they are dispersed quite regularly. [11, 18, 19]

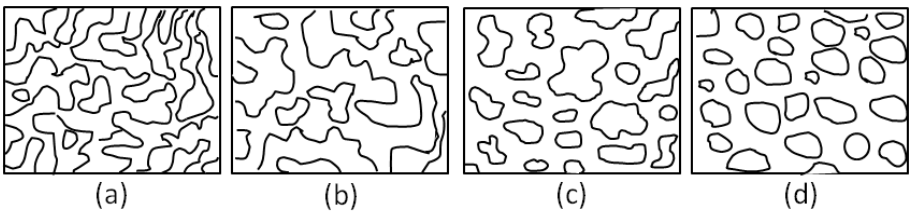

Figure 1.3 Structure change with time during spinodal decomposition.

Spinodal decomposition (SD) occurs in the unstable region, above the spinodal curve of the phase diagram (see Fig 1.4). [14, 16, 17] In the meta-stable region, between the spinodal and the binodal curves (Fig. 1.4), phase separation proceeds by another mechanism called nucleation and growth (NG). In this second case, isolated particles with an equilibrium composition initially appear and then grow up to yield an irregular two-phase structure. As discussed above, these phase separation processes are thermally-induced. [11]

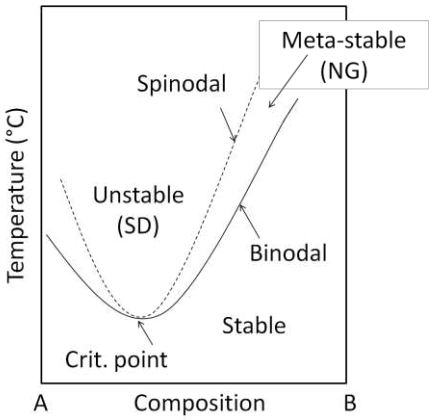

Figure 1.4 Spinodal and bimodal curves in a phase diagram.

In these systems the phase separation process can also occur via reaction-induced phase separation. That is, the access into the two-phase region is due to the

LCST depression caused by the increase in molecular weight of the epoxy, during the curing process (see Fig. 1.5). [14] The morphologies obtained as consequence of the phase separation depend on the concentration of thermoplastic with respect to the critical composition. Low concentrations provide spherical domains of thermoplastic in a thermosetting matrix; higher concentrations lead to phase-inverted structure consisting of a dispersion of spherical domains of resin in a thermoplastic matrix. [14, 20] Sometimes the domains can be interconnected. [21]

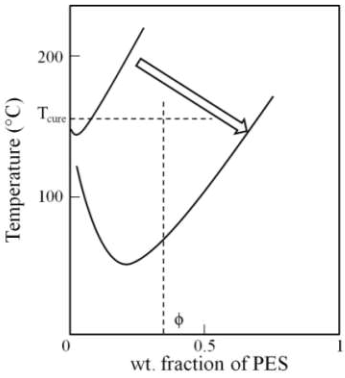

Figure 1.5 Schematic representation of variation in the epoxy monomer/PES mixture phase diagram with curing.

It is universally recognized the toughening effect of thermoplastic polymers, in particular PSF, PES and PEI, in epoxy resin. The amplitude of the increase of the fracture toughness depends on several, often interrelated, parameters. In particular, [22]:

- Properties of the monomer (number of functional groups, molecular weight, epoxy equivalent weight).
- Type of curing agent.
- Properties of the thermoplastic polymer (mainly, molecular weight).
- Concentration of the thermoplastic.
- Curing conditions.
- Thermoplastic/resin system morphology.

The increase of toughness in these systems, after the introduction of the thermoplastic, is due to the two-phase structure, where the thermoplastic particles or domains act as sites of fracture energy absorption. [3]

As already discussed, PSF, PES and PEI are the three thermoplastics most commonly used as toughening agents of epoxy resins, all obtaining varying levels of success. However, few studies compared their respective toughening abilities. [22]

Apart from PSF, PES and PEI, other thermoplastic toughening agents have been used, including poly-(butylene terephthalate) (PBT), Nylon 6 and poly(vinylidene fluoride) (PVDF). [22, 23]

Another important aspect to take into account is the adhesion between the thermoplastic particles and the matrix. To this purpose, two approaches have been developed: one is the reaction of the epoxy resin with the thermoplastic using a catalyst; the other one is to synthesize thermoplastic polymers with reactive end-groups (-NH_2 or –OH, for example). The literature is ambivalent on the effect of this modification on the toughness of the resin. [18, 22, 24]

In addition, strength points are their high thermal and mechanical properties. Because of their high modulus and Tg, the thermoplastic-modified resins do not show significant decrease in the mechanical and thermal properties [3].

Rubber-toughened epoxy resins

One of the most successful methods to increase the toughness of epoxy resins involves the addition of rubbers. Rubbers can be solid or liquid, the latter being mainly of the "reactive-type". The type of rubber used to toughen the resin is determined by a compatibility requirement, that is the rubber must initially dissolve in the resin, but precipitate during the curing process. As already described for the thermoplastic modification, rubber-modified cured resins are two-phase systems, in which spherical rubber domains are dispersed in the matrix. [3, 17, 25] The size and the volume fraction of the rubber particles depend on the rubber content and on the curing process, in particular the curing rate. Rubber domains dispersed in epoxy matrix are obtained for low concentrations of rubber (generally less than 20%). For higher concentrations, rubber blends with the resin or epoxy particles in a rubber

matrix are obtained. Regarding the curing process, slow-cure resin systems generally produces morphologies with large rubber particles between 1 and 10 µm in diameter. Indeed, the primary rubber particles formed have the time to coalesce before the resin network forms, thus preventing further coarsening. Rapid-cure systems tend to form smaller rubber particles dispersed in the matrix. [3, 26]

The most studied and employed rubbers as toughening agents for epoxy resins are the butadiene-acrylonitrile rubbers. As the name suggests, they are composed of a backbone consisting of butadiene and acrylonitrile repeating units, and reactive groups are placed in the terminal positions of the macromolecule. [3]

A number of reactive terminal functionalities have been studied, including hydroxyl, phenol, amine and carboxyl, the best results being obtained with carboxyl terminated butadiene-acrylonitrile (CTBN) rubber. [27]

A significant number of works shows that the fracture toughness of epoxy resins can significantly increase when a rubbery phase is added to the matrix. In comparison to thermoplastic-modification the level of improvements is generally more significant. However, the addition of rubbers causes reduction in other important properties of the resin; for example, stiffness and glass transition temperature of the material. [3]

Several mechanisms have been proposed to explain the enhancements in the toughness generated by the incorporation of rubber in an epoxy matrix. Among these, the "rubber tear" theory and the "shear yielding and crazing" mechanism. The first one suggests that when a crack advances around a rubber particle, the particle is stretched between the crack surfaces, behind the crack tip, and eventually it has to tear before the crack can extend further. Thus, the energy required to stretch and tear the rubber particles is responsible for the higher fracture toughness of the rubber-modified matrix. Regarding the second mechanism, some studies indicate a correlation between fracture toughness and the extent of plastic deformation on fracture surface. In addition, experimental evidence of crazing processes suggested that a mechanism based on yielding and plastic shear flow is the main source of dissipation of energy during the fracture. [26, 28-30]

With the aim of minimizing the detrimental effects of the rubbers on other desired properties of the resins, more recently some authors have suggested the use of high molecular weight solid rubbers, as alternative to reactive liquid butadiene-acrylonitrile rubbers. [31]

As a final remark of this brief review on epoxy resin toughening strategies, it should be emphasized that, albeit the fracture toughness of an epoxy resin matrix is significantly improved when a thermoplastic polymer or a rubber is added to the formulation, the increase in interlaminar fracture toughness for the composite is not generally of the same amplitude as for the bulk resin. For example, a 25-fold increase of the fracture energy of the unreinforced resin will be translated in a four-to-eight fold increase of the interlaminar fracture energy of a woven composite, only. The poor translation of resin toughness in interlaminar fracture toughness when the resin is used as matrix in composites is entrusted to be due to fiber constraints suppressing plastic deformation of the toughened resin at the crack front. [32-35]

1.5.2 Interlayer toughening of composite laminates

An alternative interesting approach to enhance the interlaminar fracture toughness is the introduction of a very thin layer of a ductile material between consecutive fiber/matrix plies, as interlayer. The interlayer could be a dense film, a porous membrane or an adhesive. Basically, the interlayer should act as a medium of crack deflection/suppression, more energy being required for the crack growth to continue. [32]

Regarding dense films, both thermoset and thermoplastic polymers has been used as interleaves. Both types of polymers increased the interlaminar fracture toughness of the laminate, but thermoplastic interleaves were found to be more effective, in consequence of their larger capability of absorbing energy. Generally, thermoset interlayers exhibited type-cohesive failures, microcracking and plastic

deformation; thermoplastic interlayers showed type-adhesive failures and a limited degree of microcracking. [36]

The main drawback of type-film interleaves is that they can act as barrier to the resin flow during the manufacturing process of the laminate. In addition, prepreg material that incorporates film could be stiff and tack-free, thus difficult to use.

Recently, the use of electrospun nanofibrous polymeric mats in epoxy laminates has been taken into account. Although electrospun nanofibrous polymeric mats look like dense films, they are actually highly porous membranes. Being made by highly resilient thermoplastic materials and being characterized by a high surface to volume ratio, high porosity and lightweight, they have a lot of potential to be used as toughening interlayers.

The idea has been proposed for the first time, in 1999, by Dzenis and Reneker in their patent. [37] The invention regards composite laminates containing a secondary reinforcement made of nanofibrous mats of polybenzimidazole (PBI), placed at each ply interface. The membranes were produced by electrospinning. The introduction of the PBI mats increased thickness and weight of the laminate of 12% and 2.5%, respectively. The Mode I and Mode II delamination tests showed increases in the critical energy release rate by 15% and 130% in Mode I and Mode II, respectively.

Following the idea of Dzenis and Reneker, other authors tried to study the effect of electrospun nanofibrous membranes in composite laminates. [38-53] In particular, a number of papers involves the use of electrospun mats which *dissolve* in the matrix during the thermal curing process of the laminate. In this case, the materials used to produce the nanofibrous mats are polysulphone (PSF), [39, 40], polyetherketone-cardo (PEK-C), [41] and poly(hydroxyether of bisphenol A). [42] For all these materials, improvements in mode I and mode II interlaminar fracture toughness of laminates were observed when they were added as interlayer, due to the phase separation of a particulate phase formed by the dissolved nanofibers and homogenously dispersed in the thermoset resin. For the PSF, glass transition temperature (Tg) and flexural properties of nanofibrous membranes toughened composites exhibited no significative reduction; [40] for PEK-C and

poly(hydroxyether of bisphenol A) modifications of the dynamic-mechanical-thermal behavior were observed, due to the presence of a PEK-C-rich and phenoxy-rich phase, respectively, while no information was available on the effect of mats on mechanical properties of the laminates.

Another approach regards the use of nanofibrous mats that maintain their nanofibrous structure in the laminate, also after the curing process, such as carbon membranes, [43, 44] and Nylon 6,6. [45-51]

Regarding electrospun carbon nano-fiber mats, they are prepared by thermal treatments (stabilization and carbonization) of polyacrilonitrile (PAN) electrospun mats. Important increases of the interlaminar shear strength (up to about 220%) were described, but no information was provided on the effect on mode I delamination properties and Tg.

Nylon 6,6 is probably the most studied nanofibre-based interlayer system. [45-51] Many authors report the increase in the delamination properties of electrospun Nylon 6,6 mats interleaved laminates with respect to a non-interleaved reference laminate, the amplitude of the increase being very different from case to case depending on several factors, such as matrix resin composition and inherent properties as well as the laminates features (resin content, production process, etc).

On this topic the research is still limited. No information is available on the effect of nanofibrous mats on the curing behavior of the epoxy matrices and on the aging behavior of the nanofibre-modified materials. Few studies investigate the effect of the presence of the membranes on the Tg and tensile or flexural mechanical properties of the laminate. The toughening mechanism activated by nanofibrous mat is not fully clarified, and probably not fully exploited.

1.6 Hydrothermal aging in composite materials

In general, in material engineering, the term “aging” is used to describe the process of alteration of the chemical or physical structure of a material, cause of loss in the its properties, sometimes until ultimate failure. Below a list of aging agents, that can act individually or collectively, such as [2]:

- High temperature exposure due to exothermal heat of reactions, low temperature exposure and thermal cycling.
- Humidity exposure.
- Brine exposure.
- Complete immersion in water at room or elevated temperature.
- Chemicals (e.g. solvents, oxygen, acids).
- Combined load and environmental exposures.
- Ultraviolet and high-energy radiations.

To evaluate the long-term effects of the aging, "accelerated" aging is usually implemented by increasing the temperature of the conditioning environment.

Focusing the attention on composite materials for advanced structural applications, in aeronautical and race automotive industry, temperature cycling and exposure to water are the most common and critical environmental conditions at which the material can be exposed, during its service life. Thus, the study of the hydrothermal aging processes of these materials and its effects on the properties is of paramount importance. [3,54]

Regarding the matrix, it is well known that the water absorption in epoxy resins follows a Fickian diffusion behavior. The diffusion kinetics is generally investigated by means of gravimetric analysis. Also, it has been observed that insufficient curing degree, presence of nano-fillers or separate phases can affect the water absorption, both in terms of diffusivity and of water absorbed at saturation. [55, 56]

The mathematical form of the second Fick's law, for large plane sheet sample and under suitable assumptions [57], for water absorption in epoxy resins is the following one:

$$\frac{M_t}{M_\infty} = \frac{4}{\sqrt{\pi}} \frac{\sqrt{Dt}}{h} \tag{1.1}$$

where M_t is the water content at the generic time t, M_∞ is the maximum water gain (at saturation), h is the thickness and D is the diffusivity. [55-58]

In some cases, typically for short-term absorption curves, a non-Fickian behavior has been observed, and several models have been proposed. Between these ones, one of most commonly used in literature is a two-stage diffusion model. As the

name indicates, the model considers two stages: the first one controlled by a gradient of concentration, according to Fick's law, the second one associated with structural relaxation of the polymeric chains, due to water uptake. The model is expressed by the following equation:

$$M_t = M_{\infty 0}(1 + k\sqrt{t})\left\{1 - exp\left[-7.3\left(\frac{Dt}{h^2}\right)^{0.75}\right]\right\} \quad (1.2)$$

where M_t is the water uptake at the time t, $M_{\infty 0}$ is the quasi-equilibrium uptake of the diffusion-dominated first stage, k a constant related to the rate of relaxation of the polymeric structure in the second stage, D the apparent diffusion coefficient and h the thickness of the sample. [59-62]

The absorbed water is in part filling the free volume of the epoxy network (free water) and in part chemically bonded (bonded water). By means of water desorption measurements, desorption activation energy analysis and NMR studies some authors classified the bonded water in two types, called Type I and Type II. The Type I involves water molecules forming single hydrogen bonds with the epoxy network; the Type II water molecules forming multiple hydrogen bonds with the network, bridges between structural segments resulting in secondary crosslinking. [58]

The amount of absorbed free or bonded water and the relative effects on the properties of the epoxy matrix is much more difficult to establish and actually not fully understood.

The plasticization of the material is the most commonly accepted phenomena due to the presence of absorbed water in epoxy resins. Variations in structural properties of material, such as Tg, Young's modulus and fracture toughness, are partially attributable to this phenomenon. [54, 63]

The water penetration process in composite materials is much more complex with respect the unreinforced matrix. Three different possible pathways of the water in the material are consider: diffusion through the matrix; capillary flow along the imperfect fiber-resin interface; and flow in micro-cracks or void present in the matrix as consequence of a poor consolidation process. [64, 65] The difference between the water diffusion coefficient in the unreinforced epoxy resin and that one

of the composite material with the same epoxy resin as matrix is attributed at the last two mechanisms. [66]

The absorbed water in composite materials has detrimental effects on their thermal and mechanical properties, being not only consequence of the interactions of the water with the neat matrix. The water may also attack the fiber-matrix interface. Studies regarding the effect of hydrothermal aging on the delamination properties of composite laminates highlighted this aspect. [67]

REFERENCES

[1] Mazumdar SK (2002). Composite Manufacturing – Materials, Product, and Process Engineering. CRC PRESS.

[2] Mallick PK (2007). Fiber-reinforced Composites – Materials, Manufacturing and Design. Taylor & Francis Group.

[3] Ellis B (1993). Chemistry and Technology of Epoxy Resins. Blackie academic & Professional.

[4] Jin FL, Li X, Park SJ. Synthesis and application of epoxy resins: A review. J Ind Eng Chem 2015;29:1-11.

[5] Long AC (2005). Design and manufacture of textile composites. CRC PRESS.

[6] Ziandoon AH, Chwei Z. Effect the stacking sequences of composite laminates under low velocity impact on failure modes by using carbon fiber reinforced polymer. Int J Eng Sci 2016;5(2):53-62.

[7] Jollivet T, Peyraac C, Lefebvre F. Damage of composite materials. Procedia Eng 2013;66:746-758.

[8] Wisnom MR. The role of delamination in failure of fibre-reinforced composites. Phil Trans R So A 2012;370:1850-1870.

[9] Launey ME, Ritchie RO. On the fracture toughness of advanced materials. Adv Mater 2009;21:2103-2110.

[10] Broek D (1984). Elementary engineering fracture mechanics. Martinus Nijhoff Publishers.

[11] Inoue T. Reaction-induced phase decomposition in polymer blends. Progress in Polym Sci 1995;20:119-153.

[12] Bucknall CB, Gomez CM, Quintard GI. Phase separation from solutions of poly(ether sulfone) in epoxy resins. Polymer 1994;35(2):353-359.

[13] Modragon I, Quintard I, Bucknall CB. Effects of cure schedule and stoichiometry on the dynamic mechanical behaviour of epoxy resin modified with polyethersulfone. Plast Rubber Compos Process Appl 1995;23:331-338.

[14] Yoon T, Kim BS, Lee DS. Structure Development via Reaction-Induced Phase Separation in Tetrafunctional epoxy/Polysulfone Blends. J Appl Polym Sci 1997;66:2233-2242.

[15] Kim BS, Chiba T, Innoue T. Phase separation and apparent phase dissolution during cure process of thermoset/thermoplastic blend. Polymer 1995;36(1):67-71.

[16] Teng KC, Chang FC. Single-phase and multiple-phase thermoplastic/thermoset polyblends: 2. Morphologies and mechanical properties of phenoxy/epoxy blends. Polymer 1996;37(2):2385-2394.

[17] Tohmas S, Sinturel C, Thomas R (2014). Micro and Nanostructured Epoxy / Rubber Blends. Wiley.

[18] Kim BS, Chiba T, Innoue T. Morphology development via reaction-induced phase separation in epoxy/poly(ether sulfone) blends: morphology control using poly(ether sulfone) with functional end-groups. Polymer 1995;36(1):43-47.

[19] Cho JB, Hwang JW, Cho K, An H, Park CE. Effects of morphology on toughening of tetrafunctional epoxy resins with poly(ether imide). Polymer 1993;34(23):4832-4836.

[20] Oyanguren PA, Aizpurua B, Galante MJ, Riccardi CC, Corta' Zar OD, Mondragon I. Design of the Ultimate Behavior of Tetrafunctional Epoxies Modified with Polysulfone by Controlling Microstructure Development. J Polym Sci B Polym Phys 1999;37:2711-2725.

[21] Oyanguren PA, Galante MJ, Andromaque K, Frontini PM, Williams RJJ. Development of bicontinuous morphologies in polysulfone–epoxy blends. Polymer 1999;40:5249–5255.

[22] Hodgkin JH, Simon GP, Varley RJ. Thermoplastic Toughening of Epoxy Resins: a Critical Review. Polym Adv Technol 1998;9(1):3-10.

[23] Kim J, Robertson R. Toughening of brittle thermosets by crystalline polymer inclusions. Polym Mat Sci Eng 1990; 63:301-305.

[24] Jin F, Park S. Improvement in fracture behaviors of epoxy resins toughened with sulfonated poly(ether sulfone). Polym Degrad Stab 2007;92:509-514.

[25] Yamanaka K, Takagi Y, Inoue T. Reaction-induced phase separation in rubber-modified epoxy resins. Polymer 1989;60:1839-1844.

[26] Garg AC, Mary YW. Failure Mechanisms in Toughened Epoxy Resins A Review. Compos Sci Technol 1988;31:179:223.

[27] Manzone LT Gillham JK. Rubber-Modified Epoxies. I. Transitions and Morphology. J Appl Polym Sci 1981;26:889-905.

[28] Collyer AA (1994). Rubber Toughened Engineering Plastics. Springer Science & Business Media.

[29] Bucknall C (2013). Toughened Plastics. Springer.

[30] Kinloch AJ, Shaw SJ, Tod DA, Hunston DL. Deformation and fracture behaviour of a rubber toughened epoxy: 1. Microstructure and fracture studies. Polymer 1983;24:1341-1354.

[31] Dispenza C, Spadaro G. Cure kinetics of a tetrefunctional rubber modified epoxy-amine system. J Therm Anal Cal 2000;61:579-587.

[32] Sela N, Ishai O. Interlaminar fracture toughness and toughening of laminated composite materials: a review. Composites 1989;20(5):423-435.

[33] Gill AF, Robinson P, Pinho S. Effect of variation in fibre volume fraction on modes I and II delamination behavior of 5HS woven composites manufactured by RTM. Compos Sci Technol 2009; 69:2368-2375.

[34] Scott M, Phillips DC. Carbon fibre composites with rubber toughened matrices. J Mater Sci 1975;10(4):551-562.

[35] Bascom WD, Bitner JL, Moulton RJ, Siebert AR. The interlaminar fracture of organic-matrix, woven reinforcement composites. Composites 1980;11(1):9-18.

[36] Tsotsis T. Interlayer Toughening of Composite Materials. Polym Compos 2009; 30:70-86.

[37] Dzenis YA, Reneker DH. Delamination resistant composites prepared by small diameter fiber reinforcement at ply interfaces. US Patent 626533; 2001.

[38] Zucchelli A, Focarete ML, Gualandi C, Ramakrishna S. Electrospun nanofibers for enhancing structural performance of composite materials. Polym Adv Technol 2011;22(3):339-49.

[39] Li G, Li P, Yu Y, Jia X, Zhang S, Yang X, et al. Novel carbon fiber/epoxy composite toughened by electrospun polysulfone nanofibers. Mater Lett 2008;62(3):511-4.

[40] Li G, Li P, Zhang C, Yu Y, Liu H, Zhang S, et al. Inhomogeneous toughening of carbon fiber/epoxy composite using electrospun polysulfone nanofibrous membranes by in situ phase separation. Compos Sci Technol 2008;68(3-4):987-94.

[41] Zhang J, Lin T, Wang X. Electrospun nanofibre toughened carbon/epoxy composites: Effects of polyetherketone cardo (PEK-C) nanofibre diameter and interlayer thickness. Compos Sci Technol 2010;70:1660-1666.

[42] Magniez K, Chaffraix T, Fox B. Toughening of a Carbon-Fibre Composite Using Electrospun Poly(Hydroxyether of Bisphenol A) Nanofibrous Membranes Through Inverse Phase Separation and Inter-Domain Etherification. Materials 2011;4:1967-1984.

[43] Chen Q, Zhang L, Rahman A, Zhou Z, Wu XF, Fong H. Hybrid multi-scale epoxy composite made of conventional carbon fiber fabrics with interlaminar regions containing electrospun carbon nanofiber mats. Compos Part A: Appl Sci Manuf 2011;42:2036-2042.

[44] Chen Q, Zhao Y, Zhou Z, Rahman A, Wu X, Wu W, et al. Fabrication and mechanical properties of hybrid multi-scale epoxy composites reinforced with conventional carbon fiber fabrics surface-attached with electrospun carbon nanofiber mats. Compos Part B: Eng 2013;44(1):1-7.

[45] Palazzetti R, Zucchelli A, Gualandi C, Focarete ML, Donati L, Minak G, et al. Influence of electrospun Nylon 6,6 nanofibrous mats on the interlaminar properties of gr-epoxy composite laminates. Compos Struct 2012;94(2):571-579.

[46] Hamer S, Leibovich H, Green A, Intrater R, Avraham Ri, Zussman E, Siegmann A, Sherman D. Mode I Interlaminar Fracture Toughness of Nylon 66 Nanofibrilmat Interleaved Carbon/Epoxy Laminates. Polym Compos 2011;32:1781-1789.

[47] Akangah P, Lingaiah S, Shivakumar K. Effect of nylon-66 nano.fiber interleaving on impact damage resistance of epoxy/carbon fiber composite laminates. Compos Struct 2010;92:1432-1439.

[48] Palazzetti R, Yan X, Zucchelli A. Influence of geometrical features of electrospun nylon 6,6 interleave on the CFRP laminates mechanical properties. Polym Compos 2014;35:137-150.

[49] Daelemans L, van der Heijden S, De Baere I, Rahier H, Van Paepegem W, De Clerck K. Nanofibre bridging as a toughening mechanism in carbon/epoxy composite laminates interleaved with electrospun polyamide nanofibrous veils Compos Sci Technol 2015;117: 244-256.

[50] Palazzetti R, Trendafilova I, Zucchelli A. The self-reinforcing effect of Nylon 6,6 nanofibres on CFRP composite laminates subjiected to low velocity impact. Compos Struct 2013;106:661-671.

[51] Beckermann GW, Pickering KL. Mode I and Mode II interlaminar fracture toughness of composite laminates interleaved with electrospun nanofibre veils. Compos Part A 2015;72:11-21.

[52] Zhang J, Yang T, Lin T, Wang CH. Phase morphology of nanofibre interlayers: Critical factor for toughening carbon/epoxy composites. Compos Sci Tech 2012;72(2):256-262.

[53] Meng F, Zhan Y, Zhao R, Liu X. New strategy to reinforce and toughen composites via introducing thorns-like micro/nanofibers. Eur Polym J 2012;48:74-78.

[54] Alessi S, Conduruta D, Pitarresi G, Dispenza C, Spadaro G. Accelerated ageing due to moisture absorption of thermally cured epoxy resin/polyethersulphone blends. Thermal, mechanical and morphological behavior. Polym Degrad Stab 2011;96:642-648.

[55] Li L, Yu Y, Wu Q, Zhan G, Li S. Effect of chemical structure on the water sorption of amine-cured epoxy resin. Corros Sci 2009;51:3000-3006.

[56] Prolongo SG, Gude MR, Urena A. Water uptake of epoxy composites reinforced with carbon nanofillers. Compos Part A: Appl Sci Manuf 2012;43:2169:2175.

[57] Lin YC, Chen X. Moisture sorption–desorption–resorption characteristics and its effect on the mechanical behavior of the epoxy system. Polymer 2005;46:11994-12003.

[58] Zhou J, Lucas JP. Hygrothermal effects of epoxy resin. Part I: the nature of water in epoxy. Polymer 1999;40:5505-5512.

[59] Bao LR, Yee AF. Moisture diffusion and hygrothermal aging in bismaleimide matrix carbon fiber composites-partI: uni-weave composites. Compos Sci Technol 2002;62:2099-2110.

[60] Bao LR, Yee AF, Lee CYC. Moisture absorption and hygrothermal aging in a bismaleimide resin. Polymer 2001;42:7327-7333.

[61] Karbhari VM, Xian G. Hygrothermal effects on high VF pultruded unidirectional carbon/epoxy composites: Moisture uptake. Compos B Eng 2009;40:41-49.

[62] Lu Z, Xian G, Li H. Effects of thermal aging on the water uptake behavior of pultruded BFRP plates. Polym Degrad Stab 2014;110:216-224.

[63] Alessi S, Conduruta D, Pitarresi G, Dispenza C, Spadaro G. Accelerated ageing due to moisture absorption of thermally cured epoxy resin/polyethersulphone blends. Thermal, mechanical and morphological behaviour. Polym Degrad Stab 2011;96:642-648.

[64] Tsenoglou CJ, Pavlidou S, Papaspyrides CD. Evaluation of interfacial relaxation due to water absorption in fiber-polymer composites. Compos Sci Technol 2006;66:2855-2864.

[65] Ray BC. Temperature effect during humid ageing on interfaces of glass and carbon fibers reinforced epoxy composites. J Colloid Interf Sci 2006;298:111-117.

[66] Zafar A, Bertocco F, Schjodt-Thomsen J, Rauhe JC. Investigation of the long term effects of moisture on carbon fibre and epoxy matrix composites. Compos Sci Technol 2012;72:656-666.

[67] Alessi S, Pitarresi G, Spadaro G. Effect of hydrothermal ageing on the thermal and delamination fracture behaviour of CFRP composites. Compos B Eng 2014;67:145-153.

2. ELECTROSPINNING

2.1 Introduction

Electrospinning is a simple and versatile technology which utilizes strong electric fields to produce polymer fibers with diameters ranging from tens to hundreds of nanometers. When the diameter of polymer fiber materials decreases from micrometers (e.g. 10÷100 μm) to nanometers (e.g. $10*10^{-3}$÷$100*10^{-3}$ μm), several interesting characteristics appear, such as very large surface area to volume ratio (this ratio for a nanofiber can be large as 10^3 times of that of a microfiber), greater concentration of surface functionalities and superior mechanical performance (e.g. stiffness and tensile strength). These properties make the polymer nanofibers optimal candidates for many important applications. [1]

Electrospinning is an old process: it was first studied by Rayleigh in 1897, more in detail by Zeleny in 1914 (on electrospraying), and patented by Formhals in 1934. Then, the work of Taylor and others on electrically driven jets laid the groundwork for electrospinning. [2] However, in the recent years it regained attention, probably due to the surging interest in nanotechnology. In Fig. 2.1 the result of an analysis of the publications related with electrospinning, in the last 15 years, is shown. The data clearly demonstrate that the electrospinning is attracting increasing attention from the scientific community.

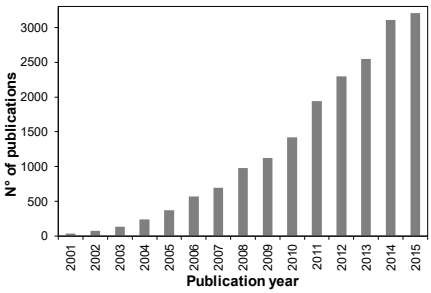

Figure 2.1 Comparison of the annual number of scientific publications regarding electrospinning. The data were obtained using Scopus search system, searching the term "electrospinning" in article title, abstract and keywords.

This chapter consists of two parts. The first part describes the process and the influence of the working parameters of the electrospinning on the characteristics of the produced membranes on the basis of the available literature. A short preliminary description of different methods to produce nanofibers is also presented.

The second part describe the preparation and morphological characterisation of electrospun hybrid rubber/thermoplastic (R/T) mats by the Author. To the best of the Author knowledge rubbers have never been electrospun before.

The choice of spinning a rubber can be easily understood, being rubbers typical toughening agents of epoxy resins. Regarding the choice of having also a thermoplastic component in the nanofibrous mat, the idea of the author was to obtain a hybrid mat, with a thermoplastic polymer which was able to maintain the nanofibrous morphology after the thermal cure of the resin, whereas the elastomer is expected to dissolve in the resin mixture and phase-separate upon cure in the form of microparticles. Since each of two components is able to activate different toughening mechanisms, the intention was to exploit their synergism. One restriction in the choice of the two components was that the rubber and polymer needed to be soluble in the same solvent, in order to produce a homogeneous solution to electrospin.

2.2 Ways to make nanofibers

Polymeric nanofibers can be produced by a number of techniques such as drawing, template synthesis, phase separation and self-assembly. [3]

- *Drawing*

Drawing is a process that can make very long single nanofibers one by one. In Fig. 2.2 a schematic representation of the main steps of the drawing process is shown. On a substrate material a drop of a polymer solution is deposited (Fig. 2.2a). A micropipette with a diameter of few micrometers is dipped into the droplet, until it reaches the edge of it (Fig. 2.2 b). Then, the polymer fiber is pulled out by means of back motion of the pipette (Fig. 2.2c), the cross section of the fiber depending on

material composition, drawing velocity and speed evaporation of solvent. Only a viscoelastic material, that can undergo strong deformations, can be made in nanofibers through the drawing process. [3,4]

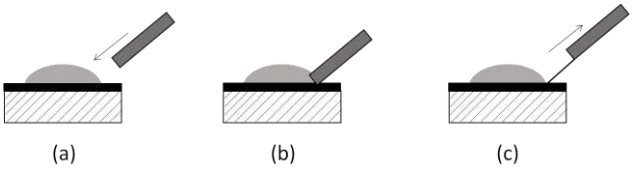

Figure 2.2 Schematic representation of drawing process.

- *Template synthesis*

As the name suggests, the template synthesis implies the use of a template or mold to obtain the desired structure. For example, for the production of polymer nanofibers a metal oxide membrane with pores of nano-scale diameter has been used. [3] Probably, the most important feature of this method lies in the fact that nanofibers of various materials, such as polymers, metals, semiconductors and carbon, can be produced. On the other hand, the process cannot manufacture continuous fibers.

-Phase separation process

In the phase separation processes, first a solvent is added to the polymer. As the name indicates, the main mechanism of the process is the separation of two phases, due to physical incompatibility. Then, the solvent extracted. This method needs a long period of time to obtain the nano-structure.

- *Self-assembly*

The self-assembly is a process in which pre-existing components organize themselves, forming structures as consequence of specific, local interactions, without external directions. Likewise phase separation, self-assembly is a time-consuming process.

2.3 Electrospinning process

A schematic illustration of the typical electrospinning apparatus in vertical set-up is shown in Fig. 2.3. There are basically three major components: a high voltage power supply able to deliver tens of kV, a spinneret (e.g. a pipette or a needle of small diameter) and a collector (usually a metal screen, a plate or a rotating mandrel).

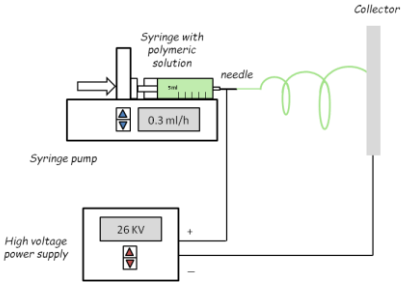

Figure 2.3 Electrospinning apparatus.

A polymer fluid, that is a polymer solution or melt, held by its surface tension on the tip of the spinneret, is subjected to an electric field and an electric charge is induced on the liquid surface. When the electric field reaches a critical value, electric forces overcome the surface tension forces, and thus a jet of the polymer fluid is ejected from the spinneret. First, the jet flows from the droplet in an almost straight line, then it bends in a complex path, during which the solvent evaporates or the melt solidifies. The nanofibers are left on the collector as non woven nanofibrous mat. [1] More in detail, in the elctrospinning process the fibers formation occurs through different steps, each one controlled by different physical phenomena. These include [5]:

- Droplet formation at the tip of the spinneret, onset of jetting.
- Development of a rectilinear jet.
- Onset of bending deformations, with looping, spiralling trajectories.
- Deposition on a collector.

The first step consists in the formation of fluid droplets at the tip of the spinneret, when the solution is pumped though the die. In absense of electric field the drop assumes an equilibrium shape, controlled by gravity and surface energy. If more spinning polymer solution is fed, droplet after droplet is formed, each of which will detach from the spinneret, falling down. A further increase of the feed flow rate may lead to the formation of a fluid jet. When an electric field is applied, the stability of the droplet/jet is perturbed. The droplet attached to the tip of the spinneret becomes electrically charged due to the applied electric field and its shape changes, as a consequence of the interaction of the charged fluid with the external electric field. The schematic rapresentation of the evolution of the shape of a fluid drop, when a increasing electric potential is applied, is shown in Figure 2.4. In particular, for the lower electrical poltential values, the droplet assumes a prolate shape (Fig 2.4 a and b); then, close to a "critical potential", the shape changes in conical, with a characteristic half-angle of the order of 30° and above (Fig. 2.4 c). The cone (called "Taylor cone") seems to be characterized by a tip with a low radius of curvature below 1 µm (Fig. 2.4 d-f). [5,6]

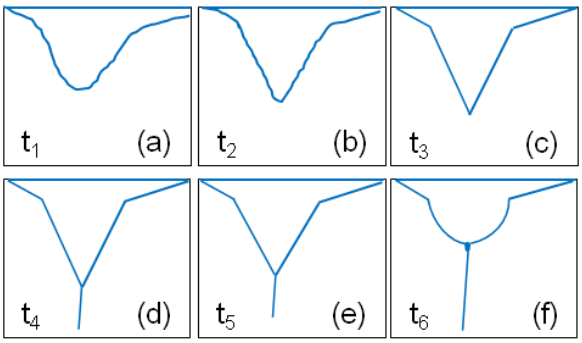

Figure 2.4 Schematic representation of the evolution of the shape of a drop at increasing electrical potential values, during electrospinning.

In the rectilinear path of the jet, after the "Taylor cone", the diameter of the jet typically decreases by a factor of about 4, corresponding to the reduction of the cross-section by a factor of about 20. A significant part of this decrease comes from

the evaporation of the solvent, and a further contribution from longitudinally deformations of the jet induced by electric force.

By means of a particle-tracking technique it has been possible to evaluate acceleration and velocity of fluid jets, during electrospinning process. The first one can reach values up to 600 m/s^2, two orders of magnitude larger than the acceleration coming from gravitational forces. Thus, gravitational force plays no significant role in electrospinning. The velocity is only few cm/s very close to the beginning of the emerging jet, but increases up to several m/s at a jet length of about 1 cm and above. [5]

According to the experimental observations, it is noted that after some distance away from the tip of the spinneret the jet is not longer able to follow a straight path, but it bends and begins to perform spiralling, looping motions (see Fig 2.5). In each loop the jet becomes thinner and elongated as the loop diameters increase. After several turns, a smaller coil on a turn of the larger coil is formed, thus the turns of the smaller coil transforms into an even smaller coil (Fig. 2.5). The envelope of these loops resembles a cone with its opening oriented towards the collector. [5-8]

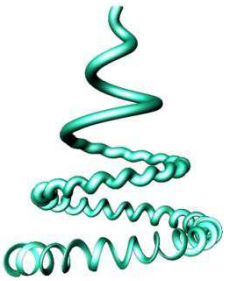

Figure 2.5 Schematic drawing of the looping part of the jet.

The deposition of the nanofiber on the collector or a substrate placed on the top of the collector is the final step of electrospinning process. The radius of the enveloped cone, that is usually of the order of 10-15 cm for a distace between the tip of the spinneret and the collector of 10-15 cm, controls the radius of the nonvowen mat that will deposit in the collector: they are of similar amplitude.

2.4 Effect of various parameters on electrospinning process

The electrospinning is governed by many parameters that can be classified into three groups:

- Solution parameters.
- Process parameters.
- Ambient parameters.

Solution parameters include polymer molecular weight, concentration, viscosity, surface tension and conductivity of the solution; process parameters are voltage, feed rate, diameter of the pipette orifice/needle, type of collector, tip of spinneret to collector distance; ambient parameters are temperature and humidity degree. [2] Each of these parameters can affect the fibers morphology and by a proper manipulation of them it is possible to get nanofibers of the desired characteristics. In the next paragraphs the effects of these parameters will be discussed.

2.4.1 Solution parameters

One of the most important solution parameters in electrospinning is *solution viscosity*. Polymer solution viscosity depends, in turn, on polymer molecular weight, polymer conformation in the solvent (i.e. polymer-solvent interactions and polymer segmental mobility) and polymer concentration. More in detail, it is expected that a solution of a high molecular weight polymer is more viscous than a solution of its lower molecular weight variant. It has been observed that high molecular weight is not always essential for the electrospinning process, if sufficient intermolecular interactions among polymer chains can be established, virtually extending the chain lenght. [2] However, in general too low molecular weight polymers solutions produce beads rather than fibers, while too high molecular weight polymer solutions give large diameter or micro-ribbon like fibers. [9]

Likewise the molecular weight, also the concentration is a parameter that can be tuned in order to modify the solution viscosity. To describe the effects of the solution concentration on the nanofibers morphology, four critical concentrations, from low to high, can be defined [1]:

(i) For very low concentrations, electrospray occurs instead of electrospinning; polymeric micro/nano-particles will be produced insead of nanofibres.

(ii) When the concentration is a little higher, a mixture of beads and fibers will be obtained.

(iii) At the optimal concentration, smooth, uniform diameter nanofibers can be manufactured.

(iv) If the concentration is too high, micro-fibers or micro-ribbons can be obtained.

As final remark regarding the solution viscosity, it is important to highlight that the range of viscosities at which spinning can be performed depends on the type of polymer and solvent used.

The initiation of electrospinning requires that the electric forces of the charged solution overcome its surface tension. Thus, it is easy to understand the importance of the *solution surface tension*. Basically, surface tension is function of the selected solvent. A too high value inhibits the electrospinning process, causing the generation of sprayed droplets. [10] Some authors have attempted to reduce the surface tension of the solution by the addition of surfactants, with improvements of the morphology of the nanofibers. [11, 12]

Solution conductivity is another important solution parameter. If the conductivity of the polymeric solution is increased more charges can be carried in the electrospinning jet. The polymer type, solvent used and availability of ionisable salts mainly affect the conductivity. Often a strategy to increase the conductivity is by adding a salt. [11] Indeed, a reduction in the fiber average diameter has been observed when a small amount of salt was added to the solution. Moreover, the critical voltage at which the electrospinning works is reduced. Another effect of the increased charge is a greater bending instability. As a result, the deposition area of the nanofibers is larger, and this also favors the formation of thinner fibers since the jet path is increased. Another approach to increase the conductivity of the solution and, at the same time, to reduce the surface tension, involves the addition of ionic surfactants. [13]

2.4.2 Process parameters

In the electrospinning process the *electric voltage* is a parameter of crucial importance. Only after attainment of threshold voltage, fiber formation occurs, the induced electrostatic force overcoming the surface tension of the solution. It has already described how the shape of the initiating drop changes with the applied voltage (see paragraph 2.3), while there are different ideas regarding the effect of the voltage of the diameter of the final fiber. Some authors showed no significative effect of electric field on the fiber diameter of polyethylene oxide. [2, 14] Other researchers suggested that when higher voltage is applied, there is more polymer ejection and this facilitates the formation of a larger diameter fiber. [2, 15, 16] Others reported that an increase in the voltage (i.e. by increasing the electric field strength) increases the electrostatic repulsive force on the fluid jet, which ultimately favours the narrowing of the fiber diameter. [2] At high voltage, a great tendency for bead formation has been observed. [3, 16, 17]. It has been also reported that the shape of the beads changes from spindle-like to spherical-like with increasing voltage. [17]

The voltage can not only affect the physical appearance of the fiber, but also its crystallinity. The electrostatic field may cause the polymer molecules to be more ordered during electrospinning, thus induces a greater crystallinity of the fiber. However, above a certain voltage, the crystallinity is reduced. [3]

Electrospinning process is caused by charges on the jet and these charges can be influenced by an external electric field. Thus, it is not surprising that there have been several attempts of control the electrospinning jets through changing the *electric field profile* between the source of the electrospinning jet and the collector. This can be obtained by using auxiliary electrodes or by changing the orientation or shape of the collector. [3]

The *feed rate* is an important process parameter, determining the amount of solution available for electrospinning. For a given voltage, there is a corresponding feed rate to obtain and maintain a stable Taylor cone. For higher feed rate, due to a greater volume of solution drawn from the needle tip, the jet will take a longer time to dry. As result, the solvent may not have time enough to evaporate, given the same

flight time. The residual solvents may cause the fibres to fuse together, obtaining an increase of the fiber diameter. In addition, when the feed rate increases, it has also been observed a corresponding increase of beads size. [18]

The *internal diameter of the needle* has a certain effect on the electrospinning process. A smaller internal diameter was found to reduce the diameter of the electrospun fiber as well as the amount of beads. When the size of the droplet at the tip of the orifice decreases, such as in the case of a smaller internal diameter of the orifice, the surface tension of the droplet increases. Thus, for the same supplied voltage, the acceleration of the jet decreases and this allows more time for solution to be stretched and elongated before it is collected. However, if the diameter of the orifice is too small, it may not be possible to extrude the droplets of solution at the tip of the orifice. [3]

During the electrospinning, *collectors* usually act as conductive substrate to collect the charged fibers. Generally, aluminium foil is used as collector, but in this case it is difficult to transfer the collected nanofibers to other substrates, for various applications. With the need of fiber transferring, different collectors have been developed, including wire mesh, parallel bars and rotating rods or wheel. [19, 20]

The *distance between tip of spinneret and collector* has been examined as another approach to control the fiber diameter and morphology, even if the effect of this parameter is not as significant as other ones. It is well known that an important stage of electrospinning is the dryness of the fibers from the solvent, thus a minimum tip to collector distance is required to give to the fibers time enough to dry before reaching the collector. If the distance is either too short or too long beads fibers can be obtained. [2, 3]

2.4.3 Ambient parameters

Ambient parameter, such as temperature and humidity, can also affect diameter and morphology of electrospun fibers. Regarding the *temperature*, for example some authors investigated the effect of this parameter on the electrospinning of polyamide-6 fibers, ranging from 25 °C to 60 °C. It has been observed that

increasing temperature favored smaller fiber diameter, as a consequence of the inverse relationship between solution viscosity and temperature. [2, 21]

Also the *umidity* may have an influence on the elctrsopinning. The variation in humidity during electrospinning of polystyrene solution has been studied, showing that that by increasing humidity there was an appearance of small circular pores on the surface of the fibers; further increase of the humidity led to the pores coalescence. [3, 22]

2.5 Preparation of electrospun hybrid rubber/thermoplastic (R/T) membranes

As described in detail in the previous paragraphs, the choice of the electrospinning working parameters, in particular of solution and process parameters, is very difficult since there are no precise rules to follow.

With the purprose of producing hybrid rubber/thermoplastic mats, the author first selected acetone as solvent, being a good solvent of both the rubber and the thermoplastic polymer, inexpensive and non-toxic. Parameters, such as polymer concentration, feed rate, voltage and needle tip to collector distance, were systematically varied. In all cases it was not possible to spin the polymers. This was probably a consequence of the low boiling point of acetone (Tb=56.2 °C), evaporating already at the tip of the needle, when the jet was ejected. To overcome this problem, acetone was replaced with dimethylformamide (DMF, Tb= 153 °C) or DMF:acetone blends (50:50 v/v).

The value of the polymers (rubber and thermoplastic) concentration (C) was chosen from a visual inspection of the flow behavior of several candidate polymer solutions prepared at different concentrations, from 4% to 25% w/v, aiming to obtain a viscous liquid but not a gel. The values of voltage (V), flow rate (Q), needle inner diameter (id) and distance between needle tip and collector (TCD) were set to be in the range of values generally usually used in electrospinning. In particular, the total polymer concentration was 9% w/v and the process parameters were set as V =

25 kV, Q = 0.4 mL/h, id = 0.9 mm and TCD = 15 cm. Different thermoplastic to rubber ratios were investigated.

In Fig. 2.6, SEM images of electrospun mats prepared with the above values of the working parameters are reported. In particular, the micrographs of the electrospun mats of solutions at 7.5% w/v rubber and 1.5% w/v thermoplastic (panels (a) and (d)), 6% w/v rubber and 3% w/v thermoplastic (panels (b) and (e)) and 4.5% w/v rubber and 4.5% w/v thermoplastic (panels (c) and (f)) are shown. The images reported in the panels (a), (b) and (c) concern the electrospinning products from solutions where the solvent was a DMF:acetone blend (50:50 v/v), the ones in the panels (d), (e) and (f) are of samples obtained from electrospinning of solutions in DMF. Regarding the samples obtained from solutions where the solvent was a DMF/acetone mixture (Fig. 2.6 a-c), the desired nanofibrous morphology was not present, irrespective of the concentrations of the two polymers. For the systems in which the solvent was only DMF, significant improvements in morphology were observed. In particular, in mats electrospun from solutions at higher rubber concentration (Fig. 2.6 d) a film with voids was obtained. Some nanofibers were also present. For 6% w/v rubber and 3% w/v thermoplastic (Fig. 2.6 e) a web of nanofibers (average diameter of about 400 nm) was produced. Defects, such as random “beads”, were also present. Finally, for the system made by equal concentrations of rubber and thermoplastic (panel f) nanofibers of average diameter of about 300 nm were produced. Fibre defects such as large beads and micro sized solution splatters were also evident. In conclusion, none of the systems spun in the selected conditions was considered satisfactory.

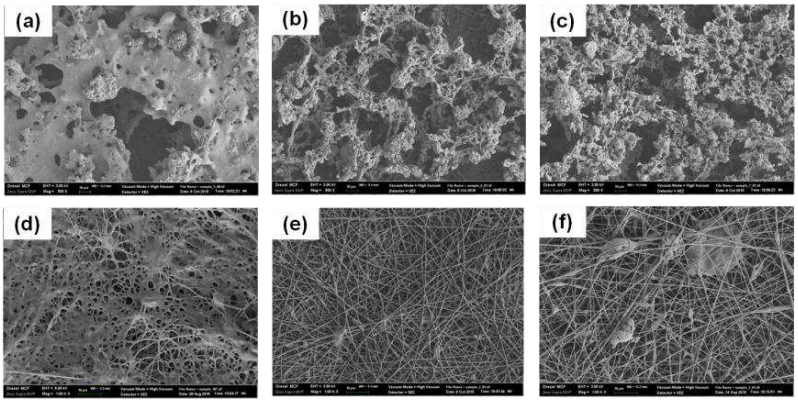

Figure 2.6 SEM images of the products obtained spinning rubber/thermoplastic solutions (% w/v) in DMF-acetone at various concentrations: (a) 7.5/1.5; (b) 6/3;(c) 4.5/4.5; and in DMF at various concentrations: (d) 7.5/1.5; (e) 6/3; (f) 4.5/4.5. V= 25 kV, Q=0.4 mL/h, id=0.9 mm and TCD=15 cm.

To understand the great difference in morphology observed when spinning the same polymers with the two different solvents (DMF and DMF/acetone), surface tension measurements of the polymer solutions at different concentration of rubber and thermoplastic, both in DMF and in DMF/acetone solvent were performed. The results are reported in Tab. 2.1. The surface tension of pure DMF and pure acetone were also measured, resulting 35.00 and 23.30 nM/m, respectively. As expected, the polymer solutions in DMF/acetone blends showed intermediate values of surface tension, with respect to the values of the two solvents. When the solvent was only DMF the surface tension increased. Not significant differences were observed for the different concentrations. The lack of nanofibrous morphologies for the samples produced from DMF/acetone solutions (Fig. 2.6 a-c) could be partially ascribed to the low values of surface tension. Thus, from this observation, DMF was used as the only solvent in the following experiments.

Table 2.1 Surface tension values of rubber/thermoplastic solutions in DMF and in DMF/acetone.

System (% w/v)	Surface tension (mN/m)
9% in DMF/Ac*	30.69
7.5/1.5% in DMF/Ac*	30.30
6/3% in DMF/Ac*	28.92
4.5/4.5% in DMF/Ac*	26.54
9% in DMF	38.00
7.5/1.5% in DMF	38.12
6/3% in DMF	39.61
4.5/4.5% in DMF	39.99
3/6% in DMF	39.56
1.5/7.5% in DMF	37.92

**DMF:Ac=50:50 v/v.

The effect of total polymer concentration, voltage and flow rate was also investigated. The reference system was the one produced from the 6/3 % w/v R/T solution, at V= 25 kV, Q=0.4 mL/h, id=0.9 mm and TCD=15 cm (the SEM image of this system is reported in Fig. 2.6 e).

Generally higher concentration solutions produce more uniform fibers with fewer beads. [2,18] For this reason, a slightly higher concentration solution was tested, all the other parameters being kept constant. Figure 2.7 compares the SEM micrographs of a mat produced from a solution at concentration of 6.5/3.5 % w/v R/T (Fig. 2.7 a, a') with the "reference" system (Fig. 2.7 b, b'). The increase of the concentration of the solution did not produce the expected morphology improvements: fiber defects did not disappear and the web consisted of larger and flatter fibers, with junction points.

In Fig. 2.8 the SEM micrographs of hybrid mats, produced from 6/3 % w/v R/T solutions, at two different voltage values, 20 kV and 25 kV, and two flow rates, 0.3 mL/h and 0.4 mL/h, are reported. Essentially, none of these mats presents significant improvements in the morphology.

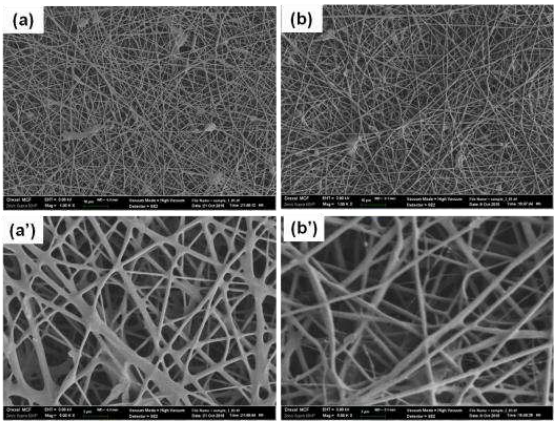

Figure 2.7 SEM images of: (a), (a') electrospun mat from 6.5/3.5 % w/v DMF solution at two different magnifications; (b), (b') electrospun mat from 6/3 % w/v DMF solution at two different magnifications. V=25 kV, Q=0.4 mL/h, id=0.9 mm and TCD=15 cm.

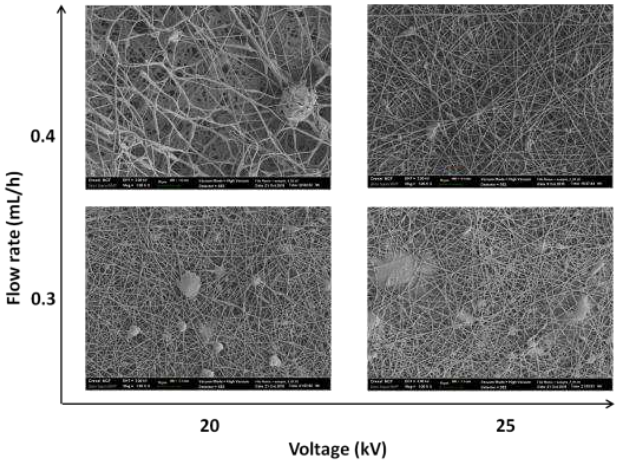

Figure 2.8 SEM images of electrospun mats from 6/3 % R/T DMF solutions obtained for two voltages and flow rates. id=0.9 mm and TCD=15 cm.

In order to produce hybrid R/T mats with improved morphology with respect to the above described ones, another attempt of the author has been to use the working parameter already used in literature for producing electrospun mats of the same thermoplastic. Thus, a new set of values was evaluated. Specifically, the new parameters values were: total polymer concentration C=7.5% w/v, voltage V=21 kV,

flow rate Q=1.2 mL/h, needle inner diamer id=0.9 mm and distance between nedle tip and collector TCD=20 cm.

Also in this case, a study of the effect of different concentrations of rubber and thermoplastic on the produced mat morphology quality was carried. Figure 2.9 shows SEM images of mats produced by electrospinning of solutions at 6% w/v rubber and 1.5% w/v thermoplastic (panels (a)), 4% w/v rubber and 3.5% w/v thermoplastic (panels (b)) and 3% w/v rubber and 4.5% w/v thermoplastic. In the same figure, a SEM micrograph of the electrospun solution of the only thermoplastic at 7.5% w/v is reported (Fig. 2.9 d), for comparison. The mat produced electrospinning the solution at higher concentration of rubber (Fig. 2.9 a) consisted of fibers (average diameter 100 nm) and micro sized solution splatters. From the 4/3.5 % R/T solution (Fig. 2.9 b) and 3/4.5 % R/T solution (Fig. 2.9 c) membranes with uniform fibers were produced. In both systems the average fiber diameter was about 200 nm. However, the 3/4.5 % R/T system shows some irregularities and beads (panel c). For this reason the best system can be considered the 4/3.5 % R/T spun at V=21 kV, Q=1.2 mL/h, id=0.9 mm and TCD=20 cm, which was selected to be tested in combination with the resin system, as it will be described in the following chapter.

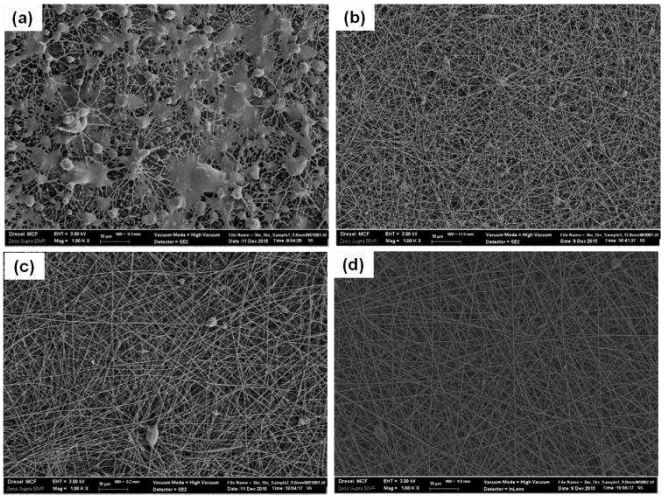

Figure 2.9 SEM images of mats obtained spinning rubber/thermoplastic solutions (% w/v) in DMF at various concentrations: (a) 6/1.5; (b) 4/3.5; (c) 3/4.5; (d) 0/7.5. V=21 kV, Q=1.2 mL/h, id=0.9 mm and TCD=20 cm.

2.6 Conclusions

This chapter consists of two parts. The first one presents the electrospinning process, describing the main features of the process and the effect of working parameters (solution, process and ambient parameters) on the properties of mats, according the literature. It has been demonstrated that while the electrospinning process requires a fairly simple and inexpensive set up, on the contrary the optimization of all working parameters can be a very complex procedure. In particular, polymer concentration, voltage and flow rate are the more critical parameters.

The second part describes the preparation and characterization of electrospun hybrid rubber/thermoplastic membranes, the rationale being to evaluate the combined toughening effect of an elastomer and a polymer on epoxy matrices. In addition, it can represent a more general method to disperse a rubber phase into localized regions of a composite laminate, the thermoplastic nanofiber mat acting as carrier and confinement aid.

The best produced hybrid rubber/thermoplastic mats have been tested with epoxy resins in form of monolayer, as described in the next chapter.

REFERENCES

[1] Huang ZM, Zhang YZ, Kotaki M, Ramakrishna S. A review on polymer nanofibers by electrospinning and their applications in nanocomposites. Compos Sci Technol 2003;63:2223-2253.

[2] Bhardwaj N, Kundu SC. Electrospinning: A fascinanting fiber fabrication technique. Biotech Advanc 2010;28:325-347.

[3] Ramakrishna S, Fujihara K, Teo WE, Lim TC, Ma Z (2005). An Introduction to Electrospinning and Nanofibers. World Scientific Publishing.

[4] Ondarcuhu T, Joachim C. Drawing a single nanofibre over hundreds of microns. Europhys Lett 1998;42:215-220.

[5] Wendorff JH, Agarwal S, Greiner A (2012). Electrospinning – Materials, Processing, and Applications. Wiley-VCH.

[6] Reneker DH, Yarin AL. Electrospinning jets and polymer nanofibers. Polymer 2008;49:2387-2425.

[7] Frenot A, Chronakis IS. Polymer nanofibers assembled by electrospinning. Curr Opin Colloid Interface Sci 2003;8:64-75.

[8] Reneker DH, Yarin AL, Zussman E, Xu H. Electrospinning of Nanofibers from Polymer Solutions. Adv Appl Mech 207;41:43-195.

[9] Koski A, Yim K, Shivkumar S. Effect of molecular weight on fibrous PVA produced by electrospinning. Mater Lett 2004;58:493-497.

[10] Hohman MM, Shin M, Rutledge G, Brenner MP. Electrospinning and electrically forced jets. II. Applications. Phys Fluids 2001;13:2221-36.

[11] Shenoy SL, Bates WD, Frisch HL, Wnek GE. Role of chain entanglements on fiber formation during electrospinning of polymer solutions: good solvent, non-specific polymer–polymer interaction limit. Polymer 2005;46:3372-3384.

[12] Wang SQ, He JH, Xu L. Non-ionic surfactants for enhancing electrospinability and for the preparation of electrospun nanofibers. Polym Int 2008;57:1079-1082.

[13] Kurban Z, Lovell A, Jenkins D, Bennington S, Loader I, Schober A, Skipper N.Turbostratic graphite nanofibres from electrospun solutions of PAN in dimethylsulphoxide. Eur Polym J 2010;46:1194-1202.

[14] Reneker DH, Chun L. Nanometre diameters of polymer, produced by electrospinning. Nanotechnology 1996;7:216-23.

[15] Zhang C, Yuan X, Wu L, Han Y, Sheng J. Study on morphology of electrospun poly (vinylalcohol) mats. Eur Polym J 2005;41:423-32.

[16] Demir MM, Yilgor I, Yilgor E, Erman B. Electrospinning of polyurethane fibers. Polymer 2002;43:3303-9.

[17] Zong X, Kim K, Fang D, Ran S, Hsiao BS, Chu B. Structure and Process Relationship of Electrospun Bioabsorbable Nanofiber Membranes. Polymer 2002;43:4403-4412.

[18] Subbiah T, Bhat GS, Tock RW, Parameswaran S, Ramkumar SS. Electrospinning of Nanofiber. J Appl Polym Sci 2005;96(2):557-569.

[19] Li D, Wang Y, Xia Y. Electrospinning of polymeric and ceramic nanofibers as uniaxially aligned arrays. Nano Lett 2003;3(8):1167-1171.

[20] Baji A, Mai YW, Wong SC, Abtahi M, Chen P. Electrospinning of polymer nanofibers: Effects on oriented morphology, structures and tensile properties. Compos Sci Technol 2010;70:703-718.

[21] Mit-uppatham C, Nithitanakul M, Supaphol P. Ultrafine electrospun polyamide-6 fibers: effect of solution conditions on morphology and average fiber diameter. Macromol Chem Phys 2004;205:2327-2338.

[22] Casper CL, Stephens JS, Tassi NG, Chase DB, Rabolt JF. Controlling surface morphology ofnelectrospun polystyrene fibers: effect of humidity andmolecular weight in the electrospinning process. Macromolecules 2004;37:573-578.

3. THE INFLUENCE OF ELECTROSPUN MATS ON THE PROPERTIES OF EPOXY RESINS

3.1 Introduction

In this chapter, the author focuses the attention on the characterization of nanofibrous mat/resin monolayers and three-layers laminates formed by the impregnated mat sandwiched between two CF fabric layers, as model system of resin/mat interleaf. The influence of the nature of the polymer used to produce the mat on the morphology of the interleaf was investigated and qualitative indications of the toughening mechanisms activated were sought. Two resin systems were selected for their different curing temperatures, their very different mechanical properties and the different impact that their cure process has on the nanofibers morphology, hence on the properties of the mat/resin systems. In addition, the effects of selected mats on both curing behavior and thermal resistance of the resins were investigated.

The various polymers and one elastomer were chosen for producing the electrospun mats, namely an acrylic rubber (R), a polysulfone (PSF), a common polyamide such as Nylon 6,6, a polyvinylidene fluoride (PVDF) and a polyacrilonitrile (PAN). In consideration of their different chemical composition and properties, different morphologies upon cure and potentially different toughening effects are expected.

Either in the form of electrospun mats or dispersed/solubilized in the epoxy monomer mixtures, these polymers have already been evaluated to some extent as toughening agents of epoxy formulations. In particular, acrylic rubbers and polysulfone (PSF) are among the most commonly used toughening agents for epoxy resins, the latter being preferred for high performance (high glass transition temperature, high elastic modulus) resins. Acrylic rubbers generally undergo phase separation yielding finely dispersed microparticles in the epoxy matrix, their toughening mechanism being mainly described as “rubber tearing” or “crazing and

shear yielding". The rubber tearing theory attributes the toughening exclusively to the rubber particles. In particular, according to this theory a crack in a rubber propagates through the brittle matrix and when impinges on a rubber particle stretch and tear the rubber dissipating the elastic strain energy.

The crazing theory proposes that toughness enhancement is due to the generation and efficient termination of crazes by rubber particles. Under tensile stress, crazes are initiated at points of maximum principal strain, which are usually near the equator of rubber particles, and propagate, again following planes of maximum principal strain. Craze growth is terminated when a further rubber particle is encountered, preventing the growth of very large crazes. The result is a large number of small crazes in contrast to a small number of large crazes formed in the same polymer in absence of rubber particles. [1-4]

Polysulfones can yield co-continuous morphologies depending on both the percentage of thermoplastic used and time and curing temperature, in this case the main toughening mechanism being "crazing and shear yielding". [5] They can be added in blend with the resin, [6, 7] in form of film [8, 9] or electrospun nanofibrous mats. [10-12]

Nylons and, more in particular, Nylon 6,6 is used as toughening agent of epoxy resins, either dispersed in form of microparticles [13] or in the form of electrospun mat interlayers. [14-18].

Electrospun mats of PVDF and PAN have also been produced to improve the interlaminar toughness of carbon-epoxy laminates, being engineering thermoplastics possessing excellent mechanical strength and toughness, high heat and chemical resistance, and low moisture absorption. [19]

For the purpose of the present investigation, all the selected polymers were used to make single component electrospun mats, with the exception of the acrylic rubber, which has been co-electrospun together with a thermoplastic polymer (R/T mats) (see Chapter 2).

Regarding the reasons to produce an hybrid mat, as already explained in Chap. 2, the purpose was to exploit the synergism of the two polymers, one that dissolves in the uncured resin and gives phase separation and the other that maintains a

nanofibrous morphology upon cure. The idea is to activate different toughening mechanisms.

The various mats have been coupled both with a high temperature curing epoxy formulation (HPE) and a room temperature curing epoxy resin (LPE), except for PVDF, that was used only with LPE, to preserve the nanofibrous morphology since the PVDF melting point is lower than the curing temperature of HPE. Indeed, it is known that when used in epoxy laminates in the form of mats that melt during the cure process, the toughness does not increase. [20]

3.2 Materials and methods

The two resin systems used, HPE (high performance epoxy resin) and LPE (low performance epoxy resin) have formulations and mechanical and thermal properties reported in section A.2 of the Appendix.

The toughening agents, i.e. acrylic rubber (R), polysulfone (PSF), Nylon 6,6, polyvinylidene fluoride (PVDF), polyacrilonitrile (PAN) and rubber/thermoplastic (R/T) blends were used in form of electrospun nanofibrous mat. Details on their production process are provided in section A.2 of the Appendix and in the Chapter 2.

All monolayers were produced by impregnation of the mat with the resin, while the three-layers systems (tls) were assembled by hand lay-up, by placing the dry membrane between the two pre-impregnated carbon fiber layers. Thus, a cure process was performed.

The high performance epoxy monolayers were cured by means a cycle cure consisting of a heating step from room temperature to 180 °C at 2 °C/min and an isothermal rest at 180 °C for 2 hr, while low performance epoxy ones at room temperature for 8 hours and then post-cured at 60 °C for 24 hours. HPE/Nylon 6,6, HPE/PAN, HPE/R/T HPR/PSF and LPE/PSF monolayers were produced in autoclave applying a pressure of 2.5 bar; LPE/Nylon 6,6, LPE/PVDF and LPE/PAN nonolayers by vacuum bagging technique. In Tab. A.2, section A.2 of the Appendix the weight fraction of mat in each produced monolayer is reported.

The systems were characterized by morphological analysis via SEM on fracture surfaces, residual reactivity by DSC analysis, and thermal properties by DMTA. The thickness of mats and monolayers was measured by a micrometer, the thickness of the mat/resin regions was evaluated by means of SEM images analysis and the data reported are the average of 3 measurements. More details of characterization techniques (DSC, DMTA and SEM) are reported in the section A.3 of the Appendix.

3.3 Results and discussion

3.3.1 Analysis of the morphological features of monolayers and three-layers systems

Figures 3.1 and 3.2 show the SEM images of the fracture surfaces of various HPE resin impregnated electrospun mats (monolayers).

In particular, in Fig. 3.1a-b, SEM micrographs of HPE/Nylon 6,6 and HPE/PAN monolayers are reported, respectively. Lower magnification images of the same systems are shown in panels a'-b'. SEM micrographs of the corresponding nanofibrous membranes are presented in panels a''-b'' for comparison. For the systems with Nylon 6,6 (Fig. 3.1a) and PAN (Fig. 3.1b) the nanofibers and the grooves left behind by the nanofibres torn out by the propagating fracture are clearly visible. The mats maintained their fibrous morphology upon thermal cure and in both systems the nanofibers appear randomly and uniformly distributed inside the resin. Moreover, several fracture planes can be observed (see Fig. 3.1a' for Nylon 6,6 and Fig. 3.1b' for PAN); this last evidence suggests that the epoxy/thermoplastic monolayers contribute in the dissipation of the fracture energy and that the nanofibres are actually exerting their toughening function.

In Fig. 3.2a-a' and b-b', the fracture surfaces of HPE/R/T and HPE/PSF monolayers impregnated with HPE at two magnifications are shown (the corresponding mats are shown in panels a"-b"). For the rubber-thermoplastic hybrid system (Fig. 3.2a-a') only few fibers are visible, probably the ones made by the

thermoplastic. The fracture surface appears significantly indented, suggesting also for this system the activation of a fracture energy dissipation mechanism.

The PSF mat (Fig. 3.2b-b') shows a very different behavior; after curing the nanofibers have lost their pristine nanofibrous morphology yielding a very coarse micro-particulate morphology. It is well known that epoxy resin/polysulfone systems exhibit an LCST-type phase behavior, a phase separation process occurring when the blend is thrust into the two-phase region, as the cure reaction proceeds. In particular, tetrafunctional epoxy resin/polysulfone systems (we can assume the HPE formulation mainly consists of the tetrafunctional monomer, see section A.2 of the Appendix for more details) show a lower critical solution temperature value of about 240 °C [21] for the blend without curing agent, and this LCST value decreases during the curing process as a consequence of the increase of the molecular weight of the resin. Indeed, the large dimensions of particles of Fig. 3.2b-b' suggest that the system actually undergoes phase inversion; the microparticles are constituted by an epoxy-rich phase dispersed into a polysulfone-rich matrix, as described in the literature for epoxy/polysulfone blends with higher PSF concentration. [21, 22] We can argue that the nanofibrous mat restrains the resin outflow when, during the curing process, the temperature increases and the resin viscosity decreases. Since we can expect the PSF nanofibres to dissolve in the resin when heated above the lower critical solution temperature, the mat cannot exert its resin retention function any longer and a significant amount of the resin flows out. As a consequence, a very thin monolayer is obtained (see Fig. 3.2b). Moreover, since the actual concentration of PSF in the residual resin-PSF mixture increases, phase inversion occurs.

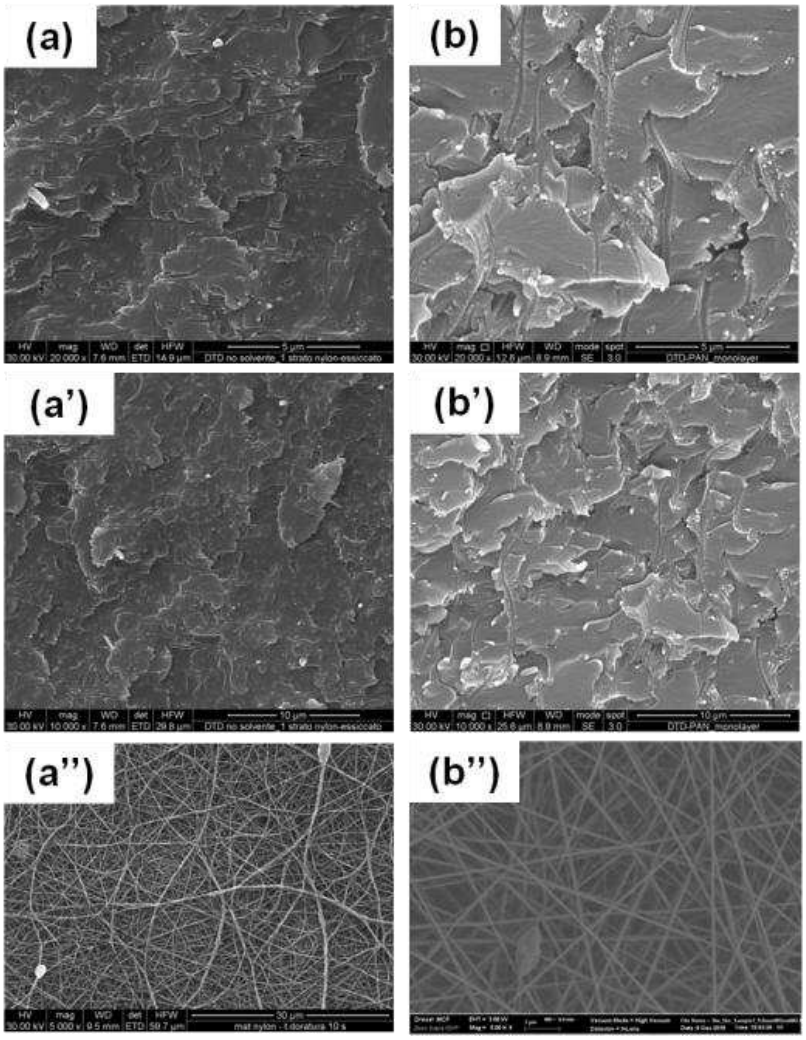

Figure 3.1 SEM micrographs of fracture surfaces of the monolayers produced with HPE and various mats, at two different magnifications, and the corresponding dry mats: (a, a', a'') Nylon 6,6; (b, b', b'') PAN.

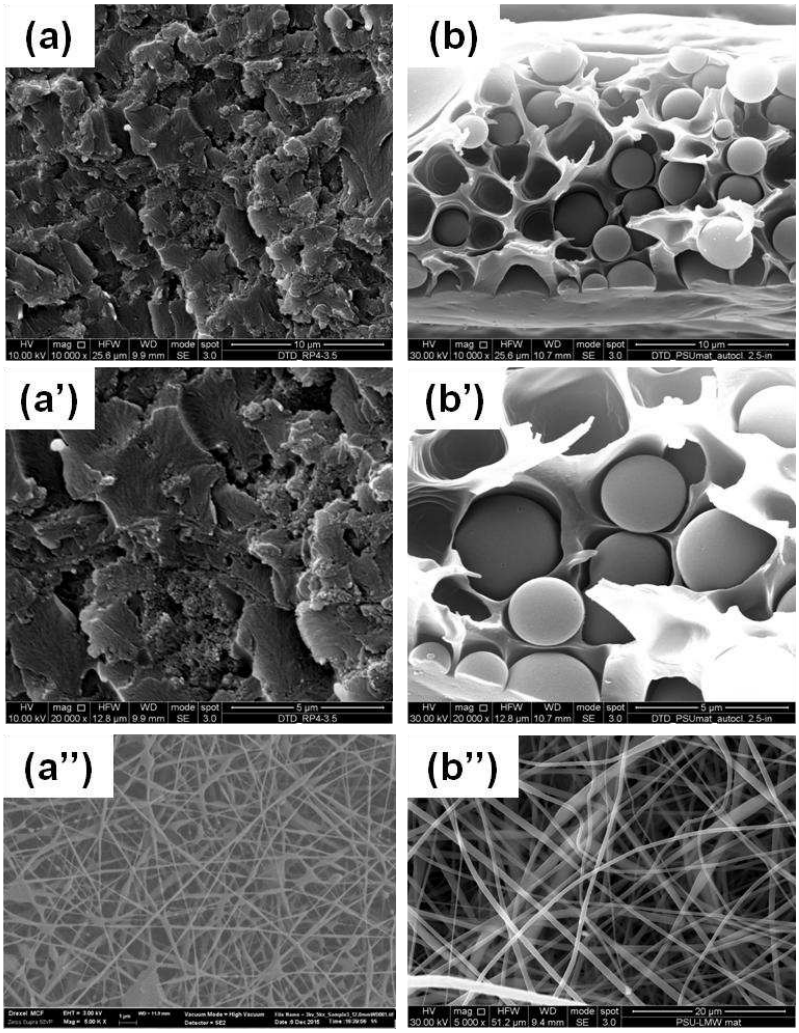

Figure 3.2 SEM micrographs of fracture surfaces of the monolayers produced with HPE and various mats, at two different magnifications, and the corresponding dry mats: (a, a', a") rubber/thermoplastic; (b, b', b") PSF.

We wanted to ascertain if sandwiching a mat between two carbon fiber fabric layers would actually mitigate the observed loss of resin, leading to a material that better mimics the resin/mat interphase in a multilayered laminate. For this reason, three-layers systems (tls) formed by two CF fabrics and a PSF mat was prepared (PSF_tls). An analogous system with Nylon 6,6 was also made to check if any effect could be appreciated also on mats that retain their morphological features upon cure.

(Nylon 6,6_tls). In Fig. 3.3 SEM images of the cross-sections of PS_tls and Nylon 6,6_tls systems are reported. In particular, for Nylon 6,6_tls a SEM micrograph of the polished and etched transversal surface is reported (Fig 3.3a), while for the PSF_tls system images of fracture surfaces (Fig. 3.3b-d) are presented. The micrograph shown in panel (b) of Fig. 3.3 was taken in the central part of the sample cross-section, while the image in the panel (c) was taken close to one of the edges. When the Nylon mat was used as interlayer between two CF fabrics (Fig. 3.3a) a well-defined and confined mat/resin region is observable. Contrariwise, in PSF_tls system no fibrous morphology is evident in any of the specimens. Particles of about 1 µm or voids of similar dimensions are present in both micrographs (referring to both the middle plane zone and the zone near to the edge, Fig. 3.3 b and c, respectively). We can speculate that the polysulfone mat dissolves in the resin upon heating and distributes in the resin that is now mostly hold in place by the two CF mats. At this lower PSF concentration, phase inversion does not occur: therefore the particles are likely attributable to the PSF-rich phase. Furthermore, some polysulfone particles are also present in regions far out of the supposedly mat boundaries (see Fig. 3.3 panel d).

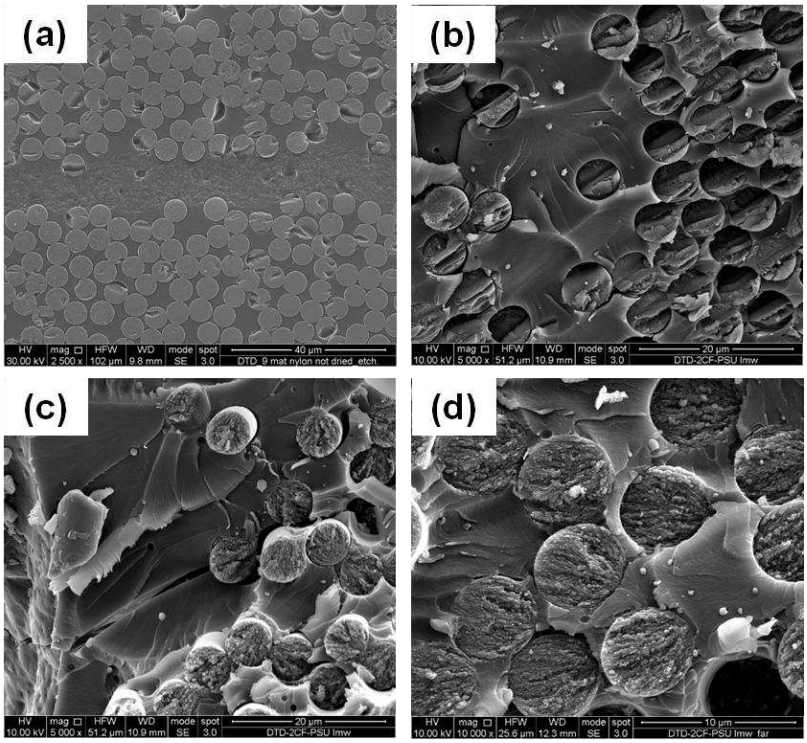

Figure 3.3 SEM micrographs of: (a) Nylon 6,6_tls system polished and etched cross-section; (b-d) PSF_tls fracture surface: (b) center, (c) close to one edge; (d) far out of the supposedly mat boundaries.

In Fig. 3.4 SEM images of fractured surfaces of LPE/Nylon 6,6 (Fig. 3.4 a, a') and LPE/PVDF (Fig 3.4 b, b') are shown, while in Fig. 3.5 the micrographs of LPE/PAN (Fig. 3.5 a, a') and LPE/PSF (Fig. 3.5 b, b') monolayers are reported. Also in this case, the micrographs of the corresponding polymeric mats used in the monolayers are shown in panels a'' and b'' of Figure 3.4 and Figure 3.5.

It can be useful to remember that the LPE/Nylon 6,6, LPE/PVDF and LPE/PAN systems have been produced by vacuum bagging technique, while LPE/PSF monolayers have been produced in autoclave, applying a pressure of 2.5 bar.

For Nylon 6,6 and PVDF cured with LPE a well-defined mat/resin region is observable in the middle plane of the monolayer and two resin layers are present above and under the mat/resin region (Fig. 3.4 a and b); in the PAN and PSF monolayers similar resin layers are not visible (Fig. 3.5 a and b). In Tab. 3.1 the

thickness of dry mat, the cured monolayer and the mat/resin region in the monolayer for LPE/Nylon 6,6, LPE/PVDF and LPE/PAN systems are compared. In LPE/Nylon 6,6 and LPE/PVDF the mat/resin region is thinner than the dry mat, the decrease being more substantial for PVDF (almost 50%). On the contrary, a significative increase of the overall monolayer thickness with respect to the dry can be observed: the percentage of increase was similar for Nylon 6,6 and PVDF (about 450%) and higher for PAN (680%). In LPE/PAN monolayer mat/resin region coincides with the whole thickness of the monolayer.

Probably, a more efficient process than vacuum bagging would be able to remove the excess of resin from the surfaces of the monolayers in the cases of Nylon 6,6 and PVDF. On the other hand, the LPE resin has a low viscosity at room temperature, therefore it can easily be absorbed by mats as well as easily desorbed when the vacuum is applied.

The observed different behavior of the various mat/resin systems with the same resin could be consequence of different nanofiber/matrix degrees of interaction, higher for the LPE/PAN monolayer than for LPE/Nylon 6,6 and LPE/PVDF.

In the panel a', b' of the figures 3.4 and 3.5 SEM images of the mat/resin region of the four systems at higher magnification are reported. In the Nylon 6,6 monolayer the thinner nanofibers seem to be tenaciously bonded to the matrix while in the PVDF monolayer, the thicker nanofibers are clearly observable as a separate phase and almost completely detached from their matrix (Fig. 3.4 a', b', respectively). However, the fracture surfaces of both systems appeared indented and corrugated, suggesting toughening effects of the resin in both cases. Regarding PAN monolayer (see Fig. 3.5 a'), only limited nanofiber-matrix debonding in the fracture surface is visible, indicating a general good nanofiber/matrix adhesion. On the other hand, the surface appears fairly flat, like in typical brittle resin systems. It can be argued that since the resin significantly swells the PAN mat, the nanofibers become effectively too "diluted" to exert a toughening effect.

In Fig 3.5 b' high magnification SEM image of LPE/PSF is shown. The nanofibrous morphology is observed after the curing process carried out at room

temperature (differently from the HPE/PSU monolayer, Fig. 3.2 b, b', that required a T_{cure}=180 °C) and a poor nanofiber/resin adhesion is noted.

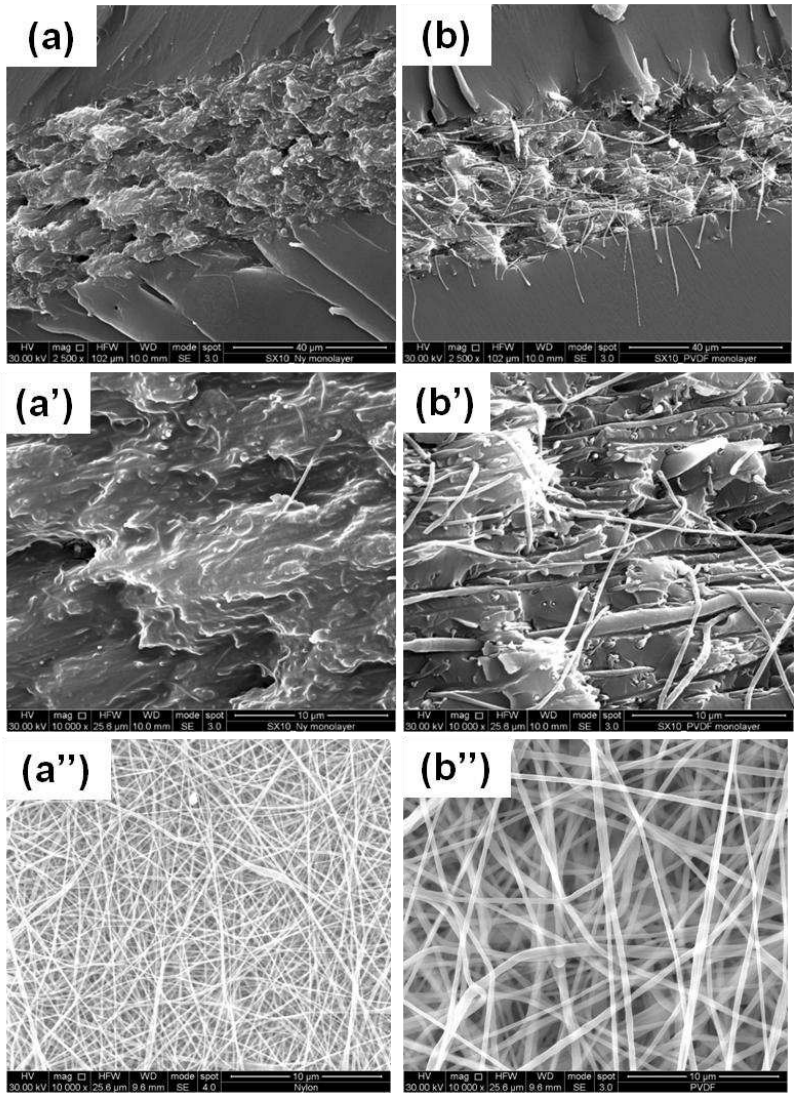

Figure 3.4 SEM micrographs of fracture surfaces of the monolayers produced with LPE and various mats, at two different magnifications, and the corresponding dry mats: (a, a', a'') Nylon 6,6; (b, b', b'') PVDF.

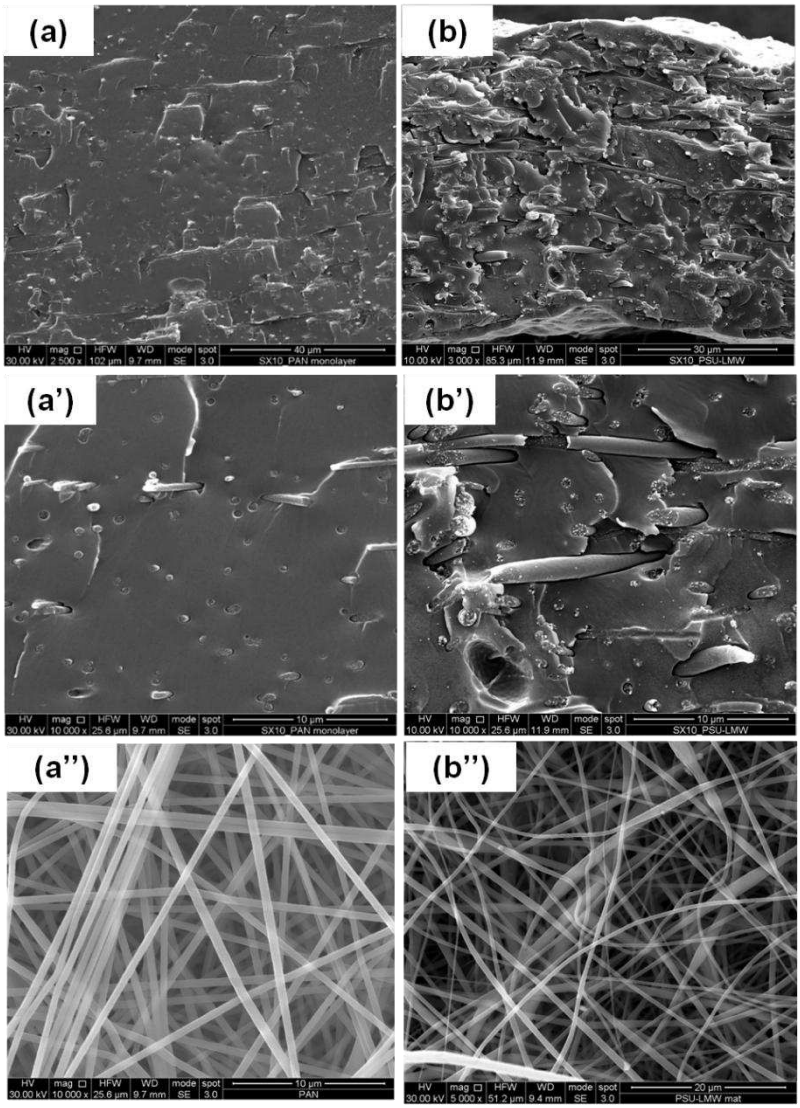

Figure 3.5 SEM micrographs of fracture surfaces of the monolayers produced with LPE and various mats, at two different magnifications, and the corresponding dry mats: (a, a', a'') PAN; (b, b', b'') PSF.

Table 3.1 Mat thickness (T_{mat}), mat/ resin region thickness ($T_{mat/resin\ region}$) and monolayer thickness (T_{monol}) in LPE/Nylon 6,6, LPE/PVDF and LPE/PAN monolayers.

System	T_{mat} (μm)	$T_{mat/resin\ region}$ (μm)	T_{monol} (μm)
LPE/Nylon 6,6	60±4	43±5	317±41
LPE/PVDF	60±4	32±2	330±30
LPE/PAN	60±6	467±49	467±40

Finally, in Fig. 3.6 SEM images of HPE/Nylon 6 (panel a), HPE/PSF (panel b), LPE/Nylon 6,6 (panel c) and LPE/PSF (panel d) monolayers are reported, to compare systems with same nanofibrous mat but different matrix formulation (HPE or LPE). Morphologies are similar for the two Nylon 6,6 monolayers (HPE/Nylon 6,6 and LPE/Nylon 6,6); the nanofibres survive the curing process, and appear randomly distributed and strongly bound to the matrix. For both systems different fracture planes are noted, indication that toughening effects are occurring. On the contrary, as already pointed out, the PSF mat shows a different behavior if coupled with the high temperature curing resin (HPE) or the room temperature curing formulation (LPE). In particular, for HPE/PSF (Fig. 3.6 b) micro-particles appear, while in LPE/PSF the nanofibers keep their morphology, although they look detached from the matrix, suggesting poor nanofiber/resin adhesion.

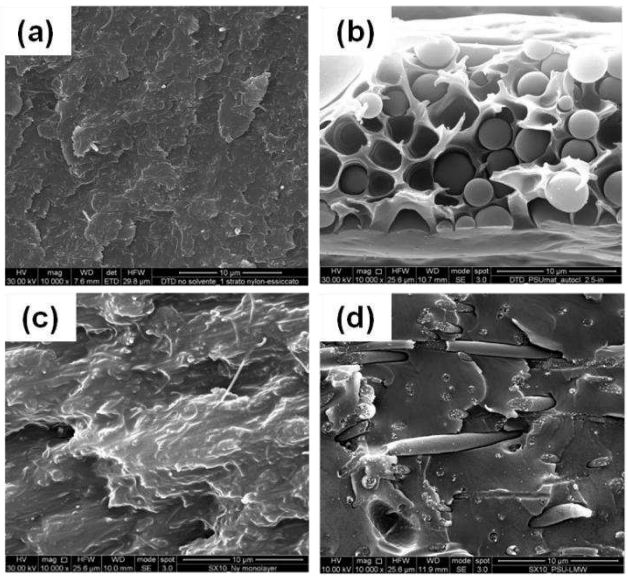

Figure 3.6 SEM micrographs of fracture surfaces of different monolayers: (a) HPE/Nylon 6,6; (b) HPE/PSF; (c) LPE/Nylon 6,6 (d) LPE/PSF.

3.3.2 Effect of nanofibrous membranes on curing and dynamic mechanical thermal behavior of epoxy resins

The influence of the Nylon 6,6 and PSF mats on the curing behavior of the HPE matrix was investigated by means of DSC analysis. For the purpose of this investigation, different weighed amounts of the uncured resin were dropped on dry mat samples. As a result, different polymer/resin compositions were obtained in order to simulate different possible local concentrations.

In Fig. 3.7 the thermograms of Nylon 6,6 mat and uncured resin are reported, as well as those of uncured resin/Nylon mat samples at different resin to mat ratio. In particular, three different weight percentages of mat in the resin are considered: 5%, 10% and 20%. The curve of Nylon 6,6 mat shows a broad endothermic peak at low temperature (the peak temperature was about 65 °C), probably due to the presence of moisture absorbed by the polymer. At higher temperature (T=265 °C) a second narrow endothermic peak is present, attributable to the melting of the crystalline domains of the polymer. In both the thermograms of the uncured resin and the uncured resin/mat samples (see Fig. 3.7), a large exothermic peak, that refers to the curing reactions of the resin, is evident.

In Fig. 3.8 DSC curves of the uncured resin/PSF mat samples are reported and compared with those of the two individual components, i.e. PSF mat and uncured resin. In the thermogram of PSF mat the flex point at about 165 °C, better visible in the inset, can be attributable to the glass transition temperature of the polymer. Regarding the uncured resin/PSF mat samples, also for these systems the main feature in the thermogram is the exothermic peak of the resin.

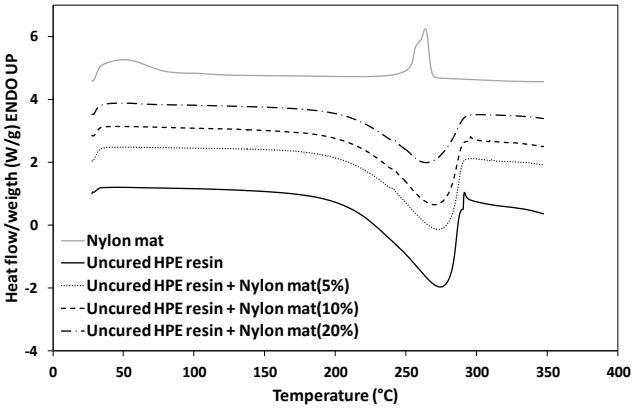

Figure 3.7 Calorimetric analysis of Nylon 6,6 mat, uncured resin and uncured resin with different amounts of Nylon 6,6 mat.

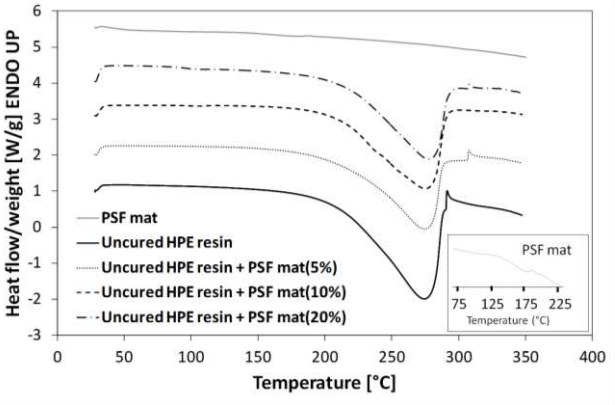

Figure 3.8 Calorimetric analysis of PSF mat, uncured resin and uncured resin with different amounts of PSF mat.

From the curves of Figs. 3.7 and 3.8, the onset and peak temperatures, and the curing reaction heat (ΔH) for the neat resin and the resin in the presence of Nylon mat or PSF mat are reported in Tab. 3.2. For all systems that contain also mats, the curing reaction heat has been calculated taking into account the weight fraction of resin in the specimen. In addition, for samples with Nylon mat, the melting heat of Nylon has been considered, because this phenomenon occurs in the same range of temperatures as curing (see Fig. 3.7).

The nanofibrous mats, both Nylon 6,6 and PSF, seem to interfere with the curing process of HPE resin: a significant increase of the T_{onset} value is observed for all systems containing the mat with respect the neat resin, while ΔH is lower when the membrane is present. The shift of the peak temperature toward lower values for the samples with Nylon 6,6 could be partially attributed to the concomitant phenomenon of Nylon melting (T_{peak}= 265 °C).

The increase of T_{onset} for both type of systems can be caused by a less efficient heat transfer when the resin is cured in the presence of the mat, while the reduced heat of reaction can be due to a lower conversion of epoxy groups owing to the presence of the non-reactive interface with the polymer nanofibres. Indeed, the effect is more pronounced for Nylon than for PSF.

Table 3.2 Thermal properties of the uncured HPE resin, uncured HPE resin/Nylon mat and uncured HPE resin/PSF samples, as obtained from DSC analysis.

System	T_{onset} (°C)	T_{peak} (°C)	$\lvert\Delta H\rvert$ (J/g)
Uncured HPE	~130	274	827.03
Uncured HPE + Nylon mat_5%	~150	273	705.13
Uncured HPE + Nylon mat_10%	~150	270	741.29
Uncured HPE + Nylon mat_20%	~150	264	632.45
Uncured HPE + PSU mat_5%	~140	274	796.23
Uncured HPE + PSU mat_10%	~150	275	760.85
Uncured HPE + PSU mat_20%	~150	277	714.97

In Fig. 3.9 DMTA results for the neat resin and for HPE/Nylon 6,6 monolayer, in terms of storage modulus, E', loss modulus, E'', and loss factor, tanδ, are reported. In general, a peak in tanδ curve, corresponding to a flex point in the E' curve, is attributable to the structural relaxation of the network and the corresponding temperature is assumed as the glass transition temperature, Tg, of the material. In the DMTA relative to the net resin, two main relaxation peaks appear in the tan δ curve, at 215 °C and 260 °C. The lower peak temperature can be related to the relaxation of the network as formed upon the curing process; the higher one can be due to the relaxation of the same network after the thermal post-cure induced by

the permanence at temperatures higher that the resin Tg during the DMTA test itself. The increase of the storage modulus in the temperature range between the two relaxation peaks confirms the proposed network densification, owing to the further crosslinking reactions occurring during the test.

The epoxy/ Nylon mat monolayer shows a more complex dynamic mechanical behavior, with many relaxations occurring in different temperature ranges. In particular, the E' curve presents a first inflection point at about 50 °C, due to the glass transition temperature of the Nylon 6,6. [23] A second and third relaxation occur at higher temperatures, which are better shown by the E'' curve peaks. They refer to structural relaxations of portions of the network having different rigidity. In particular, the one at lower temperature (140 °C) could be attributed to the relaxation of epoxy network portions closer to the interface between the epoxy matrix and the nanofibrous mat. The higher temperature relaxation (170 °C) is lower than the main relaxation peak of the neat resin (matrix) and it likely refers to the network portion further away from the nanofibrous mats. The effect of the thermal post-cure induced by the DMTA is not visible in the DMTA curve of the monolayer because the measurement was interrupted before reaching the melting temperature of Nylon.

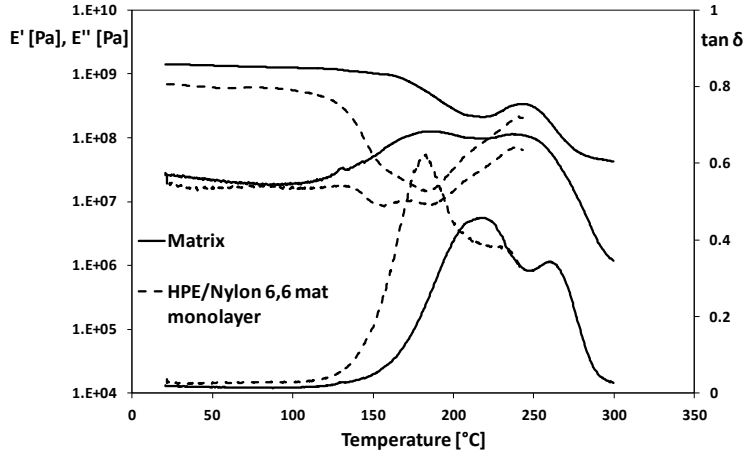

Figure 3.9 DMTA of cured neat resin (Matrix) and HPE/Nylon 6,6 monolayer.

DMTA was also performed on LPE/Nylon 6,6, LPE/PVDF, LPE/PAN and LPE/PSF monolayers (see Figure 3.10). We observe (i) for the neat resin a glass transition temperature of 90 °C; (ii) for PSF and PAN monolayers DMTA curves that are almost coincident with those of the neat resin (a single relaxation); (iii) for Nylon 6,6 and PVDF monolayers two main relaxation phenomena. In particular, the tanδ curve of LPE/Nylon 6,6 monolayer shows two different peaks, the first one at 90°C and the second one at 110 °C. The first peak can be due to the relaxation of outer neat resin layers present in the monolayer (see Fig. 3.4a), the second one is probably attributable to the central mat/resin region. In LPE/PVDF monolayer, the main peak of tanδ curve is also at 90 °C and a shoulder is present at higher temperature. Also for this system an inner layer with mat and resin was sandwiched between two net resin layers (Fig. 3.4b). Being the Nylon and PVDF nanofibers concentrated in a thinner region, they have an impact on the relaxation temperature of the resin fraction they have incorporated. Conversely, the PAN mat was significantly swollen by the resin and apparently not interacting with it, therefore the resin relaxation is not affected by mat. Likewise, the poor adhesion between PSF nanofibers and resin supports the absence of effects on the glass transition temperature of the resin in LPE/PSF.

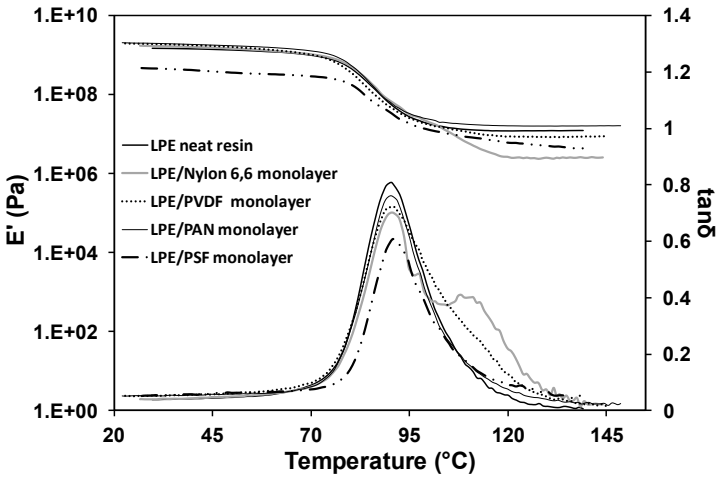

Figure 3.10 DMTA results of LPE matrix, LPE/Nylon 6,6, LPE/PVDF, LPE/PAN and LPE/PSF monolayers.

3.4 Conclusions

In this chapter, mat/resin monolayers and three layer systems, consisting of a electrospun mat sandwiched between two CF fabric layers, were produced and characterized by SEM microscopy to gather some indications on (i) the resin uptake and retention ability of the mats; (ii) their compatibility with the resin; and (iii) the toughening mechanism that can be activated by the nanofibers. In particular, electrospun mats made of various thermoplastic monomers (Nylon 6,6, PSF, PVDF and PAN) and a rubber/thermoplastic blend were tested with two different epoxy formulations, characterized by different cure temperatures and mechanical properties. For PSF mats the two different cure temperatures resulted in two different morphologies, nanofibrous for the low cure temperature resin, and particulate for the high cure temperature/high performance resin. Calorimetric and dynamic-mechanical-thermal analyses were also performed to evaluate the effect of the mats on the cure behavior and glass transition of the resin. In particular, Nylon 6,6 and PVDF appear to be the most compatible nanofiber materials towards both resin systems and their mats seem to be promising candidates as toughening elements of epoxy-based laminates. They also show minimal effects on the Tg of the matrix. These results encourage in proceeding with testing their performance in carbon-reinforced laminates.

REFERENCES

[1] Collyer AA (1994). Rubber Toughened Engineering Plastics. Springer Science & Business Media.

[2] Bucknall C (2013). Toughened Plastics. Springer.

[3] Kinloch AJ, Shaw SJ, Tod DA, Hunston DL. Deformation and fracture behaviour of a rubber toughened epoxy: 1. Microstructure and fracture studies. Polymer 1983;24:1341-1354.

[4] Garg AC, Mai YW. Failure Mechanisms in Toughened Epoxy Resins - A Review. Compos Sci Technol 1988;31:179-223.

[5] Cho JB, Hwang JW, Cho K, An JH, Park CE. Effect of morphology on youghening of tetrefucnctional epoxy resins with poly(ether imide). Polymer 1993;34(23):4832-4836.

[6] Kim BS, Chiba T, Innoue T. Phase separation and apparent phase dissolution during cure process of thermoset/thermoplastic blend. Polymer 1995;36(1):67-71.

[7] Yoon T, Kim BS, Lee DS. Structure Development via Reaction-Induced Phase Separation in Tetrafunctional epoxy/Polysulfone Blends. J Appl Polym Sci 1997;66:2233-2242.

[8] Yun NG, Won YG, KimSC. Toughening of carbon fiber/epoxy composite by inserting polysulfone film to form morphology spectrum. Polymer 2004;45:6953-6958.

[9] Kim JY, Lee HK, Kim SC. Surface structure and phase separation mechanism of polysulfone membranes by atomic force microscopy. J Membrane Sci 1999;163:159-66.

[10] Li G, Huang Z, Li P, Xin C, Jia X, Wang B, He Y, Ryu S, Yang X. Curing kinetics and mechanisms of polysulfone nanofibrous membranes toughened epoxy/amine systems using isothermal DSC and NIR. Thermochim Acta 2010;497:27-34.

[11] Li G, Li P, Yu Y, Jia X, Zhang S, Yang X, et al. Novel carbon fiber/epoxy composite toughened by electrospun polysulfone nanofibers. Mater Lett 2008;62(3):511-4.

[12] Li G, Li P, Zhang C, Yu Y, Liu H, Zhang S, et al. Inhomogeneous toughening of carbon fiber/epoxy composite using electrospun polysulfone nanofibrous membranes by in situ phase separation. Compos Sci Technol 2008;68:987-94.

[13] Kim JK, Robertson RE. Toughening of thermoset polymers by rigid crystalline particles. J Mater Sci 1192;27:161-174.

[14] Palazzetti R, Zucchelli A, Gualandi C, Focarete ML, Donati L, Minak G, et al. Influence of electrospun Nylon 6,6 nanofibrous mats on the interlaminar properties of gr-epoxy composite laminates. Compos Struct 2012;94(2):571-579.

[15] Hamer S, Leibovich H, Green A, Intrater R, Avraham Ri, Zussman E, Siegmann A, Sherman D. Mode I Interlaminar Fracture Toughness of Nylon 66 Nanofibrilmat Interleaved Carbon/Epoxy Laminates. Polym Compos 2011;32:1781-1789.

[16] Akangah P, Lingaiah S, Shivakumar K. Effect of nylon-66 nano.fiber interleaving on impact damage resistance of epoxy/carbon fiber composite laminates. Compos Struct 2010;92:1432-1439.

[17] Palazzetti R, Yan X, Zucchelli A. Influence of geometrical features of electrospun nylon 6,6 interleave on the CFRP laminates mechanical properties. Polym Compos 2014;35:137-150.

[18] Daelemans L, van der Heijden S, De Baere I, Rahier H, Van Paepegem W, De Clerck K. Nanofibre bridging as a toughening mechanism in carbon/epoxy composite laminates interleaved with electrospun polyamide nanofibrous veils Compos Sci Technol 2015;117: 244-256.

[19] Magniez K, De Lavigne C, Fox BL. The effects of molecular weight and polymorphism on the fracture and thermo-mechanical properties of a carbon-fibre composite modified by electrospun poly (vinylidene fluoride) membranes. Polymer 2010;51:2585-2596.

[20] Zhang J, Yang T, Lin T, Wang CH. Phase morphology of nanofibre interlayers: Critical factor for toughening carbon/epoxy composites. Compos Sci Tech 2012;72(2):256-262.

[21] Yoon T, Kim BS, Lee DS. Structure Development via Reaction-Induced Phase Separation in Tetrafunctional epoxy/Polysulfone Blends. J Appl Polym Sci 1997;66:2233-2242.

[22] Oyanguren PA, Aizpurua B, Galante MJ, Riccardi CC, Corta' Zar OD, Mondragon I. Design of the Ultimate Behavior of Tetrafunctional Epoxies Modified with Polysulfone by Controlling Microstructure Development. J Polym Sci B Polym Phys 1999;37:2711-2725.

[23] Mark JE (2007). Physical Properties of Polymers Handbook. Springer, New York, USA.

4. ELECTROSPUN NYLON 6,6 MATS IN HIGH PERFORMANCE EPOXY LAMINATES

4.1 Introduction

The purpose of this chapter is to study the interlaminar toughening behavior of electrospun nanofibrous mats when placed as inter-layers in carbon fiber reinforced epoxy laminates, and their effects on properties of the laminates, such as porosity, mechanical and thermal resistance. The toughening mechanisms activated by the mats are also investigated.

According to the preliminary results obtained from the analyses performed on monolayers and three-layers systems, presented in the previous Chapter, Nylon 6,6 membranes were selected. In particular, from the morphological analysis of the fracture surfaces of mat-resin monolayers, Nylon showed to exert toughening properties towards both the two resin systems used, one with high temperature of cure and high thermo-mechanical performance (High Performance Epoxy, HPE), the other curing at room temperature, with higher fracture toughness but lower Tg (Low Performance Epoxy, LPE). In this chapter the author focused the attention on the HPE resin, and thus its composites, while the LPE laminates will be described in the Chapter 5.

This Chapter consists of three parts. The first part deals with the effect of the curing pressure on the morphological and thermal properties of high performance epoxy laminates interleaved with a Nylon 6,6 mat, placed in the middle plane. A second part investigates the influence of the number of mats on both thermal and mechanical properties of laminates comparing two arrangements, one containing a single mat placed in the middle plane of the laminate and the other containing one mat at each interlayer. Finally the third part reports the results of mode I interlaminar fracture toughness test on the laminates containing Nylon 6,6 membranes, and the toughing mechanism activated by the nanofibrous mat is also discussed.

4.2 Materials and methods

The epoxy resin used as matrix of the laminates on which the author focused the attention in this chapter consisted of a blend of a tetrafunctional monomer (TGDDM), a bifunctional monomer (DGEBA) and an amine curing agent (DDS). The weight ratio of two epoxy monomers TGDDM: DGEBS was 84:16, the used amount of the curing agent was 26 phr (per hundred of resin by weight). All reagents were provided by Sigma Aldrich (Italy).

High modulus unidirectional carbon fiber fabric of nominal areal weight 300 gr/m^2 and Young's modulus 398 MPa, purchased by Dalla Betta Group s.r.l., was used as reinforcement.

The laminates were manufactured by hand lay-up of 10 layers of carbon fiber fabric, in the interleaved systems one or more electrospun mat being placed in two different arrangements: in the middle plane or at each interlayer. Thus, a curing process consisting of a heating ramp from room temperature to 180 °C at 2 °C/min and an isothermal rest at 180 °C for 2 h was carried in autoclave, applying a pressure of 2.5 or 3.5 bar, or in press.

More details on materials, thermal and mechanical properties of the matrix and procedures of the preparation of the laminates are described in the sections A.1 and A.2 of appendix. In particular, in Tab. A.3 carbon fiber type, curing process and carbon fiber weight fraction of laminates characterized in this Chapter, are indicated.

Dynamic Mechanical Thermal Analysis (DMTA), Three Point Bending (TPB) test, Mode I delamination test (on Double Cantilever beam (DCB) samples), Short beam shear (SBS) test and morphological analysis via Scanning Electron Microscopy (SEM) have been performed. All the details of the thermal and mechanical tests and the procedures of preparation of SEM samples are provided in the paragraph A.3 of the appendix.

4.3 Results and discussion

4.3.1 Effect of the curing pressure on morphology and visco-elastic properties of CF-reinforced laminates with a single mat interleaf in the mid-plane.

In this section the author presents the results of a study carried out on four different laminates: HPECF_A1, HPECF_A2, HPECFN_A1, HPECFN_A2 (see Tab. A.3 of appendix). HPECF_A1 and HPECFN_A1 laminates were produced in autoclave, with a pressure of 2.5 atm (leading to comparable carbon fiber weight fractions, W_{CF}, of 52% and 53%, respectively); while HPECF_A2 and HPECFN_A2 were obtained applying a pressure of 3.5 atm (with a final W_{CF} of 62% and 64%, respectively). In order to evaluate the quality of the laminates in terms of carbon fiber/resin interface, thickness of mat/resin interlayer and interface between the carbon fibers-reinforced plies and the Nylon 6,6 interlayer, morphological analysis via SEM was carried out on the various laminates. In particular, Figure 4.1a shows the SEM micrograph for the transverse plane of the fractured surface of HPECFN_A1 laminate at relatively high magnification. Only limited carbon fiber-matrix debonding is visible, suggesting a general good carbon fiber/matrix adhesion. As expected, similar results were observed for the HPECF_A1, HPECF_A2 and HPECFN_A2 systems (micrographs not reported for brevity). In Fig. 4.1 b and c, SEM micrographs at lower magnification of polished and etched cross-sections of the HPECF_A1 and HPECFN_A1 systems are reported, respectively. Analyzing these images it seems that there no significative difference in the quality of two laminates, in terms of porosity, that is the presence of a Nylon mat does not affect the consolidation process. Similar results can be noted for HPECF_A2 and HPECFN_A2 (SEM micrographs not reported). In the presence of the mat (HPECFN_A1) a well-defined resin-rich interlayer in the middle plane, that is located between ply 5^{th} and 6^{th}, can be observed (panel c). As expected, the thickness of this interlayer is strongly affected by the applied pressure upon cure: it is about 210 µm for HPECFN_A1 (curing pressure of 2.5 bar) and 100 µm for HPECFN_A2 (curing pressure 3.5 bar). No evidence of discontinuity in the matrix

across the boundary between the carbon reinforced ply and the nanofibrous mat can be observed even at high magnification, both in HPECFN_A1 and HPECFN_A2 (see Fig. 4.1 d, for HPECFN_A1).

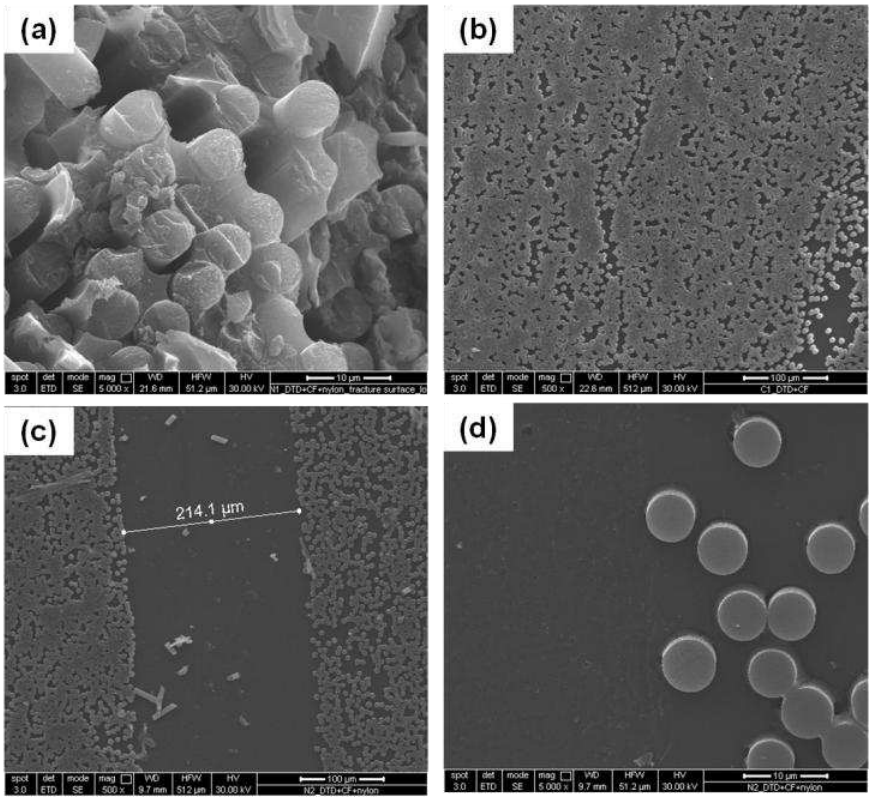

Figure 4.1 SEM micrographs of: (a) HPECFN_A1 fractured section from flexural test; (b) HPECF_A1 and (c), (d) HPECFN_A1 laminates polished transverse sections at two magnifications.

Figure 4.2 a shows the results of DMTA analysis performed on the composite laminate without Nylon mat (HPECF_A2 laminate), before and after the thermal post curing treatment, compared to the neat resin DMTA curves, as reference. The general trend observed for the neat resin was maintained for the laminate, with only a slight increase of E' and decrease of tanδ values in the composite samples, due to the stiffening effect of carbon fibers in the epoxy network. The post-curing

treatment at 230 °C led, as expected, to a more crosslinked network, with a Tg of about 260 °C.

With respect HPECF_A2 system, the introduction of the Nylon mat caused in HPECFN_A2 an increase of the damping capacity in the non post-cured composite, as revealed by the larger area under tanδ curve, and a slight decrease of the glass transition temperature (see Fig. 4.2b). After post-cure the DMTA curve of HPECFN_A2 closely resembles the one of the corresponding laminate without mat (HPECF_A2). Similar behavior was observed for the systems cured at lower pressure, hence with a lower carbon fiber weight fraction (HPECF_A1 and HPECFN_A1) (here not reported). The presence of the embedded nanofibrous mat had a negligible influence on the composite's Tg.

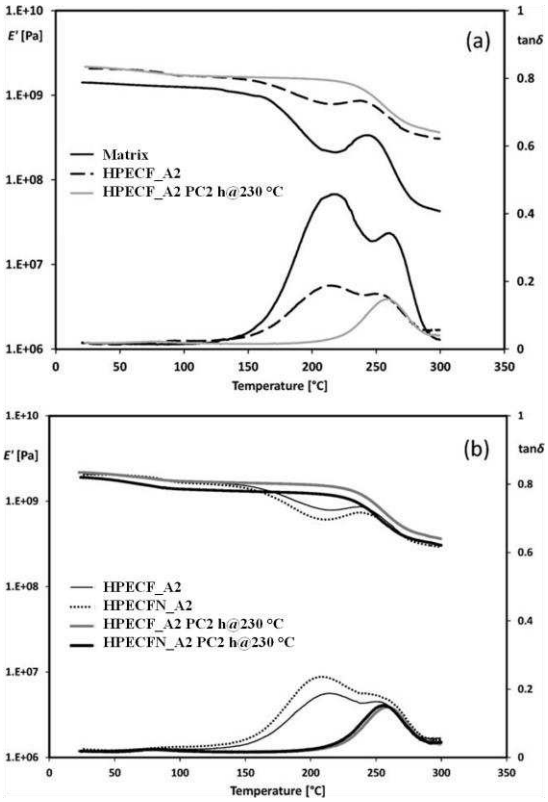

Figure 4.2 DMTA results of: (a) neat resin (Matrix) and HPECF_A2 laminate, before and after post-cure; (b) HPECF_A2 and HPECFN_A2 laminate panels.

This first part of the study highlights that the presence of a Nylon 6,6 nanofibrous mat did not affect the quality of the laminate while a difference in the thickness of the mat/resin interlayer was observed when different applied pressure values were used during the curing process in autoclave. No detrimental effect were observed on T_g of the interleaved systems.

4.3.2 Effect of the number of mat-toughened interleaves on the morphology, visco-elastic and mechanical properties of CF-reinforced laminates

In this paragraph the comparison between systems having a different number of Nylon 6,6 electrospun mats as interlayer is presented. In order to evaluate the quality of the manufactured panels, a morphological analysis via SEM has been conducted on the samples cross-sections after an etching treatment (for the details of the procedure see section A.3 of the Appendix). In Fig. 4.3 a-c representative micrographs of the three systems described in this paragraph, one without mat, as reference system, one with a Nylon 6,6 mat in the middle plane and third one with a Nylon mat for each interlayer, are shown. In HPECF_P and $HPECFN_1$_P randomly distributed voids were observable. Fewer pores were present in $HPECFN_9$_P. In support of this qualitative analysis, the porosity degree values, calculated by image analysis, are reported in Tab. 4.1. The porosity degree of $HPECFN_9$_P was halved with respect to HPECF_P and $HPECFN_1$_P. The improvements in the laminate consolidation when Nylon 6,6 mats were added at each interlayer were likely due to the mats acting as "resin reservoirs", that is the excess of resin present on the pre-impregnated fabrics during hand lay-up can be absorbed by mats and then released by them when the laminate is pressed for curing. In Fig. 4.3 b, concerning $HPECFN_1$_P, a well-defined Nylon mat/resin region at the middle plane is clearly evident; instead in $HPECFN_9$_P the mat/resin interleaves are thinner and some of them visible only at higher magnifications. A close look to an interleaf (Fig. 4.3 e) reveals the fingerprints of the nanofibers left after the etching treatment. The image shows that the nanofibers were randomly and uniformly distributed into the resin, but confined in the interlayer region.

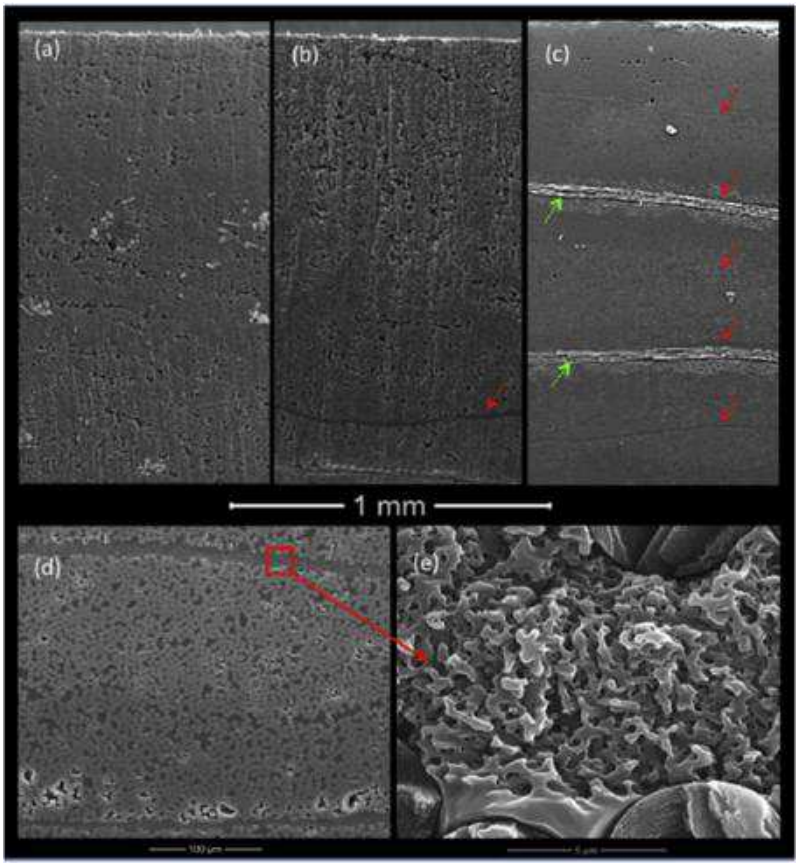

Figure 4.3 SEM micrographs of cross-sections: (a) HPECF_P; (b) HPECFN$_1$_P; (c) HPECFN$_9$_P; (d) zoomed part from (c); (e) enlarged detail of (d). In Fig. (b) and (c) the red and green arrows indicate the mat/resin interlayers and the stitching threads of carbon fiber fabric, respectively.

Table 4.1 Properties of the laminates, with one (HPECFN$_1$_P) and nine (HPECFN$_9$_P) Nylon 6,6 mats as interlayers and with no mats HPECF_P) as reference.

System	Porosity degree, % ϕ	Glass transition temperature T_g (°C)	Transverse flexural modulus E_f (GPa)	Interlaminar shear strength ILSS (MPa)
HPECF_P	9.9±0.4	265	5.82±0.39	44.67±0.96
HPECFN$_1$_P	10.8±0.4	263	5.39±0.19	46.05±0.62
HPECFN$_9$_P	5.2±0.2	263	5.51±0.07	59.10±4.21

In Fig. 4.4 DMTA results, carried out on neat resin and laminates, are presented and the relative glass transition temperatures are reported in Tab. 4.1. The tanδ curve of the resin shows a relaxation peak at high temperature (Tg=265 °C). With respect to the neat resin (Matrix in the figure), the laminates show similar dynamic mechanical thermal behavior, with an increase of E' in the whole temperature range analyzed and in particular in the rubbery plateau, and a decrease of tanδ. Comparing to HPECF_P and $HPECFN_1$_P, in $HPECFN_9$_P an enlargement of the main tanδ peak and the presence of a second small peak, at about 180 °C, can be observed, probably due to localized plasticization effects in the matrix caused by the presence of the mats at each interlayer. Interestingly, the comparison of the glass transition temperatures (see Tab. 4.1) of the laminates highlighted no detrimental effects of Nylon mats on thermal resistance.

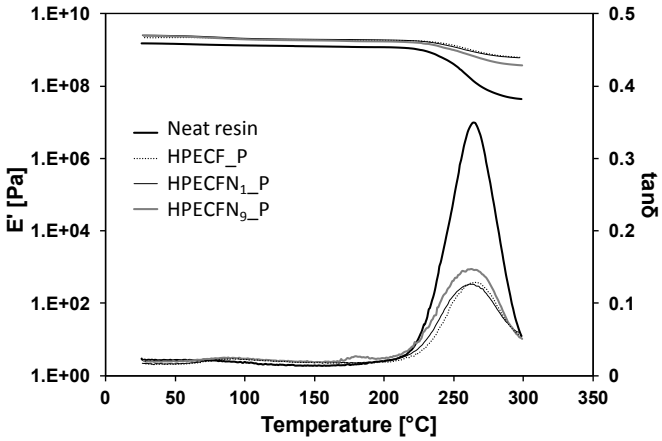

Figure 4.4 DMTA results of neat resin and the three laminate panels.

Transverse flexural modulus, E_f, and interlaminar shear strength, ILSS, evaluated for the three systems, are reported in Tab. 4.1, too. The addition of nanofibrous Nylon 6,6 mats did not affect the E_f, while the ILSS increased of only 3% in the $HPECFN_1$_P system but of about 30% for $HPECFN_9$_P, comparing to HPECF_P. The low increase of ILSS in $HPECFN_1$_P is likely attributable to the relatively high porosity degree. For $HPECFN_9$_P the significant increase of ILSS is referable to the toughening effect exerted by the mats.

4.3.3 Study of the interlaminar toughening effect of the Nylon 6,6 mat interleaf

According to the geometry of the DCB sample [1, 2], Mode I delamination tests were performed on the laminates in which only a mat, placed in the middle plane, was present. Interest of the author was also to investigate the effect of the interlayer thicknesses. For these reasons the laminates studied in this part are HPECFN_A1 and HPECFN_A2 and, as reference, HPECF_A1 and HPECF_A2.

In Fig. 4.5 a and c, representative Load vs Crack Opening Displacement (COD) curves for systems without and with Nylon are shown, respectively. The discrete dots in each curve identify the points at which visual crack length measurements were acquired to evaluate the critical Strain Energy Release Rate, G_{IC}. [2, 3] A qualitative analysis of curves reveals an instable delamination growth, generally called of the "stick-slip" type, characterized with periods of slow delamination growth followed by a very rapid growth, yielding sharp drops in the load-displacement curve, and a reloading phase. [4-6] This behavior was observed in all tested samples and is probably caused by the non-homogeneous fiber/matrix distribution at the meso-scale, typical of crimped UD fabrics. Indeed, in the fractured surfaces of all DCB samples after complete delamination (Fig. 4.6 a-c), transverse weft ties and carbon fiber yarns crimps as well as resin-rich scattered zones are well visible, which can likely be the main cause of the observed stick-slip growth behavior.

From a visual inspection of the delaminated surfaces, it is evident that delamination in the Nylon 6,6 interleaved systems always began within the mat/resin interlayer, while during propagation deviated towards either the upper or the lower CF plies. As result, in areas far from the initial crack front, the resin impregnated Nylon mat appeared unevenly fractured. This is evident in Fig. 4.6 b, c, where a close-up visual inspection of the fracture surfaces reveals, in the propagation zones, "mat-rich" regions on one delaminated face of the sample, which correspond to "mat-poor" regions on the equivalent part of the opposite delaminated face.

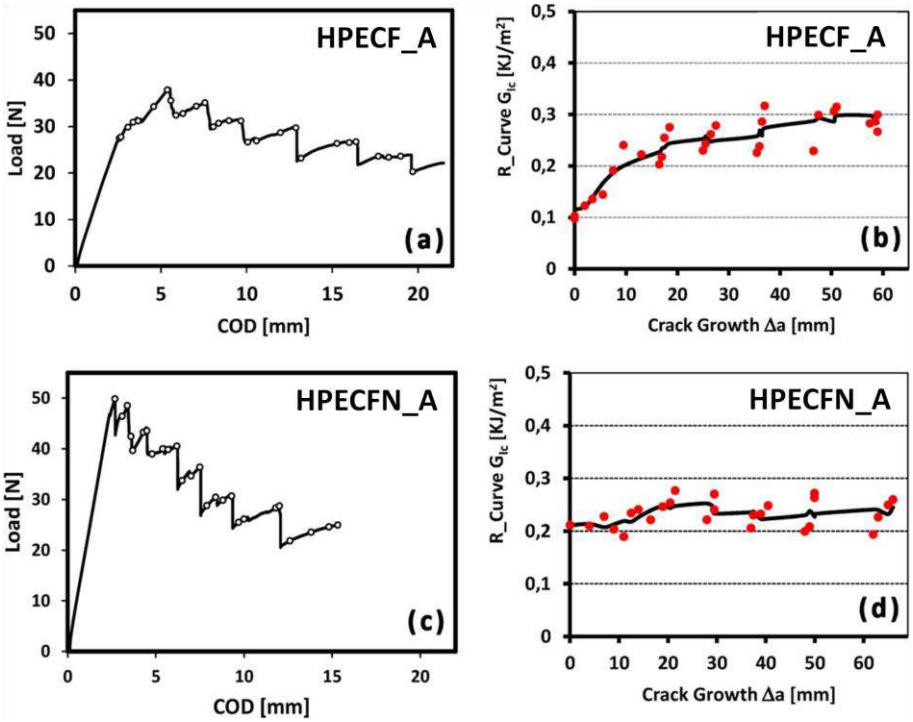

Figure 4.5 Representative Load versus Crack Opening Displacement (COD) (left) and corresponding R-Curves (right).

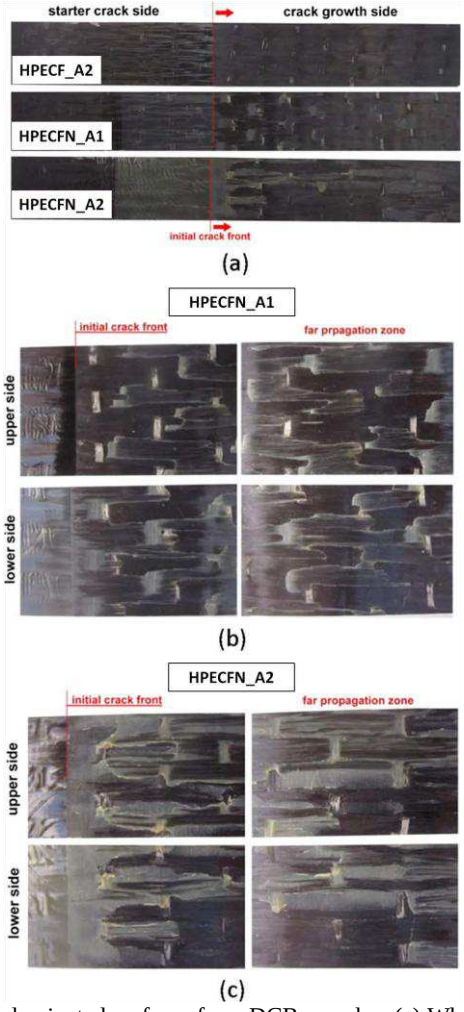

Figure 4.6 Photos of delaminated surfaces from DCB samples. (a) Whole samples; (b) close-up photos of HPECFN_A1 and (c) HPECFN_A2

One main difference visually observed during delamination of systems with and without Nylon mat, as shown in Fig. 4.7, was the absence of fiber bridging behind the growing crack front in the HPECFN_A systems (Fig. 4.7 b). This is probably due to the delamination in the mat modified systems mainly confined within the Nylon mat interlayer.

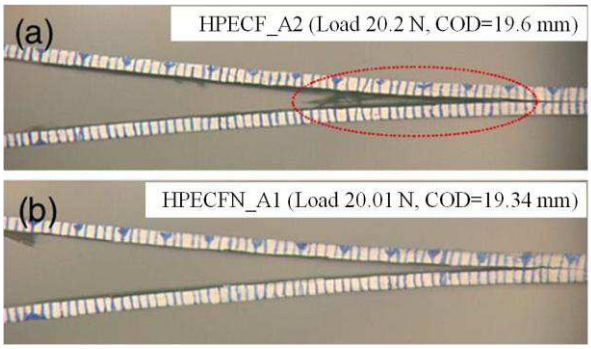

Figure 4.7 Photos of representative HPECF_A and HPECFN_A samples during delamination, evidencing the different fiber bridging density development by the two systems.

The R-Curves determined from the plot reported in Fig. 4.5 a, c are displayed in Fig 4.5 b, d, respectively. They can be considered representative of both HPECF_A and HPECFN_A systems, respectively (the different carbon fiber weight fractions and the different interlayer thickness did not produce any meaningful difference in these plots). Although the "stick-slip" delamination behavior is causing some scattering in the R-Curves, it is evident that the HPECF_A systems had a typical growing R-Curve, which was mainly related to the presence of fiber bridging, while the HPECFN_A systems showed an almost flat R-Curve.

In Fig. 4.8 the values of the initiation and propagation fracture energy, G_{IC_init} and G_{IC_prop} are reported for four investigated systems. The introduction of the electrospun Nylon nanofibrous mat in the composite always caused a significant increase of $G_{IC\_init.}$ with respect the systems without mat. The G_{IC_init} of Nylon mat interleaved systems was pretty similar, irrespective of the different carbon fiber weight fraction and thickness of the mat/resin region, and this was in accordance with the fact that in both systems the fracture failure started within the Nylon/epoxy interleaf (cohesive failure). Regarding $G_{IC\_prop.}$, this value was higher for the HPECF_A systems, due to the more consistent development of fiber bridging.

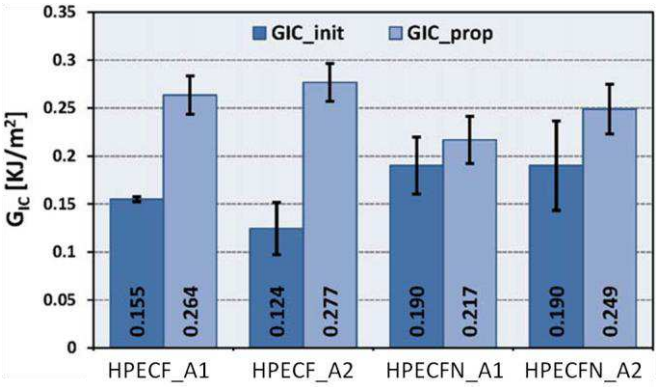

Figure 4.8 Values of initial and propagation G_{IC} for the all studied systems.

The results of DCB tests were further supported by the SEM morphological analysis of delaminated surfaces. In Fig. 4.9 SEM images of delamination surfaces of HPECF_A1 are reported. Panel a refers to areas close to the interlaminar precrack, (indicated as "near zone"), spanning just few millimeters from the initial delamination front, while panel b to areas at least 30 mm further back from the initial delamination front (indicated as "far zone"). In general, a good fiber/matrix adhesion was observable, with a balanced presence of sites of cohesive matrix fracture and interfacial fracture. Cluster of fibers were present in the "far zone" (panel b), probably consequence of fiber bridging phenomena. Similar morphologies are noted for the delaminated surfaces of HPECF_A2 (SEM images not reported for brevity).

In Fig 4.10 delaminated surfaces SEM micrographs of HPECFN_A1 (panel a, b and e) and HPECFN_A2 (panel c, d and f) are reported. Micrographs shown in Fig. 4.10 a, c, e, f are zoomed on the "near zone"; micrographs of Fig. 4.10 b, d refers to the "far zone". With regards to both HPECFN_A1 and HPECFN_A2 systems, different fracture mechanisms can be proposed from inspection of the two zones, as already suggested by the visual inspection of the delaminated surfaces (Fig. 4.6). In the "near zone" (Fig. 4.10 a, c) the delaminated surfaces of both systems were covered by the epoxy/mat layer, indicating that the delamination initially run within this interlayer (cohesive fracture). On the contrary, in the "far zone" (Fig. 4.10 b, d) "epoxy/mat-rich" patches partially covered the underlying carbon fibers, or showed

the marks left by the carbon fibers, thus suggesting that the crack developed also at the carbon fibers/matrix interface (cohesive/adhesive mixed fracture). The different thickness of the mat/resin interleaf of the two HPECFN_A systems affected the features of the initial crack front zone. While in HPECFN_A1, system characterized by the lower W_{CF} and the thicker interleaf, the fractured surface showed a compact epoxy/mat layer (Fig. 4.10 a), in HPECFN_A2 this layer is so much thinner that reveals the impregnated carbon fibers located underneath, when observed at low magnification (Fig. 4.10 c). In the "far zones" (panel b for HPECFN_A1 and d for HPECFN_A2, Fig. 4.10) the presence of clustered fibers is much reduced if compared to HPECF_A1 (Fig. 4.9 b), supporting the above-formulated hypothesis of fiber bridging hindrance operated by the mat/resin interleaf.

Micrographs at higher magnification of the delaminated surfaces shown in Fig. 4.10 a, c are reported in Fig. 4.10 e, f, respectively. The nanofibrous morphology of the interleaved mat is revealed either by the presence of the random nanofibers or their fingerprint left upon delamination, especially in the sample with thinner nanofiber interleaf HPECFN_A2 (Fig. 4.10 f).

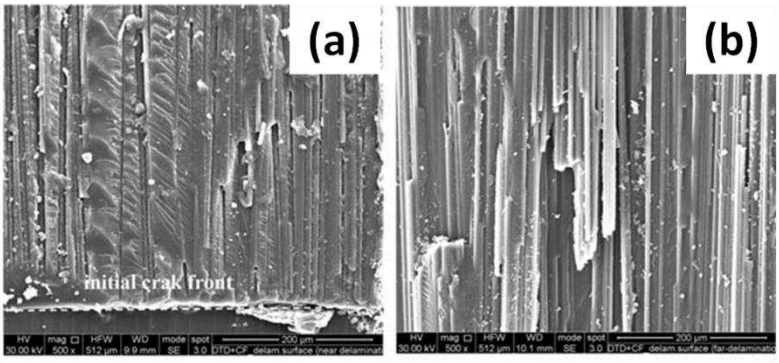

Figure 4.9 SEM micrographs of HPECF_A1 delaminated surfaces after DCB test: (a) area close to the interlaminar precrack; (b) area far from the interlaminar precrack.

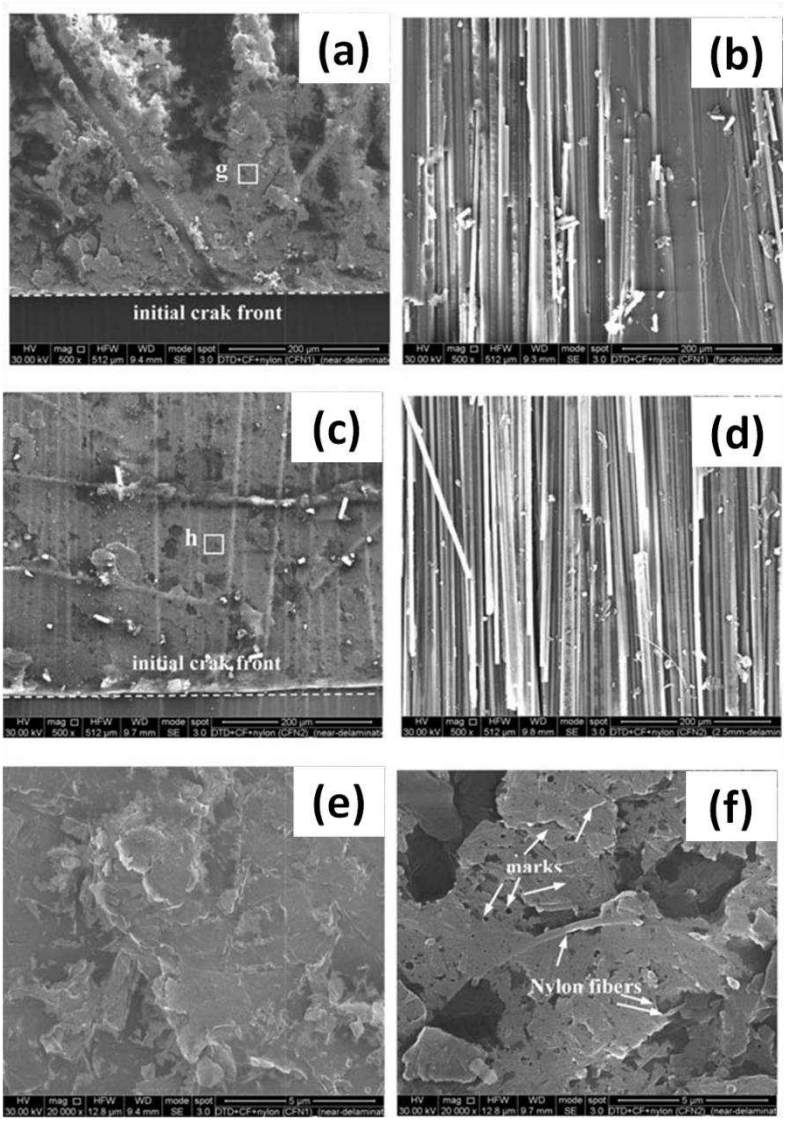

Figure 4.10 SEM micrographs of delaminated surfaces after DCB test: (a) HPECFN_A1, area close to the interlaminar precrack; (b) HPECFN_A1, area far from the interlaminar precrack; (c) HPECFN_A2, area close to the interlaminar precrack; (d) HPECFN_A2, area far from the interlaminar precrack; (e) HPECFN_A1, high magnification of area close to the interlaminar precrack; (f) HPECF2_A2, high magnification of area close to the interlaminar precrack.

4.4 Conclusions

The effect of electrospun Nylon 6,6 nanofibrous membranes, interleaved at the mid-section or at each interlayer of unidirectional carbon fiber reinforced epoxy composite, has been assessed towards morphological, thermo-mechanical and the mechanical analysis of the laminate. A highly cross-linked, high glass transition temperature but low fracture toughness epoxy resin wass consider as matrix.

The applied pressure during the curing stage significantly affected the thickness of the nanofibers containing resin-rich interlayer and a significant reduction in laminate porosity was obtained when mats were placed at each interlayer, probably acting as resin reservoirs and thus collaborating to a more uniform distribution of the resin across the laminate upon curing. No detrimental effects on Tg and trasversal flexural modulus were observed.

Mode I delamination test on DCB samples showed an increase of the initial fracture toughness up to 50% between the interleaved and not interleaved systems, benefiting of toughening properties of Nylon 6,6 nanofibrous mats.

REFERENCES

[1] ASTM D 5528 – 01. Standard Test Method for Mode I Interlaminar Fracture Toughness of Unidirectional Fiber-Reinforced Polymer Matrix Composites (2007).

[2] Mallick PK (2007). Fiber-reinforced Composites – Materials, Manufacturing and Design. Taylor & Francis Group.

[3] Moore DR, Pavan A, Williams JG (2001). Fracture Mechanics Testing Methods for Polymers Adhesives and Composites. ESIS publication.

[4] Suppakul P, Bandyopadhyay S. The effect of weave pattern on the mode-I interlaminar fracture energy of E-glass/vinyl ester composites. Composites Sci Technol 2002;62(5):709-717.

[5] Gill AF, Robinson P, Pinho S. Effect of variation in fibre volume fraction on modes I and II delamination behaviour of 5HS woven composites manufactured by RTM. Composites Sci Technol 2009;69(14): 2368-2375.

[6] Phong NT, Gabr MH, Okubo K, Chuong B, Fujii T. Improvement in the mechanical performances of carbon fiber/epoxy composite with addition of nano-(polyvinyl alcohol) fibers. Compos Struct. 2013;99:380-387.

5. COMPARATIVE ANALYSIS OF NYLON 6.6 AND PVDF ELECTROSPUN MATS IN LOW PERFORMANCE EPOXY- CARBON FIBRE LAMINATES

5.1 Introduction

In this chapter the author focused the attention on the interlaminar toughening properties of electrospun polymer membranes in carbon fiber reinforced laminates, in which the matrix is an epoxy formulation characterized by high fracture toughness but low Tg. It is called low performance epoxy (LPE).

Preliminary analysis performed on LPE resin/mat monolayers (see Chapter 3) showed that Nylon 6,6 and Polyvinylidene fluoride (PVDF) can act as toughening agents, when added to the resin. In addition difference in the swelling properties of these two polymer mats by the LPE resin were observed. For these reasons Nylon 6,6 and PVDF were the selected polymer to use as nanofibrous interlayers in laminates.

The effect of the mats on thermal, mode I and mode II delamination properties of the laminates were investigated, making some assumptions on different toughening mechanisms exerted by the mat in the laminate.

5.2 Materials and methods

The selected matrix for the laminates studied in this chapter consisted of an epoxy monomer and an amine hardener, while a non- crimp unidirectional carbon fiber fabric (nominal areal weight 300 gr/m^2) was used as reinforcement.

The studied laminated in this chapter are LPECF_V, LPECFN_V and LPECFP_V (see Tab. A.3 of the appendix). They were assembled by hand lay-up. Electrospun Nylon 6,6 or Polyvinylidene fluoride (PVDF) interleaved laminates were prepared by laying the nanofibrous mat between the 6th and the 7th layer of 12

carbon fiber fabric layers. The curing process was carried out by means the vacuum bagging technique, at room temperature for 8 hr. Then, a post-cured process was carried out in oven, for 24 h at 60 °C. Denomination, carbon fiber weight fraction and other information of the laminates are described in Tab. A.3 of the appendix.

Dynamic Mechanical Thermal Analysis (DMTA), Mode I delamination test (on Double Cantilever beam (DCB) samples), Mode II End Notched Flexure (ENF) test and morphological analysis via SEM have been performed on samples from laminates.

More details of materials, preparation procedures and characterization techniques are reported in the sections A.1, A.2 and A.3 of appendix, respectively.

5.3 Results and discussion

DMTA, mode I and mode II delamination tests have been carried out on mat interleaved laminates, as well as on the laminate that does not contain the mat, for comparative purposes.

In Fig. 5.1 storage modulus E' and loss factor tanδ of all systems, as obtained from DMTA, are reported. In regards to laminate without mat (LPECF_V system), an inflection point in E' curve, corresponding a peak in tanδ, can be noted. The glass transition temperature value (measured as tanδ peak temperature) was about 93 °C.

Focusing the attention on the interleaved systems, for both laminates (LPECFN_V and LPECFP_V systems), E' curves show two inflection points, probably consequence of the overlap of two different relaxation phenomena. The corresponding tanδ curves show each one only a peak, the temperature value at which the peak occurs being higher than LPECF_V system, and somewhat higher for LPECFP_V than for LPECFN_V. As already discussed for the monolayers (see paragraph 3.4, Chapter 3), these phenomena can be explained as consequence of the presence in the laminates of a layer made of mat and resin.

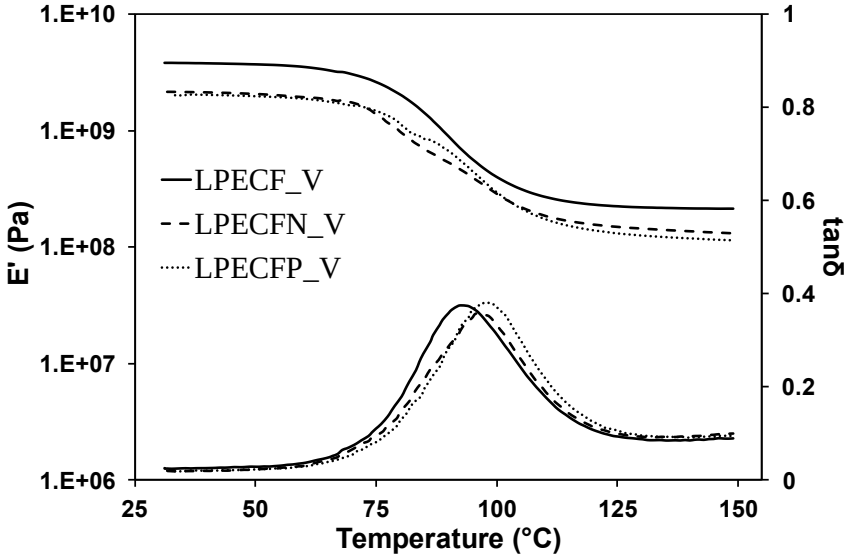

Figure 5.1 DMTA results of the Nylon 6,6 mat interleaved laminate (LPECFN_V), PVDF mat interleaved laminate (LPECFP_V) and laminate without mat, as reference (LPECF_V).

Representative load/displacement curves (panels a-c) and the corresponding R-curves (panels a'-c') from Mode I delamination tests for LPECF_V, LPECFN_V and LPECFP_V systems are reported in Fig. 5.2. The trend of R-curves was similar for all systems, with a general increase of fracture energy during propagation. This effect is generally attributed to fiber bridging, observed in the delamination front during the test for all three systems (see Fig. 5.3). It is well known that fiber bridging is observed mainly for the unidirectional DCB specimens than for the multidirectional ones. Acting as a toughening mechanism in UD laminates by hampering crack growth, fiber bridging is of little or no practical relevance for most of the multiply laminated composite structures. In fact, it can be considered an artifact of the DCB test on unidirectional materials which makes the G_{IC_prop} values much less meaningful than the G_{IC_init}. [1-4]

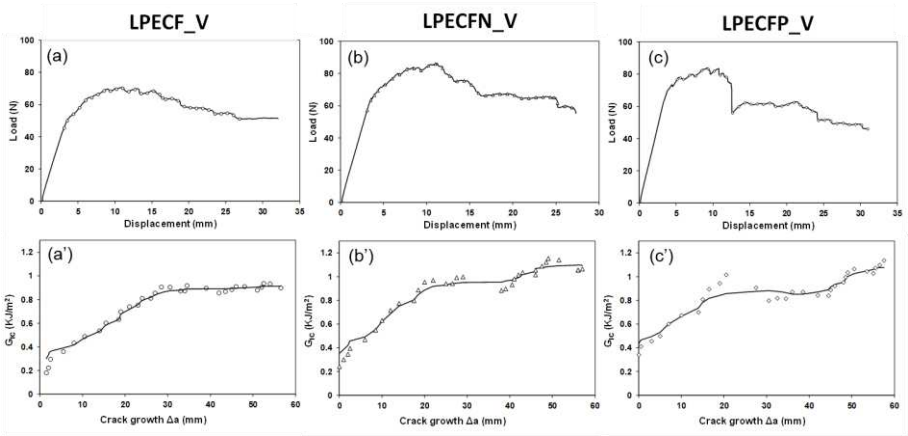

Figure 5.2 Representative (a) (b) (c) Load versus Displacement curves and (a') (b') (c') corresponding R-curves for Nylon 6,6 mat interleaved laminate (LPECFN_V), PVDF mat interleaved laminate (LPECFP_V) and laminate without mat (LPECF_V).

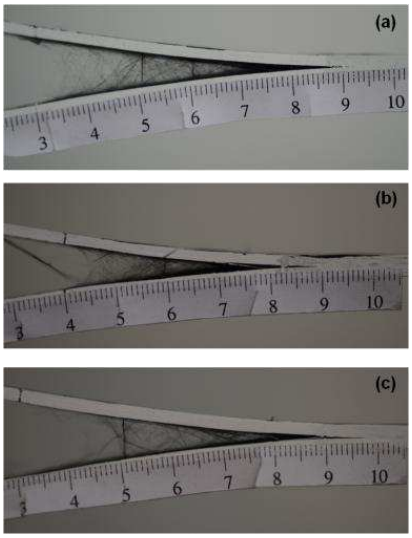

Figure 5.3 Photos of representative (a) LPECF_V, (b) LPECFN_V and (c) LPECFN_V laminates samples during DCB test.

Both G_{IC_init} and G_{IC_prop} values for the three systems are reported in Fig. 5.4 but in view of the above considerations only G_{IC_init} will be discussed. G_{IC_init} was higher for the mat interleaved systems, compared to LPECF_V, which was a clear indication that the mats play a role as toughening materials. In particular, the

increase of G_{IC_init} was significant for LPECFP_V, being twice the value measured for LPECF_V.

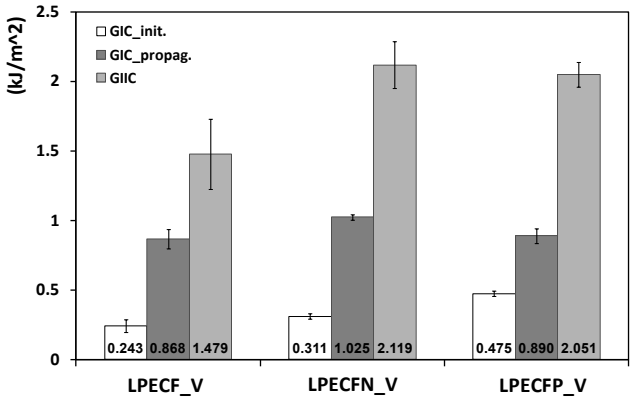

Figure 5.4 Values of G_{IC_init}, G_{IC_prop} and G_{IIC} for LPECF_V, LPECFN_V and LPECFP_V laminates.

In order to study the toughening mechanism exerted by nanofibrous mats obtained from the two polymers, the delaminated surfaces of LPECFN_V and LPECFP_V after DCB tests have been observed by SEM. In Fig. 5.5 a, c and e and Fig. 5.5 b, d and f SEM micrographs of LPECFN_V and LPECFP_V laminates are reported, respectively. Panels a, b, c and d are zoomed on an area close to the initial delamination front, while panels e and f are taken from an area that is far from the delamination front. The images at lower magnification of the zone adjacent to the initial crack (Fig. 5.5 a, b) showed for both systems the presence of large zones covered with resin/mat, indicating a prevalent cohesive fracture. This was in agreement with the increase of G_{IC_init} in the LPECFN_V and LPECFP_V systems with respect to LPECF_V, due to the presence of the mat. The higher magnification micrographs of the same area revealed a different behavior for Nylon and PVDF. In LPECFN_V surfaces (Fig. 5.5 c) the fracture propagated through mat/resin layer. Nanofibres that were oriented perpendicularly to the delamination surface appeared to be fractured, thus supporting the already proposed idea of strong nanofiber/resin interactions. In LPECFP_V the nanofibers have been pulled out and deformed (Fig.

5.5 d). Similar behavior has been observed in the fracture surfaces of the corresponding monolayers (see Paragraph 3.3 of Chapter 3). This could explain two different toughening mechanisms activated by the two mats. It can be argued that the increase of toughness in LPECFN_V (higher G_{IC_init}) with respect to LPECF_V was prevalently due to the increase of the toughness of the uniform resin/mat interlayer. While for LPECFP_V, where the PVDF mat did not show significant interaction with the resin, the mechanically interlocked nanofibers were acting similarly to a Velcro undergoing shearing and plastic deformation.

Finally, panels e and f of Fig. 5.5, zooming the zone of crack growth, far from the crack initiation, indicated a mixed adhesive/cohesive fracture, with extensive carbon fiber bridging for both systems. For LPECFN_V system, higher magnification images highlighted the occurring of nanofiber-bridging phenomena during the crack growth (insert in panel (d)).

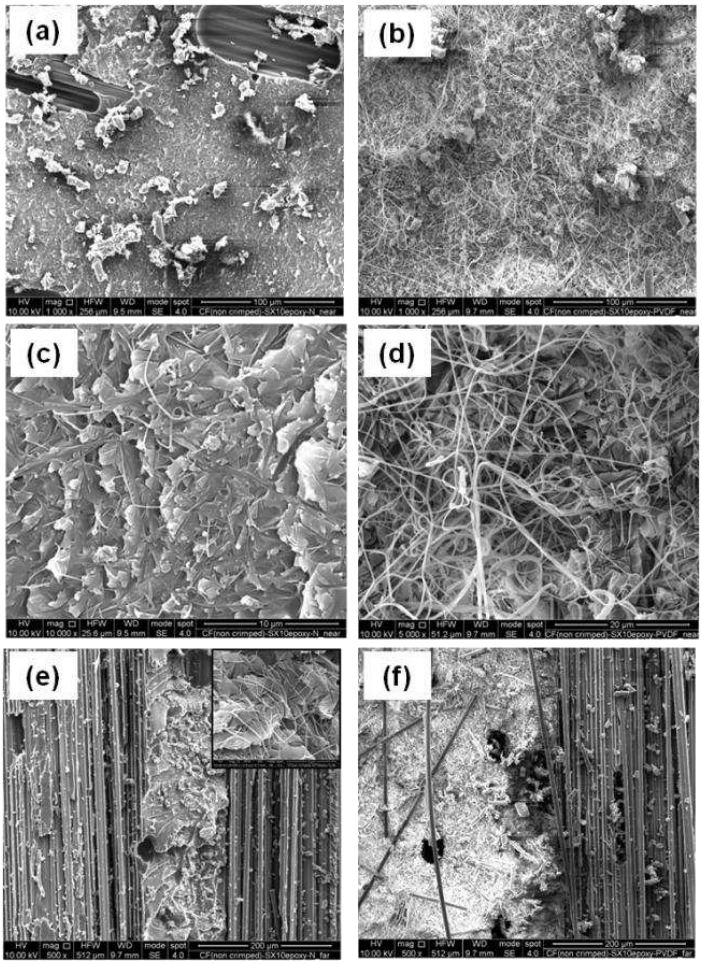

Figure 5.5 SEM micrographs of delaminated surfaces after Mode I delamination test: (a) and (c) LPECFN_V, area close to the interlaminar precrack different magnifications; (b) and (d) LPECFP_V, area close from the interlaminar precrack, different magnification; (e) LPECFN_V, area far from the interlaminar precrack; (f) LPECFP_V, area far from the interlaminar precrack.

Also Mode II delamination test (ENF test) has been carried out on LPECF_V, LPECFN_V and LPECFP_V laminates. The force/displacement curves obtained from this test and presented in Fig. 5.6 reported an increase of the maximum load for LPECFN_V and LPECFP_V laminates with respect LPECF_V, with a slightly smoother collapse of the load. The values of G_{IIC}, as derived from the analysis of load/displacement curves, are also reported in Fig. 5.4. A marked increase of G_{IIC}

was observed for both the interleaved laminates (about 40%), with no significative difference between LPECFN_V and LPECFP_V.

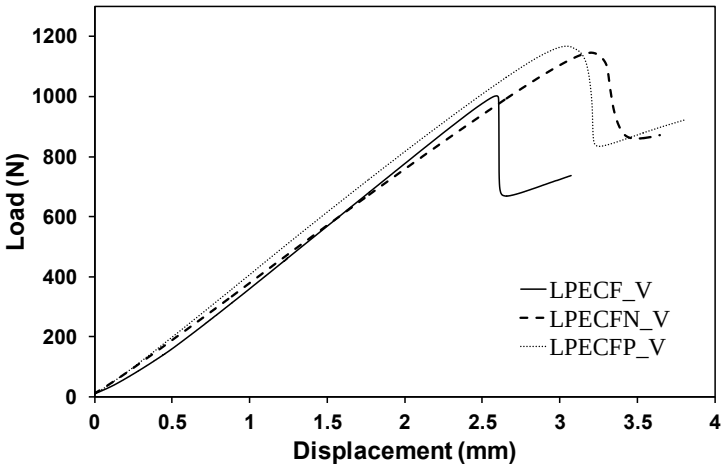

Figure 5.6 Load versus displacement curves from Mode II delamination test (ENF) for all studied systems.

5.4 Conclusions

Carbon fiber reinforced epoxy laminates, being the matrix a low Tg but high toughness epoxy resin and with Nylon 6,6 and Polyvinylidene fluoride (PVDF) electrospun mats as interlayer have been prepared and characterized.

No significant effects were observed on dynamic mechanical thermal behavior of the laminates, as consequence of the presence of mats. Mode I and Mode II delamination tests highlighted the toughening properties of both nanofibrous selected mats, although according to different mechanisms. For the Nylon 6,6 mat interleaved system the increase of the toughness was probably due to an uniform resin/mat interlayer, while for the PVDF membrane the toughening mechanism seemed to consist in a mechanically interlock of nanofibers acting similarly to a "Velcro" adhesive.

REFERENCES

[1] Huang XN, Hull D. Effects of fibre bridging on GIC of a unidirectional glass/epoxy composite. Compos Sci Technol 1989;35(3): 283-299.

[2] Spearing SM, Evans AG. The role of fiber bridging in the delamination resistance of fiber-reinforced composites. Acta Metall 1992;40(9): 2191-2199.

[3] Sakai M, Miyajima T.Fracture toughness and fiber bridging of carbon fiber reinforced carbon composites. Compos Sci Technol 1991;40(3): 231-250.

[4] Tamuzs V, Tarasovs, Vilks U. Progressive delamination and fiber bridging modeling in double cantilever beam composite specimens. Eng Fract Mech 2001;68(5):513-525.

6. HYDROTHERMAL AGING OF EPOXY RESINS

6.1 Introduction

This chapter describes the studies carried out on the hydrothermal aging behavior (combined effect of water and temperature) of selected epoxy resins, and its effects on their thermal and mechanical properties.

It consists of three parts. The first part is a comparison of two epoxy resin systems with significantly different crossilinking densities; a commercial resin composed of an epoxy monomer with trade name SX10Evo, and a Bisphenol A diglycidyl ether (DGEBA)-based resin. The aging was carried out at a relatively low temperature, 50 °C, for both systems to be far from their glass transition temperature.

The second part investigates the influence of the methyl substituents between the two phenols (i.e. the segmental chain mobility) on the hydrothermal aging behavior of epoxy resins. Bisphenol A diglycidyl ether (DGEBA) and bisphenol F diglycidyl ether (DGEBF) monomers based epoxy resins were used as model epoxy resin compounds. In this case the aging was performed at two temperatures, 50 °C and 80 °C.

The last part deals with the water absorption and desorption behavior of an epoxy formulation based on a blend of 4,4'-methylenebis(N,N-diglycidylaniline) (TGDDM) and bisphenol A diglycidyl ether (DGEBA) monomers. This study provides preliminary information that will be useful for the analysis of the hydrothermal aging behavior of composite laminates with the same epoxy formulation as matrix of the material.

6.2 Materials and methods

Four different resin systems were used: the first two consisted of an bi-functional epoxy monomer (DGEBA or DGEBF) and an amine (DDS) as curing

agent, a third was a blend of a tetrafunctional monomer (TGDDM), a bifunctional monomer (DGEBA) and an amine curing agent (DDS) while the last one was composed of an epoxy monomer with trade name SX10Evo and a type-M (medium) curing agent. All details regarding the amounts of different components used in the formulations, curing conditions and main properties are reported in the section A2 Appendix.

Water absorption processes were carried out by immersing samples in baths of deionized water at different temperatures. In some cases after absorption step one or more desorption processes were performed at different conditions. During the treatments the amount of absorbed/desorbed water was monitored by means of weighting of the samples.

Dynamic-mechanical-thermal analysis (DMTA) were carried out at different stages of the aging, in order to evaluate the effect of the aging (see section A3 of the appendix).

Photo-elastic tests, studying the evolution of the swelling stresses during the water absorption processes, have been carried out by Photoelasticity Laboratory of the Univeristà degli Studi di Palermo. Details of the test are reported in [1-4].

6.3 Results and discussion

6.3.1 Hydrothermal aging behavior of epoxy resins with different crosslinking density

This paragraph focuses the attention on two epoxy formulations with very different Tg values: the first one was a typical commercial epoxy resin, curing at room temperature and after thermal low temperature post-cure process reaching a Tg of about 90 °C (SX10Evo) while the second one was a DGEBA + DDS epoxy system achieving after cure and post-cure a Tg of about 230 °C.

In Fig. 6.1 the water uptake curves (amount of absorbed water against square root of time of immersion), obtained by weighing the samples during the aging treatment, of DGEBA and SX10Evo systems are showed. For both systems aging

treatment was carried out until the DGEBA system reached a complete stress free condition (about 1300 hours), according to photoelastic stress analysis. The materials exhibited an absorption behavior qualitatively similar: in the initial phase the amount of absorbed water, M_r, increased linearly with the square root of time, then, prolonging the exposure time, the absorption rate gradually decreased, the full saturation being not reached in the explored time window. Comparing the two systems, SX10 absorbed a significantly less amount of water than DGEBA. It is suggested that the lower crossiling density in the SX10 determined a more flexible network structure, able to reduce the amount of free volume [5-8]. This would explain the lower amount of absorbed water, with respect to DGEBA.

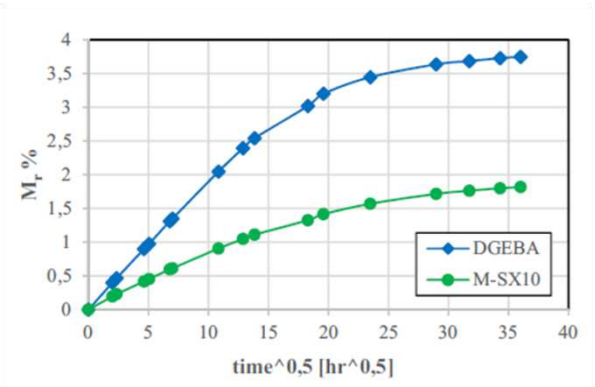

Figure 6.1 Water uptake curves at 50°C of DGEBA and SX10 systems.

DMTA was performed at different stages of the aging process:

i) Start of the aging treatment (after post-cure).

ii) After 1 week of immersion, that is at the reach of maximum swelling stress, as indicated by phoelastic stress analysis.

iii) At the reach of complete stress relaxation of the DGEBA system (i.e. after 1300 hours).

The results are reported in terms of tanδ versus temperature, in Fig. 6.2a for DGEBA system and in Fig. 6.2b for SX10Evo system. Focusing the attention on DGEBA, the not aged system (DGEBA post-cured) tanδ curve presents a narrow peak, the temperature value corresponding to the peak being about 226 °C, while

after 1 week of immersion in water at 50 °C it was observed a widening of the peak and a small decrease of the temperature value of the peak, up to about 223 °C. Finally, more significative modifications were observed after 1300 h of aging: at lower temperature a marked shoulder of the main peak was observable.

The behavior of SX10 is quite different. In fact, during aging the tanδ peak does not move significantly with respect the initial condition (M-SX10 Post-cured), indicating a stable Tg. In addition, after 1300 hrs of immersion the formation of a small shoulder towards higher temperatures is noted. This effect might indicate an attempt of the material to post-cure, probably induced by the long permanence at 50 °C.

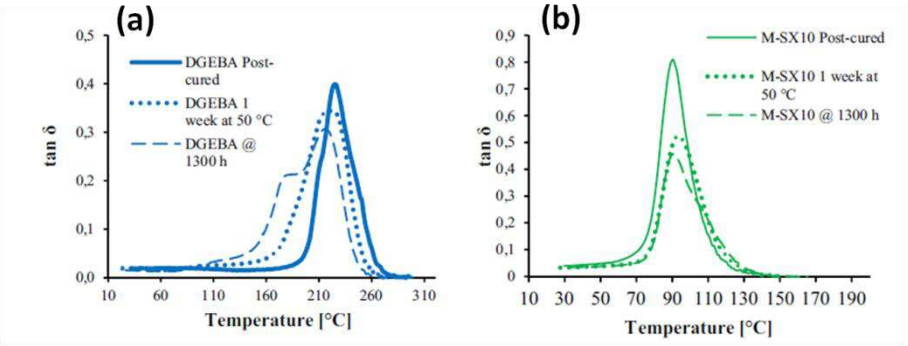

Figure 6.2 Loss factor (tanδ) against temperature from DMTA before and after aging of (a) DGEBA system; (b) SX10Evo system.

Photoelastic Stress Analysis (PSA) was also implemented during the aging treatment in order to study the evolution of stresses arising throughout the water uptake process.

In Fig. 6.3 a schematic representation of the rectangular sample tested by Photoelastic Stress Analysis (PSA) is reported. Figure 6.4 shows some isocromatic maps in white light of DGEBA system acquired during the aging, zoomed in the region of interest (see Fig. 6.3).

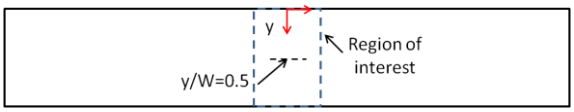

Figure 6.3 Schematic representation of a PSA sample.

The first image "Initial" (i.e. at the begging of the hydrothermal aging, immediately after the post-cure process) presented the sample in a completely stress free condition. The images taken during the permanence in the 50 °C water bath were showing a symmetric distribution of isocromatic black fringes, due to the internal stresses induced by the non-uniform swelling. The last image, after 1300 hours, highlighted an almost completely restored stress free condition, due to the homogenization of swelling on the whole volume of the material.

Figure 6.4 also shows that the higher stresses at the edge and in the center of the sample were reached at relatively early stages of absorption. In fact, comparing the images at 65 hr, 161 hr and 306 hr the number of fringes between the edge and the black fringe is progressively reduced, indicating a relaxation of stresses.

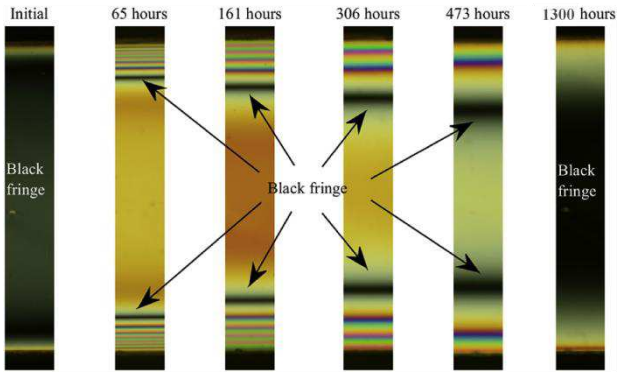

Figure 6.4 Evolution of the isochromatic fringes of DGEBA during aging treatment (water absorption), obtained in a circular dark field polariscope in white light.

A quantitative analysis of the photoelastic images allowed to evaluate the stresses along the y-axis of symmetry of the sample, from the edge to the centre (y/W=0.5) of the sample, being W the total width of the specimen (see Fig. 6.3). The stress function that was obtained was the difference of principal stresses ($\sigma_1 - \sigma_2$),

along the vertical symmetry axis. Due to the beam-shape sample, and hence the high length to width ratio, the normal stress component along the y direction was negligible, thus $(\sigma_1 - \sigma_2) = (\sigma_x - \sigma_y) \sim \sigma_x$. In particular, Figure 6.5 reports the comparison of values of σ_x of the DGEBA and SX10 systems, during all water absorption process, at the position y/W=0.5. As it is possible to observe, DGEBA always reached significantly higher stress values than SX10, more amount of water being absorbed by DGEBA (see Fig. 6.1). In addition, the plot of σ_x at y/W = 0.5 versus time of immersion shows that when the DGEBA system regained a fully stress free condition (σ_x=0), SX10 had instead a negative value of σ_x, indicating that the swelling was still non uniform.

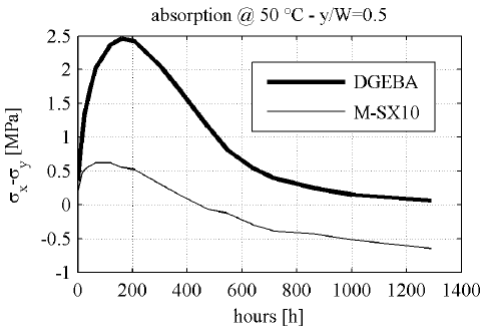

Figure 6.5 Plot of σ_x at the position y/W = 0.5 versus time of immersion for DGEBA system and SX10 system, from photoelastic stress analysis.

6.3.2 Influence of methyl groups in the hydrothermal aging behavior of epoxy resins

In this part a comparison of aging behavior of DGEBA and DGEBF based epoxy resins is presented.

First of all, the results of the gravimetric studies carried out on DGEBA and DGEBF, during absorption and desorption processes, are presented. Figure 6.6 reports the comparison of the water absorption curves, for aging at two different temperatures, 50 °C and 80 °C. The test was performed until it was not observed a significative mass change (i.e. saturation condition). As expected higher temperature

condition required less time to reach the saturation condition than the absorption process at lower temperature.

For both aging temperatures, it was found that DGEBA absorbed more water than DGEBF, although the gap seemed to decrease at 80 °C. This was believed to be related to the higher crossilinking density of DGEBA, consequence of the presence of the $–CH_3$ groups in the monomer. The more flexible DGEBF network causes several Van der Waals interactions in the molecular chains, leading to a small free-volume with respect to the more rigid network of DGBA. This causes a lower water uptake of DGEBF with respect to DGEBA and this effect is marked at low ageing temperature. At high temperature the increased kinetics of water absorption and the increased molecular mobility could provide an explanation for the reduction of the gap with DGEBA in absorbed water.

The diffusion coefficient (diffudivity) D, calculated by the Fick's second law for both systems and for both aging temperature conditions, are reported in Tab. 6.1. D value was always higher for DGEBA with respect to DGEBF.

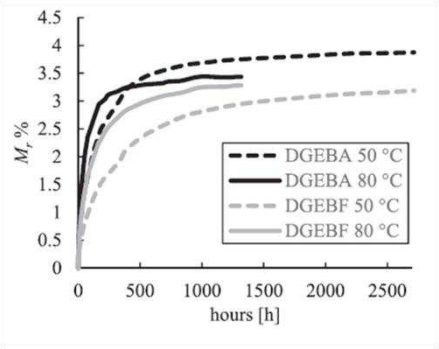

Figure 6.6 Water absorption curves of DGEBA and DGEBF systems, during hydrothermal aging process at 50 °C and 80 °C.

Table 6.1 Diffusivity (D) of DGEBA and DGEBF, calculated at different conditions of hydrothermal aging.

System	D at 50°C (10^{-8} cm^2/s)	D at 80°C (10^{-8} cm^2/s)
DGEBA	0.93	2.83
DGEBF	0.58	1.71

The samples aged at 80 °C have been also subjected to a controlled desorption process, immediately following the end of absorption. It has been carried out for about 2800 h, i.e. up to the formation of a consolidated plateau trend in the desorption gravimetric curves. The results of this treatment are reported in Fig. 6.7, in terms of absorbed water amount normalized by absorbed water at saturation versus time, for both studied systems. From Fig. 6.7 it was observed that DGEBA had an initial faster desorption rate. In addition, both DGEBA and DGEBF reached plateau keeping residual water. Since the desorption process was carried out at room temperature, activated only by an external controlled dry airborne environment, it was assumed that the desorbed water was mainly free water.

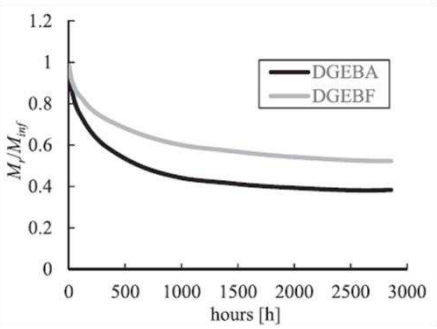

Figure 6.7 Water desorption curves of DGEBA and DGEBF systems, after absorption process at 80 °C.

DMTA has been performed at four different aging conditions, in order to monitor the dynamic-mechanical behavior. The selected stages were:

i) Initial not aged samples (after post-cure).

ii) Under maximum swelling stresses, as detected by photoelastic analysis. The time at which the two systems reached this condition was different, as well as was different for same system but different temperature of aging (50 °C or 80 °C).

iii) At saturation (last point in the water absorption curves, Fig. 6.6).

iv) At plateau of desorption (last point in the desorption curves, Fig. 6.7).

In Fig. 6.8 the DMTA results are reported in terms of tanδ against temperature curves, for the two studied systems and for both temperatures. Starting from a single

peak in the tanδ curve for both systems, the value of temperature being referred to the glass transition temperature of the material at not aged condition, with the progress of water uptake the tanδ curve always shifted toward lower temperatures, with a broadening of the curve and the formation of other peaks or shoulder. For the condition corresponding to the maximum stress, at both 50 °C and 80 °C it is observed that the Tg value was only slightly affected in DGEBA, while it significantly decreased in DGEBF, even if tanδ curve showed always a broadening of the peak. DMTA performed at the end of the absorption period (i.e at saturation) presented a significant Tg reduction in both systems, with also the occurring of two peaks. This modification suggested that the water absorption induced the formation of heterogeneities in the epoxy network, with the occurring of plasticization/degradation phenomena. In particular DGEBA Tg showed a lower decrease than DGEBF. Looking at the water uptake curves (see Fig. 6.6), as already highlighted DGEBA absorbed a larger amount of water than DGEBF. This can be referred to a more dense starting network, due to the presence of the $–CH_3$ groups, which induced a lower sensibility to plasticization effects. DMTA performed at the end of desorption period showed a tendency of both materials to recover the initial Tg. It was though noted that the DGEBF tanδ peak remained quite far away from the initial position (Tg of 171 °C against 202 °C of the un-aged condition), while DGEBA system was able to almost fully recover the initial Tg (Tg of 217 °C against 226 °C of the un-aged condition).

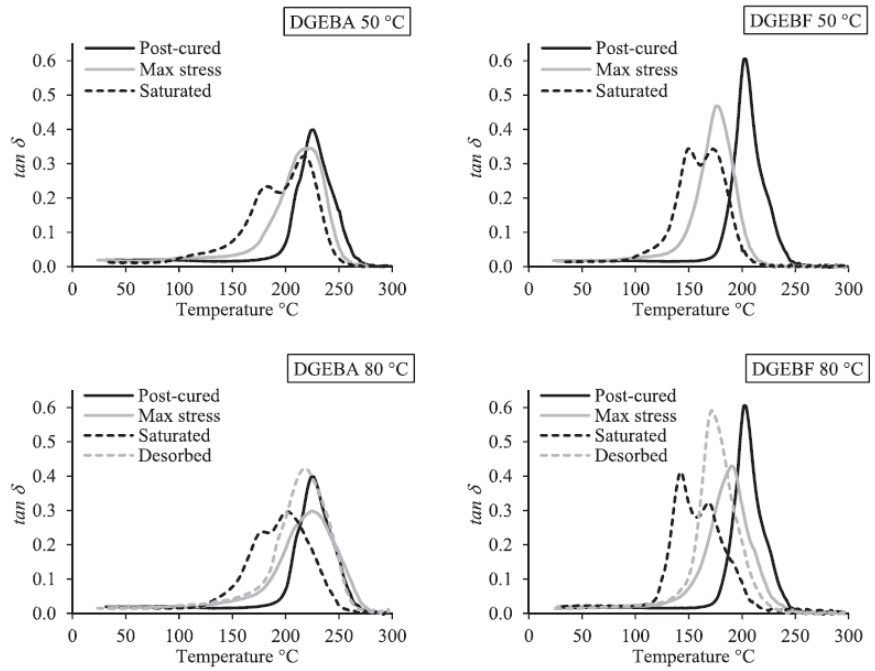

Figure 6.8 DMTA results for DGEBA and DGEBF systems, at different stages of aging. Temperature of absorption process is indicated.

A swelling stresses evolution study has been carried also in this case by means photoelastic technique. In particular quantitative analysis of swelling stresses has been performed on the y-axis of the sample, in two points: one near the edge, y/W=0.1, and one at the center, y/W=0.5 (see these two points in Fig. 6.3). The results of this test are showed in Fig. 6.9, in terms of σ_x versus time curves. The panel (a) is for the aging condition 50 °C, the panel (b) for the aging at 80 °C. It is evident that the swelling stress curves have a similar trend for DGEBA and DGEBF and irrespective of the temperature of absorption. The maximum stresses in the two observed points were reached soon compared to the total time required to reach saturation. At this regard, it should be clarified that the curves in Fig. 6.9 are interrupted earlier than the whole time to saturation, to better appreciate the swelling stress development.

Fig. 6.9 also shows that for both systems the center point (y/W= 0.5) always remained in traction, $\sigma_{x>0}$, while the point near the edge (y/W= 0.1) was in traction in a small initial phase, then passing in compression.

While the general trend and peak value of swelling stresses are similar for DGEBA and DGEBF, the most noteworthy difference involves the kinetic, the DGEBF having a slower swelling stresses evolution kinetic. This tendency was reproduced at both aging temperatures. The conclusion of this comparison is that the two materials achieved similar values of maximum swelling stress, but with different kinetics. The kinetic of swelling stress development followed that one of water diffusion, thus DGEBF was slower in diffusing water and in reaching maximum swelling stress than DGEBA.

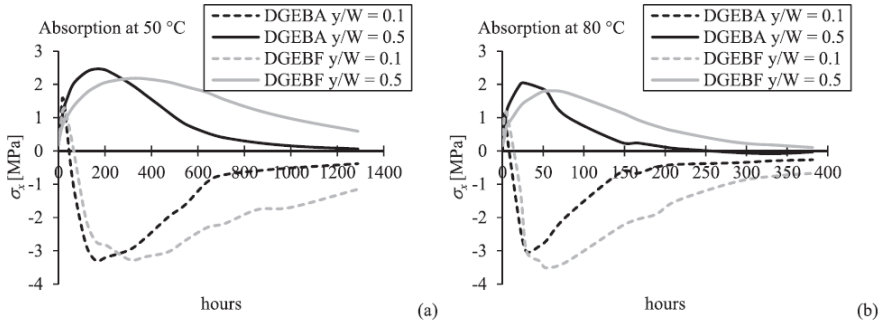

Figure 6.9 Stress curves near the edge (y/W= 0.1) and at the centre (y/W= 0.5) of specimen for DGEBA and DGEBF (a) at 50 °C (b) and 80 °C as temperature of absorption.

6.3.3 Preliminary study of hydrothermal aging behavior of a TGDDM/DGEBA monomers based epoxy resin

This paragraph focuses the attention on the hydrothermal aging behavior of an epoxy resin based on a blend of TGDDM and DGEBA monomers. As already said in the paragraph 6.1 it represents a preliminary investigation of a study regarding the hydrothermal aging behavior of composites in which the matrix is the same epoxy formulation.

In Fig. 6.10 the water absorption/desorption profile of the epoxy matrix is reported. Regarding the absorption step, performed at 90°C, in the initial phase the

amount of absorbed water, M_t, increased linearly with the square root of time, then, prolonging the exposure time, the absorption rate gradually decreased, the full saturation being not reached in the explored time window. The first stage of desorption process, carried out at room temperature, was slower than the water uptake, as showed from the thermo-gravimetric curve, and after three months the materials retained almost 50% of the total amount of absorbed water. For this reason a more drastic thermal treatment was applied (T=150 °C). By means of this treatment the matrix eliminated the residual water in about 50 hr.

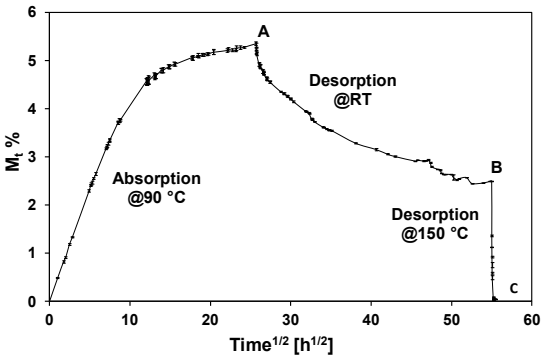

Figure 6.10 Water absorption/desorption profile of the resin. The solid line is only a guide for the eye.

The effect of the water absorption/desorption processes on the dynamic-mechanical-thermal behavior of the resin has been also investigated. In Fig. 6.11 the DMTA results, conducted on resin samples after aging, are presented and compared with the non-aged system. For the non-aged system, in tanδ curve only a peak at the temperature of 264 °C was present. After the water absorption stage at 90 °C for 4 weeks (point A in Fig. 6.10) two broad peaks appeared, at about 190 °C and 250 °C. These two broad relaxations suggest the co-existence of material portions or domains with different crosslinking densities. The observed behaviour can be explained with an uneven distribution of the absorbed water into the epoxy network, inducing a non uniform swelling and a different extent of plasticization in the different domains, and/or to the occurrence of some degradation phenomena. The first effect should be reversible upon drying, while the latter is irreversible.

A main peak with a shoulder was evident in the tanδ curve of the resin after the first step of desorption (point B of the curve in Fig. 6.10), as indication of a partial recovery of the initial properties of the material, while after the second desorption step a full recovery of the thermo-mechanical behavior was achieved, with a single peak at 268 °C in tanδ curve. This last behaviour indicates that only few degradation effects upon ageing occurred and it also evidences some post curing effects on the lower cross-linked parts.

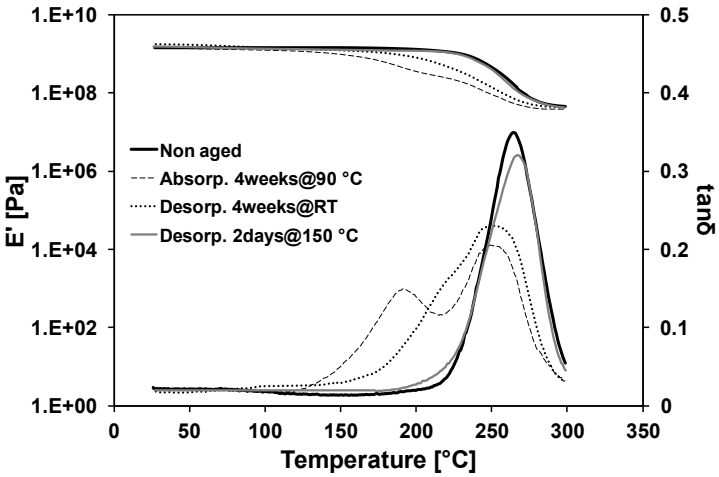

Figure 6.11 DMTA results of the epoxy resin, before and after aging.

6.4 Conclusions

In this chapter the hydrothermal aging behavior of epoxy resins with different features is studied by means of gravimetric measurements, dynamic-mechanical-thermal analysis (DMTA) and Photoelastic Stress Analysis (PSA). It is always observed that systems with higher crossilinking density (higher Tg) absorb higher amounts of water. Higher network density determines lower segmental chain mobility, hence higher free volume and higher water uptake.

For the first time, the photoelastic technique has been used to evaluate the transient swelling stresses induced by water absorption. The analysis has allowed to

establish that in hydrothermally aged epoxy resins the stress filed is induced by the non-uniform swelling between the inner and the outer parts of the sample. The kinetics of the swelling stresses evolution have been correlated with both the water diffusion kinetics and the network structure.

REFERENCES

[1] Pitarresi G, Scafidi M, Alessi S, Di Filippo M, Billiaud C, Spadaro G. Absorption kinetics and swelling stresses in hydrothermally aged epoxies investigated by photoelastic image analysis. Polym Degrad Stab 2015;111:55-63.

[2] Toscano A, Pitarresi G, Scafidi M, Di Filippo M, Spadaro G, Alessi S. Water diffusion and swelling stresses in highly crosslinked epoxy matrices. Polym Degrad Stab 2016;133:255-263.

[3] Pitarresi G, Toscano A, Scafidi M, Di Filippo M, Alessi S, Spadaro G. Photoelastic stress analysis assisted evaluation of fracture toughness in hydrothermally aged epoxies. Frattura ed Integrità Strutturale 2014;30:127-137.

[4] Alessi S, Di Filippo M, Pitarresi G, Scafidi M, Toscano A. Fracture Toughness of hydrothermally aged epoxy systems with different crosslink density. Procedia Eng 2015;109:507-516.

[5] Alessi S, Caponetti E, Güven O, Akbulut M, Spadaro G, Spinella A. Study of the curing process of DGEBA epoxy resin through structural investigation. Macromol. Chem. Phys 2015;216(5):538-546.

[6] Starkova O, Chandrasekaran S, Prado L, Tolle F, Mülhaupt R, Schulte K. Hydrothermally resistant thermally reduced graphene oxide and multi-wall carbon nanotube based epoxy nanocomposites. Polym. Degrad. Stab. 2013;98(2):519-526.

[7] Starkova O, Buschhorn ST, Mannov E, Schulte K, Aniskevich A. Water transport in epoxy/MWCNT composites. Eur. Polym. J. 2013;49(8):2138-2148.

[8] Jackson MB, Kaushik M, Nazarenko S, Ward S, Maskell R, Wiggins J. Effect of free volume hole-size on fluid ingress of glassy epoxy networks. Polymer 2011;52:4528-4535.

7. HYDROTHERMAL AGING OF LAMINATES WITH NANOFIBROUS MATS AS INTERLAYERS

7.1 Introduction

In the design of fiber reinforced polymer composite materials the aging behavior study is of primary importance. In particular, water exposure and temperature cycles are the most common environmental conditions which the material, used in structural components, experiences during its service life. For this reason, hydrothermal aging behavior of epoxy matrix and carbon fiber reinforced epoxy laminates has been investigated to a great extent. [1-8] Conversely, to the best of the Author knowledge, no work has been found regarding hydrothermal aging of carbon reinforced epoxy composites modified with nanofibrous mats as interlayers. It is interesting to evaluate if the nanofiber membranes act as barrier for the water transport across the material or they favor the water absorption, creating "secondary" interfaces and hence increasing the susceptibility of the material to hydrothermal aging.

This chapter presents the results of a study carried out on laminates toughened with electrospun Nylon 6,6 nanofibrous mats, evaluating the accelerated hydrothermal aging behavior of these materials. The same aging treatment has been carried out specimens from a laminate without mats, in order to compare the results. The visco-elastic and mechanical properties of these laminates have already discussed in the paragraph 4.3.2 of Chapter 4 while the hydrothermal aging behavior of the neat resin (used as matrix) has been described in the paragraph 6.3.3 of the Chapter 6. In this chapter, thermal and mechanical properties of the composite laminates, with and without mats, are investigated at various stage of conditioning process, i.e. after water absorption and desorption.

7.2 Materials and methods

This chapter involves three laminates: HPECF_P, HPECFN$_1$_P and HPECFN$_9$_P (see Tab. A.3 of appendix), the matrix formulation being a blend of TGDDM and DGEBA as epoxy monomers and DDS as curing agent.

Hydrothermal aging has been performed on specimens of DMTA-type (i.e. sample of nominal dimensions 30 mm x 8 mm x thickness) and SBS-type (i.e. sample of nominal dimensions 20 mm x 6 mm x thickness), in three stages:

- Water absorption, conducted by immersing the samples in deionized water at 90 °C, for 4 weeks.
- Room temperature desorption, carried out keeping the samples in a box with calcium chloride, at room temperature.
- Accelerated desorption, during the which the coupons were placed in oven, at 150 °C, until to remove all absorbed water.

The amount of absorbed water, M_t, was calculated according to the following equation:

$$M_t, \% = \frac{W_t - W_i}{W_i} * 100 \tag{7.1}$$

where W_t is the weight at time t and W_i is the initial weight.

A two-stage diffusion model was used to fit the water uptake data (see paragraph 1.6, chapter 1). The model is described by the following equation:

$$M_t = M_{\infty 0}(1 + k\sqrt{t)}\left\{1 - exp\left[-7.3\left(\frac{Dt}{h^2}\right)^{0.75}\right]\right\} \tag{7.2}$$

where M_t is the amount of absorbed water time t, M_{∞_0} is the quasi-equilibrium uptake of the first stage, k a constant related to the rate of relaxation of the polymeric structure in the second stage, D the apparent diffusion coefficient and h the thickness of the sample.

Dynamic-mechanical-thermal analysis (DMTA), Three Point Bending (TPB) tests and Short Beam Shear (SBS) tests were performed before and after aging.

More information regarding the characterization methods are provided in the appendix.

7.3 Results and discussion

Figure 7.1 shows the water absorption and desorption curves of DMTA samples with transverse reinforcement for all composite laminates, with and without mats, and for the resin, as reference. In panel (a) the absorption curves are reported. In this case the absorption data for the laminates were normalized with respect to the weight fraction of the matrix, so that they could be directly compared with those of the neat resin, and the lines were the fitting curves obtained using the two-stage diffusion model (Eq. 7.2). In absorption, resin and all the laminates showed a qualitatively similar behavior: initially M_t increased linearly with the square root of time, then it continued to increase with a lower slope, the full saturation being not reached in the explored time window.

In Tab. 7.1 the fitting parameters, i.e. the apparent diffusion coefficient, D, a constant related to the rate of relaxation of polymeric chains in the second stage, k, and the quasi-equilibrium uptake, $M_{\infty 0}$, and the coefficient of determination R^2, are reported. R^2 was close to 1 for all systems, indicating a satisfactory quality of fitting for matrix and all laminates. D of the resin was similar to the values reported in literature for comparable systems [1] and significantly lower than the composite systems. This last result could be explained considering the capillary transport of water into pores and microcracks, mechanism involving only laminates and not neat resin. [9, 10] No substantial differences were observed in the D values for the mat-modified systems ($HPECFN_1$_P and $HPECFN_9$_P) and the not mat-modified one (HPECF_P). Comparing the k values calculated for the all systems, it was possible to conclude that the presence of the carbon fibers and Nylon mats did not influence significantly this parameter, related to matrix plasticization effects.

As already described in the paragraph 4.3.2 of Chapter 4, the three systems were characterized by a different porosity degree, ϕ (9.9% HPECF_P, 10.8% for $HPECFN_1$_P and 5.2% for $HPECFN_9$_P) (see Tab. 4.1, Chapter 4). As expected, $M_{\infty 0}$ was lower for the system with the lowest porosity degree ($HPECFN_1$_P).

The fitting parameters determined for water absorption curves of the SBS-type samples confirmed the same trends.

Desorption curves (see panel (b) of the Figure 7.1) showed a faster water release for the systems with higher porosity. For all systems a plateau was reached after about 200 h, with residual water detained by the laminates. Thus, a thermal treatment at high temperature was required to eliminate the total amount of absorbed water.

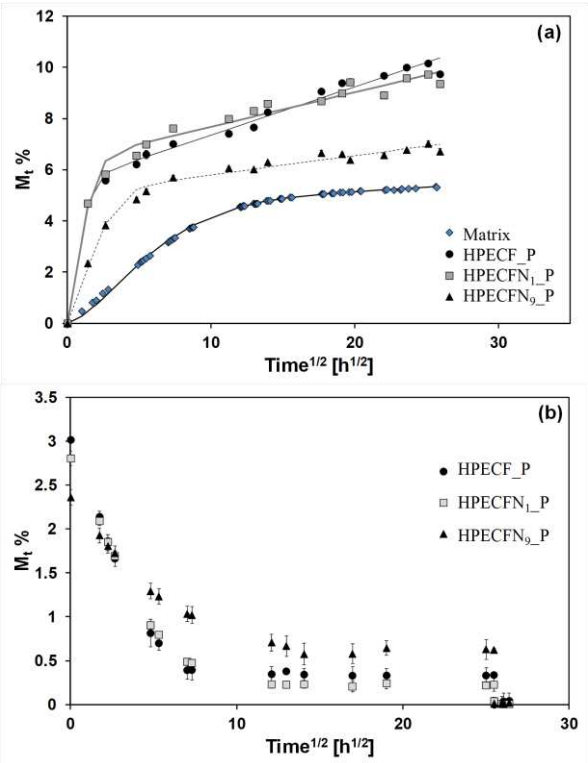

Figure 7.1 Water (a) absorption and (b) desorption profiles of the neat resin (Matrix) and composite laminates. In (a), the lines are the fitting curves obtained using Eq. 7.2.

Table 7.1 Coefficient of determination, R^2, apparent diffusion coefficient, D, polymer relaxation k and quasi-equilibrium uptake value, $M_{\infty 0}$, determinate according Eq. 7.2 for neat resin and composite laminates. The two different geometries are denoted as DMTA and SBS.

System	R^2	D (mm^2/s)	k($s^{0.5}$)	$M_{\infty 0}$, %
Resin_DMTA	0.99788	4.17×10^{-6}	1.06×10^{-4}	4.58
HPECF_P-DMTA	0.99002	1.49×10^{-4}	5.78×10^{-4}	5.45
$HPECFN_1$_P-DMTA	0.98284	9.95×10^{-5}	3.57×10^{-4}	6.32
$HPECFN_9$_P-DMTA	0.98874	3.85×10^{-5}	2.48×10^{-4}	5.04
HPECF_P-SBS	0.98714	1.43×10^{-4}	6.55×10^{-4}	4.55
$HPECFN_1$_P-SBS	0.99361	1.08×10^{-4}	4.09×10^{-4}	5.26
$HPECFN_9$_P-SBS	0.99562	3.78×10^{-5}	3.39×10^{-4}	4.51

The effect on the hydrothermal aging on the thermal resistance (by means DMTA) and on the mechanical properties (by means transverse flexural test and short beam shear test) of all laminates has been investigated.

Figure 7.2 shows the results of DMTA, performed on the HPECF_P and $HPECFN_9$_P laminates, before and after aging. The values of temperature corresponding to peaks in tanδ curves, at the different tested aging conditions are reported in Tab 7.2. For the HPECF_P system (Fig. 7.2 a), after post-cure (Non aged) only peak at about 265 °C was noted in tanδ curve, while after the absorption step a shift of the main peak in tanδ curve to lower temperature (260 °C) and the appearance of a secondary peak at about 170 °C, corresponding to a flex point in E' curve, were shown. These were the effects of plasticization operated by water on epoxy network. A fully recovery of the thermal properties was observed once the water desorption process was completed, with a small increase in Tg with respect to the non aged system, probably due to a slow post-cure process occurring on the plasticized system during the prolonged immersion in water at 90 °C.

DMTA results on the $HPECFN_9$_P system (see panel (b) of Fig. 7.2) after water absorption showed a single tanδ peak with a broad shoulder. The temperature at the peak shifted toward higher values (266 °C). The shoulder was no longer present after partial or complete water desorption and the main peak was maintained at the high temperature.

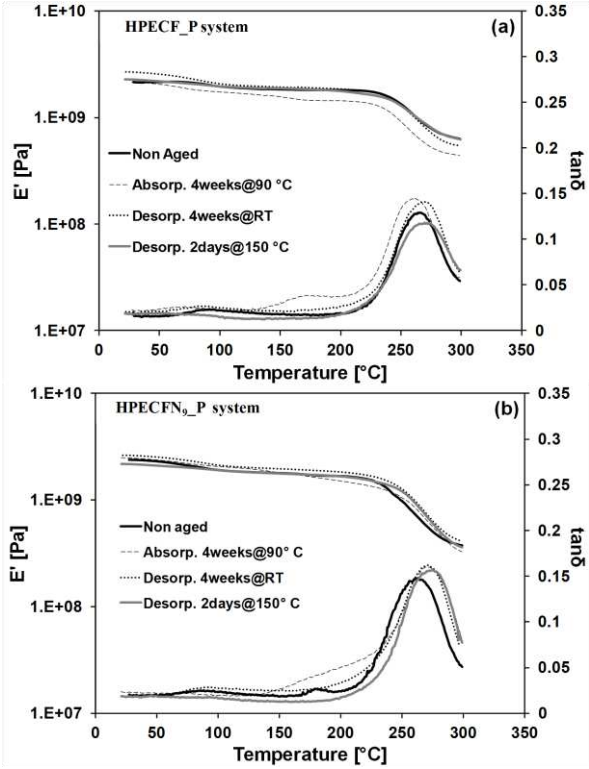

Figure 7.2 Storage modulus, E', and loss factor, tanδ, from DMTA before and after aging of (a) HPECF_P system; (b) HPECFN$_9$_P system.

Table 7.2 Peak temperature in tanδ curve for HPECF_P and HPECFN$_9$_P, before and after aging.

System	T of tanδ curve, at peak, (°C)			
	Non aged	Absorp. 4weeks@90°C	Desorp. 4weeks@RT	Desorp. 2days@150°C
HPECF_P	265	260-170	270	270
HPECFN$_9$_P	263-180	266-shoulder	266	270

The results of mechanical characterizations, carried out on the laminates before and after the absorption/desorption steps are summarized in Fig. 7.3, in terms of flexural modulus, E_f, and interlaminar shear strength, ILSS, the first being evaluated from three-point bending test, the second one from short beam shear test. After absorption flexural modulus decreased of about 15% with respect the initial value, but it was recovered after complete water desorption (the differences observed were

within the experimental error). Such a decrease in stiffness was likely induced by the increased mobility of the resin due to the already discussed plasticization effects. No significant differences were observed by the different systems, with and without mats.

A similar trend was noted for the ILSS data. The reduction in strength caused by water uptake was almost entirely recovered upon drying. The improvement of 30% achieved by the introduction of mats at each interlayer with respect to HPECF_P was maintained at each stage of the hydrothermal aging process.

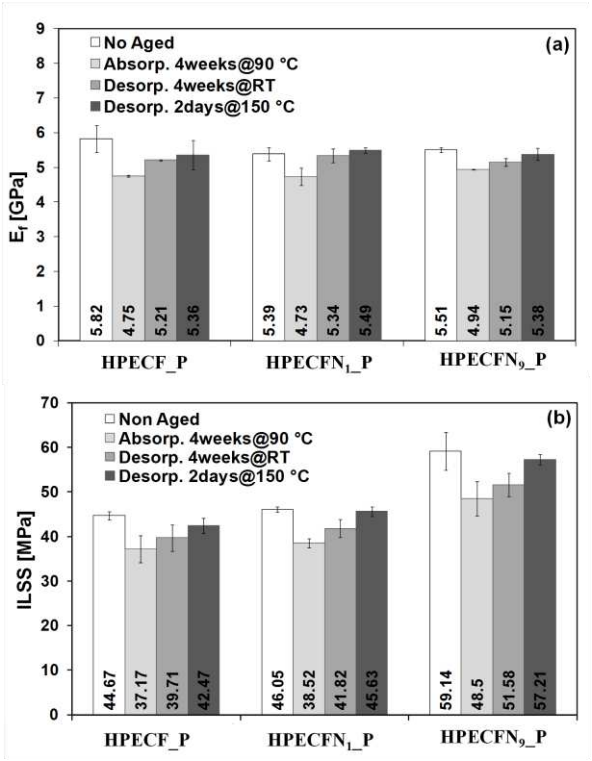

Figure 7.3 (a) Transverse flexural modulus, E_f, and (b) interlaminar shear strength, ILSS, of composites for different aging conditions.

7.4 Conclusions

In this chapter the hydrothermal aging behavior of laminates with Nylon 6,6 electrospun mats placed either at the middle plane only or at each interlayer is investigated. The water uptake behavior was modeled by a two-stage diffusion model and compared with the behavior of the neat resin and of the laminate without mats. Interestingly, a lower water uptake was observed for the laminates with mat-modified interfaces and this was possibly due to a significantly reduced porosity.

All the systems aged in the conditions here investigated were plasticised by water but they recovered their original thermal and mechanical properties after drying. No evidence of irreversible degradation phenomena caused the hygroscopic Nylon 6,6 nanofibers was found.

REFERENCES

[1] Zhou J, Lucas JP. Hygrothermal effects of epoxy resin. Part I: the nature of water in epoxy. Polymer 1999;40:5505-5512.

[2] Zhou J, Lucas JP. Hygrothermal effects of epoxy resin. Part II: variations of glass transition temperature. Polymer 1999;40: 5513-5522.

[3] Li L, Yu Y, Wu Q, Zhan G, Li S. Effect of chemical structure on the water sorption of amine-cured epoxy resin. Corros Sci 2009;51:3000-3006.

[4]Li L, Yu Y, Su H, Zhan G, Li S, Wu P. The Diffusion Mechanism of Water Transport in Amine Cured Epoxy Networks. App Spectrosc 2010;64(4):458-465.

[5] Alessi S, Conduruta D, Pitarresi G, Dispenza C, Spadaro G. Accelerated ageing due to moisture absorption of thermally cured epoxy resin/polyethersulphone blends. Thermal, mechanical and morphological behavior. Polym Degrad Stab 2011;96:642-648.

[6] Abot JL, Yasmin A, Daniel IM. Hygroscopic Behavior of Woven Fabric Carbon–Epoxy Composites. J Reinf Plast Compos.2005;24(2):195-207.

[7] Barbosa APC, Fulco APP, Guerra ESS, Arakaki FK, Tosatto M, Costa MCB, Melo JDD. Accelerated aging effects on carbon fiber/epoxy composites. Compos B Eng 2017;110: 298-306.

[8] Alessi S, Pitarresi G, Spadaro G. Effect of hydrothermal ageing on the thermal and delamination fracture behaviour of CFRP composites. Compos B Eng 2014;67:145-153.

[9] Zafar A, Bertocco F, Schjodt-Thomsen J, Rauhe JC. Investigation of the long term effects of moisture on carbon fibre and epoxy matrix composites. Compos. Sci. Technol 2012;72:656-666.

[10] Lu Z, Xian G, Li H. Effects of thermal aging on the water uptake behavior of pultruded BFRP plates. Polym Degrad Stab 2014;110:216-224.

APPENDIX A - Experimental

A.1 Materials

Tetraglycidylether of 4,4'diaminodiphenil methane (TGDDM), bisphenol A diglycidyl ether (DGEBA) and 4,4' diaminodiphenyl sulfone (DDS) were supplied by Sigma Aldrich (Italy). Araldite PY 306 CH, epoxy monomer based on bis(4-glycidyloxyphenyl)methane (DGEBF) was provided by Huntsman Advanced Materials (Belgium). SX10Evo epoxy monomer and type M (medium) amine hardener were purchased by Mates Italiana s.r.l.

UNIC CUT 300/10 HM-U659 10 HM unidirectional carbon fiber fabric (nominal areal weight 300 gr/m^2 and Young's modulus 398 GPa) and Sigmatex 300gsm/Unifiber C/T700SC 12K non-crimp unidirectional carbon fiber fabric (nominal areal weight 300 gr/m^2) were provide by Dalla Betta Groups s.r.l and Mates Italiana s.r.l, respectively.

A thermoplastic and an acrylic rubber were used for producing electrospun nanofibrous mats[1]. Dimethylformamide (DMF) and Acetone (Ac) were supplied by Sigma Aldrich.

Polysulfone (PSF), Nylon 6,6, Polyacrilonitrile (PAN) and Polyvinylidene fluoride (PVDF) electrospun mats were kindly provided by Università degli Studi di Bologna-Dipartimento di Ingegneria Industriale.

A.2 Preparation procedures

Electrospun polymeric mats

Nanofibrous hybrid rubber/thermoplastic (R/T) mats were produced by using an electrospinning apparatus (Polymers & Composites Laboratory, Chemical and

[1] Also called membranes.

Biological Engineering Department, Drexel University, Philadelphia (USA)), composed of an high voltage power supply (Glassman high voltage power supply), a syringe pump (Cole Parmer 74900 series syringe pump) and a 10 ml disposable syringe. As collector aluminum foils were used.

The polymeric solution was prepared stirring at room temperature until complete dissolution of the polymer in the solvent.

Neat resin systems

In this work four different epoxy formulations have been used. The first one consisted of a blend of a tetrafunctional monomer (TGDDM), a bifunctional monomer (DGEBA) and an amine curing agent (DDS). The weight ratio of two monomers TGDDM:DGEBA was 84:16, while the amount of the hardener was 26 phr (per hundred of resin by weight). This formulation is indicated as "high performance epoxy resin" (HPE). The resin was prepared by mechanical stirring of the three components at 80 °C for 30 min, and at 130 °C for further 30 min until complete dissolution of the curing agent. Then, the mixture was poured into the mold. The mold consists of two aluminum plates, previously covered with release film, and a silicon frame (4 mm thick). The curing process was carried out in a hydraulic press equipped with a temperature control system. The cycle cure, chosen on the basis of preliminary calorimetric analysis, consisted of a heating step from room temperature to 180 °C at 2 °C/min, an isothermal rest at 180 °C for 2 hr and a cooling step to room temperature without temperature control.

Calorimetric analysis has been performed in order to evaluate the best conditions of post-cure. Two post-cure conditions were selected: 2 hr at 200 °C, corresponding to a residual reaction heat of about 5%, and 2 hr at 230 °C, for which no residual heat was detected.

The second epoxy system used is a blend of the SX10Evo monomer and the type-M curing agent, used in weight ratio monomer:hardener 100:26, as suggested by the supplier. This formulation is indicated as "low performance epoxy resin" (LPE). After manual mixing of the two components, the blend was casted into the

mold and cured at room temperature for 8 hr. Then, the resin plaque was post-cured in oven, for 24 h at 60 °C, as recommended by the supplier.

The other two formulations consisted of DEGBA and DGEBF epoxy monomers, respectively. They were prepared by mixing a stoichiometric amount of DDS to the epoxy, fully dissolved after mechanical stirring for 30 min at 130 °C. The resin blends have then been casted into the mold. Both systems were cured in three steps: the first one consisted of a temperature gradient of 2 °C/min from room temperature to 180 °C, resting at this temperature for 2 h, and cooling at the same rate to room temperature. DGEBA based resin was post-cured at 200 °C for 2 h, followed by a slow cooling to room temperature in about 24 h while DGEBF based formulation was post-cured at 180 °C for 2 h, followed by the same cooling rate applied for DGEBA.

Dynamic-mechanical-thermal analysis (DMA), three point bending (according to EN ISO 178-2003 standard) and fracture toughness tests (according to ASTM D5045-96 standard) have been performed on two cured epoxy systems. In Tab. A.1 glass transition temperature, T_g, flexural modulus E_f, and fracture toughness, K_{IC}, of resins are reported.

Table A.1 Glass transition temperature, Tg, flexural modulus, E_f, and fracture toughness, K_{IC}, of the resin systems.

System	T_g (°C)	E_f (GPa)	K_{IC} (MPa*$m^{0.5}$)
TGDDM/DGEBA/DDS (HPE)	262	3.6±0.06	0.50±0.03
SX10Evo/type-M hardener (LPE)	90	2.9±0.12	0.68±0.04
DGEBA/DDS	230	3.3±0.07	0.55±0.09
DGEBF/DDS	194	3.4±0.04	0.64±0.07

Epoxy resin/electrospun nanofiber mat monolayer

Monolayer systems were produced by impregnation of the mat with the selected epoxy resin. Nanofibrous mat was impregnated by soaking it into the epoxy resin blend, at 130 °C for the TGDDM/DGEBA/DDS system, or at room temperature for the SX10Evo/Type-M hardener formulation. These temperatures were chosen in order to keep resin viscosity sufficiently low. The excess of resin was removed by

rolling the monolayer between two release films. Thus, the thermal curing process was applied. The curing process was performed in autoclave, at a pressure of 2.5 atm, for the TGDDM/DGEBA/DDS formulation and for LPE/PSF system, and by vacuum bagging technique for the other SX10Evo/Type-M hardener/mat monolayers. The used cure cycles were the same as for the corresponding epoxy resin neat systems.

Table A.2 summarizes nomenclature and characteristics of the manufactured monolayers. Mat weight fractions were calculated as mat weight to final monolayer weight ratio.

Table A.2 Denomination, components, production process and mat weight fraction W_{mat} of all the produced monolayers.

System	Resin formulation*	Electrospun mat	Production process**	W_{mat}, %
HPE/Nylon	TDD	Nylon 6,6	Autoclave	9.0
HPE/PAN	TDD	PAN	Autoclave	8.5
HPE/R/T	TDD	Rubber/thermoplastic	Autoclave	8.0
HPE/PSF	TDD	PSF	Autoclave	19.4
LPE/Nylon	SX	Nylon 6,6	Vac. bagg	2.3
LPE/PVDF	SX	PVDF	Vac. Bagg	4.9
LPE/PAN	SX	PAN	Vac. bagg	1.8
LPE/PSF	SX	PSF	Autoclave	5.9

*TDD and SX are the abbreviations for TGDDM/DGEBA/DDS and SX10Evo/typeM hardener resin systems, respectively.
*** For autoclave curing, the applied pressure was 2.5 atm.

Three-layers systems

Laminates composed of 2 layers of carbon fiber fabric, resin and a nanofibrous mat, placed between the two layers, (labeled three-layers systems (tls)) were produced in order to have preliminary information on the behavior of the mat in composite laminates. Systems consisting of 2 layers of carbon fiber fabric and resin, without electrospun mat interleaving, were prepared as reference.

Hand lay-up process was used to assemble these systems. UNIC CUT 300/10 HM-U659 10 HM and TGDDM/DGEBA/DDS epoxy formulation were fabric and resin used to produce them. The mat modified systems were prepared by laying the

membrane between the two carbon fiber layers. The curing process was performed in autoclave, at pressure of 2.5 atm, following the cycle cure already described for the preparation of other systems with the same matrix formulation.

Carbon fiber reinforced epoxy laminates

Carbon fiber/epoxy $[0]_n$ (where n is the number of layers of carbon fiber fabric used) laminates were produced by hand lay-up. In the mat interleaved systems, one or more membranes was added placing them in the middle plane or at each interlayers during the lay-up process. A stripe of 15 µm thick FEP release film was laid at mid-thickness, along one edge of the panel and perpendicularly to the fiber direction, in order to obtain DCB and ENF specimens, for the mode I and mode II interlaminar fracture toughness characterization, respectively.

The curing process were carried out in autoclave, at pressure of 2.5 atm and 3.5 atm, or by means the vacuum bagging technique, according the thermal profiles already described in the previous paragraphs, for the other systems.

In Tab A.3 all the panels produced are presented. In it nomenclature, resin formulation, carbon fiber and type of mat used, production process and weigh fraction of carbon fiber for each system are summarized. The carbon fiber weight fractions were calculated from known weight of carbon fibers in the panel and the measured weight of the panel after cure.

Table A.3 Denomination, components, production process and carbon fiber weight fraction, W_{CF}, of all the produced laminates.

System	Resin*	Carbon fiber fabric**	Electrospun mat (number of mats)	Production process***	W_{CF}, %#
HPECF_A1	TDD	UNIC CUT	no	Autocl. 2.5	52
HPECF_A2	TDD	UNIC CUT	no	Autocl. 3.5	62
HPECFN_A1	TDD	UNIC CUT	yes, Nylon (1)	Autocl. 2.5	53
HPECFN_A2	TDD	UNIC CUT	yes, Nylon (1)	Autocl. 3.5	64
LPECF_V	SX	Sigmatex	no	Vac. bag.	66
LPECFN_V	SX	Sigmatex	yes, Nylon (1)	Vac. bag.	63
LPECFP_V	SX	Sigmatex	yes, PVDF (1)	Vac. bag.	62
HPECF_P	TDD	UNIC CUT	no	Press	69
$HPECFN_1$_P	TDD	UNIC CUT	yes, Nylon (1)	Press	70
$HPECFN_9$_P	TDD	UNIC CUT	yes, Nylon (9)	Press	65

*TDD and SX are the abbreviations for TGDDM/DGEBA/DDS and SX10Evo/typeM hardener resin systems, respectively.
**UNIC CUT and Sigmatex are abbreviation for UNIC CUT 300/10 HM-U659 10 HM and Sigmatex 300gsm/Unifiber C/T700SC 12K carbon fiber fabric reinforcements, respectively.
*** For autoclave curing, the number indicates the applied pressure in atmosphere.
# The carbon weight fraction has been determined as dry carbon fiber fabric weight to final laminate weight (after cure) ratio.

Hydrothermal aging treatment

Hydrothermal aging was carried out both on neat resin samples and on laminate specimens, by immersing dry samples in deionized water at different temperatures and for different times. In some cases, after absorption, desorption steps were carried out

The weight of the specimens was measured at increasingly longer time intervals, by a balance with 10 µg resolution. Excess of water was removed from surfaces by blotting paper.

The amount of absorbed water, M_t, was calculated according to the following equation:

$$M_t, \% = \frac{W_t - W_i}{W_i} * 100 \qquad \text{(A.1)}$$

where W_t is the weight at time t and W_i is the initial weight. M_t values reported are the average of at least 5 specimens for each system.

A two-stage diffusion model has been used to fit the data. The mathematical form of this model is given by the following equation:

$$M_t = M_{\infty 0}(1 + k\sqrt{t})\left\{1 - exp\left[-7.3\left(\frac{Dt}{h^2}\right)^{0.75}\right]\right\} \quad \text{(A.2)}$$

where, M_t is the water uptake at the generic time t, $M_{\infty 0}$ the quasi-equilibrium uptake of the diffusion-dominated first stage, k a constant related to rate of relaxation of the polymeric structure in the second stage, D the apparent diffusion coefficient and h the specimen thickness. $M_{\infty 0}$, D and k have been determined.

A.3 Characterizations

Surface tension measurement

Surface tension measurements were carried out on polymer solutions at different concentrations, by a KSV Instruments CAM 200 Contact Angle and Surface Tension Meter, equipped with a disposable syringe and a 2.14 mm diameter needle (see Fig. A.1).

The reported surface tension values were average of 25 measurements for each polymeric solution.

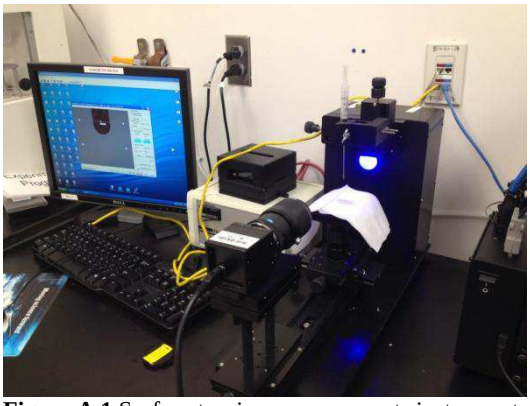

Figure A.1 Surface tension measurements instrument.

Differential scanning calorimetry (DSC)

DSC analysis was performed on uncured resin, electrospun mats and uncured resin/mat samples, by a Perkin Elmer Precisely Jade calorimeter. The tests were carried out at a heating ramp of 10 °C/min from room temperature to about 350 °C, under nitrogen flow. Heat flow, normalized to sample weight, against temperature were recorded. For uncured resin/mat samples, the curing reaction was calculated taking into account the weight fraction of resin in the specimen.

Dynamic mechanical thermal analysis (DMTA)

A Rheometrics DMTA V instrument was used to evaluate the dynamic mechanical thermal behavior of neat cured epoxy resins, epoxy resin/mat monolayers and composite laminates. For laminate systems, the test was performed on transversal samples, i.e. cut to their length to be perpendicular to fiber direction. Tension setup was used for monolayers whereas for neat resin and laminates single cantilever bending setup was employed. Tests were carried out in temperature swift mode at heating ramp of 2 °C/min or 5 °C/min, under nitrogen flow. For samples with TGDDM/DGEBA/DDS, DGEBA/DDS and DGEBF/DDS formulations the range of temperature was 30 °C÷300 °C while for the specimens with SX10Evo/Type M hardener resin 30 °C÷150 °C. For all tests, the frequency and strain values were set at 1 Hz and 0.02%.

Storage and loss moduli (E' and E'') and loss factor (tanδ) versus temperature were recorded. Glass transition temperature Tg was evaluated as temperature corresponding to peak in tanδ curve.

Three point bending (TPB) test

TPB test was performed on composite laminates, according with the guidelines of the UNI EN ISO 1425 standard [1]. In particular transverse reinforcement samples were tested, in order to evaluate the effect of the mats on the properties of the resin. The specimens were 60 mm long and 15 mm wide. The tests were

conducted by an Instron 3367 electro-mechanical machine, equipped with a 1 kN load cell.

Six samples for each systems were tested. The flexural modulus was evaluated.

Mode I interlaminar fracture toughness test

The study of the interlaminar fracture toughness in Mode I crack opening of laminates was performed on double cantilever beam (DCB) samples, cut from manufactured panels, according with the guidelines of ASTM D5528 standard. [2]

In Fig. A.1 an image of used set-up is shown.

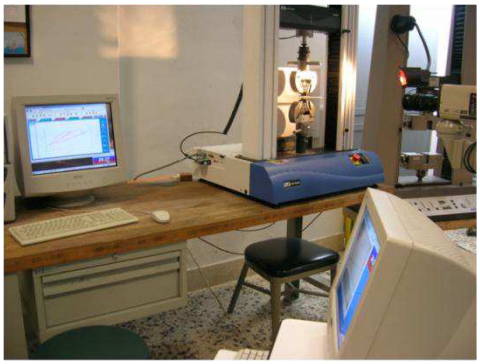

Figure A.2 Set-up for double cantilever beam test.

The test was carried out on an electromechanical machine, under displacement control, whereas crack extension was monitored by means of a camera, equipped with appropriate zoom lenses. The image sampling was opportunely synchronized with the load and crosshead displacement values acquired by the testing machine.

Metallic hinges were glued on the two surfaces of the DCB samples, in the delaminated end, to allow gripping with the mechanical jaws of the dynamometer. The thickness side of the samples was painted with white paint to improve the contrast of marks drawn every 1 mm.

The Modified Beam Theory (MBT) method [2] was implemented in order to calculate the Critical Strain Energy Release Rate values, G_{IC}. According this method a crack length correction term Δ, was added to the visually measured crack length,

deriving from a linear interpolation of the cubic root of the compliance versus the visually observed value of the crack length.

The Resistance Curves (R-Curves) were obtained plotting G_{IC} against the crack growth. In addition, the initiation and propagation fracture energy, G_{IC_init} and G_{IC_prop} respectively, were extrapolated. The first one, representative of delamination onset, was calculated according the Visual Observation (VIS) technique, indicated in the standard; the second one, representative of stabilized propagation fracture energy, was obtained by averaging the G_{IC} values over the second half of the total crack growth, in the R-curves.

At least a number of five DCB samples for each system was tested.

Mode II interlaminar fracture toughness

Mode II interlaminar fracture energy was determined by means of end notched flexure (ENF) test, using an electro-mechanical test machine with a 30 kN capacity load cell. The test was carried out on samples with an interlaminar precrack starter, according with le guideline of the ASTM D 7905 – 14 standard. Non-precracked (NPC) method was applied. [3]

The ENF test is not ideal test for deriving Mode II R-curve, due to the unstable intrinsic nature of the ENF test. For this reason, only the initiation value of interlaminar fracture energy, G_{IIC}, was calculated.

At least five specimens for each system were tested.

Short beam shear (SBS) test

SBS tests were conducted on the same dynamometer used for all the mechanical test, using the 30 kN load cell. This test was carried out according to the ASTM D2344 standard. [4] In particular, specimens were characterized by length to thickness ratio equal to 6 and width to thickness ratio equal to 2.

Interlaminar shear strength (ILSS) was calculated using the following formula:

$$ILSS = 0.75 * \frac{P_m}{b * h} \tag{A.3}$$

where P_m is the maximum load recorded during the test, b is the specimen width and h the specimen thickness.

For each analyzed system, six samples were tested and average and standard deviation of ILSS were calculated.

Scanning Electron Microscopy (SEM)

Surface morphology was observed by means of a Philips 505 Quanta 200 field-emission SEM. Different sample surfaces have been analyzed and in particular:

- Electrospun nanofiber mats surface.
- Fracture surface of epoxy resin/electrospun mat monolayers and three-layers systems.
- Cut and polished transverse section of composite laminates.
- Cut, polished and etched cross section of composite laminates.
- Mode I and Mode II delamination surfaces of composite laminates.

The etching process was conducted by immersing the sample in a super-acid solution, for 5 minutes. The purpose of the etching treatment was to remove the mat and thus to enhance the contrast with the resin. The same treatment was also carried out on not mat-modified laminates to compare systems subjected to the same surface preparation.

The samples were mounted on SEM aluminum stubs by means of graphite adhesive or silver glue. Before testing, all the analyzed surfaces were gold sputtered, in order to make them conductive.

The ImageJ software has been used for image analysis, to estimate the porosity degree of laminates. This software converted the SEM image in a binary image, in which voids were black and filled parts (with resin or carbon fibers) were white. SEM images at 700X magnification were used. A "cleaning" process of binary images was carried out, aiming to remove unwanted noise. Several samples from different parts of the laminate were observed and average and standard deviation of the porosity degree, ϕ, for each system were evaluated.

REFERENCES

[1] UNI EN ISO 14125. Fibre-reinforced plastic composites-Determination of flexural properties (2000).

[2] ASTM D 5528 – 01. Standard Test Method for Mode I Interlaminar Fracture Toughness of Unidirectional Fiber-Reinforced Polymer Matrix Composites (2007).

[3] ASTM D7905-14. Standard Test Method for Determination of the Mode II Interlaminar Fracture Toughness of Unidirectional Fiber Reinforced Polymer Matrix Composites (2014).

[4] ASTM D 2344/D2344M – 13. Standard test method for short-beam strength of polymer matrix composite materials and their laminates (2013).

LIST OF PAPERS

- Effects of Nylon 6,6 nanofibrous mats on thermal properties and delamination behavior of high performance CFRP laminate.
  Alessi S, Di Filippo M, Dispenza C, Focarete ML, Gualandi C, Palazzetti R, Pitarresi G, Zucchelli A.
  Polymer Composites 2014, vol. 36(7), p. 1303-1313.

- Absorption kinetics and swelling stresses in hydrothermally aged epoxies investigated by photoelastic image analysis.
  Pitarresi G, Scafidi M, Alessi S, Di Filippo M, Billaud C, Spadaro G.
  Polymer Degradation and Stability 2015, vol. 111, p. 55-63.

- Hydrothermal aging of carbon reinforced epoxy laminates with nanofibrous mats as toughening interlayers.
  Di Filippo M, Alessi S, Pitarresi G, Sabatino MA, Zucchelli A, Dispenza C.
  Polymer Degradation and Stability 2016, vol. 126, p. 188-195.

- Water diffusion and swelling stresses in highly crosslinked epoxy matrices.
  Toscano A, Pitarresi G, Scafidi M, Di Filippo M, Spadaro G, Alessi S.
  Polymer Degradation and Stability 2016, vol. 133, p. 255-263.

- Photoelastic stress analysis assisted evaluation of fracture toughness in hydrothermally aged epoxies.
  Pitarresi G, Toscano A, Scafidi M, Di Filippo M, Alessi S, Spadaro G.
  Frattura ed Integrità Strutturale 2014, vol. 30, p. 127-137.

- Fracture Toughness of hydrothermally aged epoxy systems with different crosslink density.
  Alessi S, Di Filippo M, Pitarresi G, Scafidi M, Toscano A.
  Procedia Engineering 2015, vol. 109, p. 507-516.